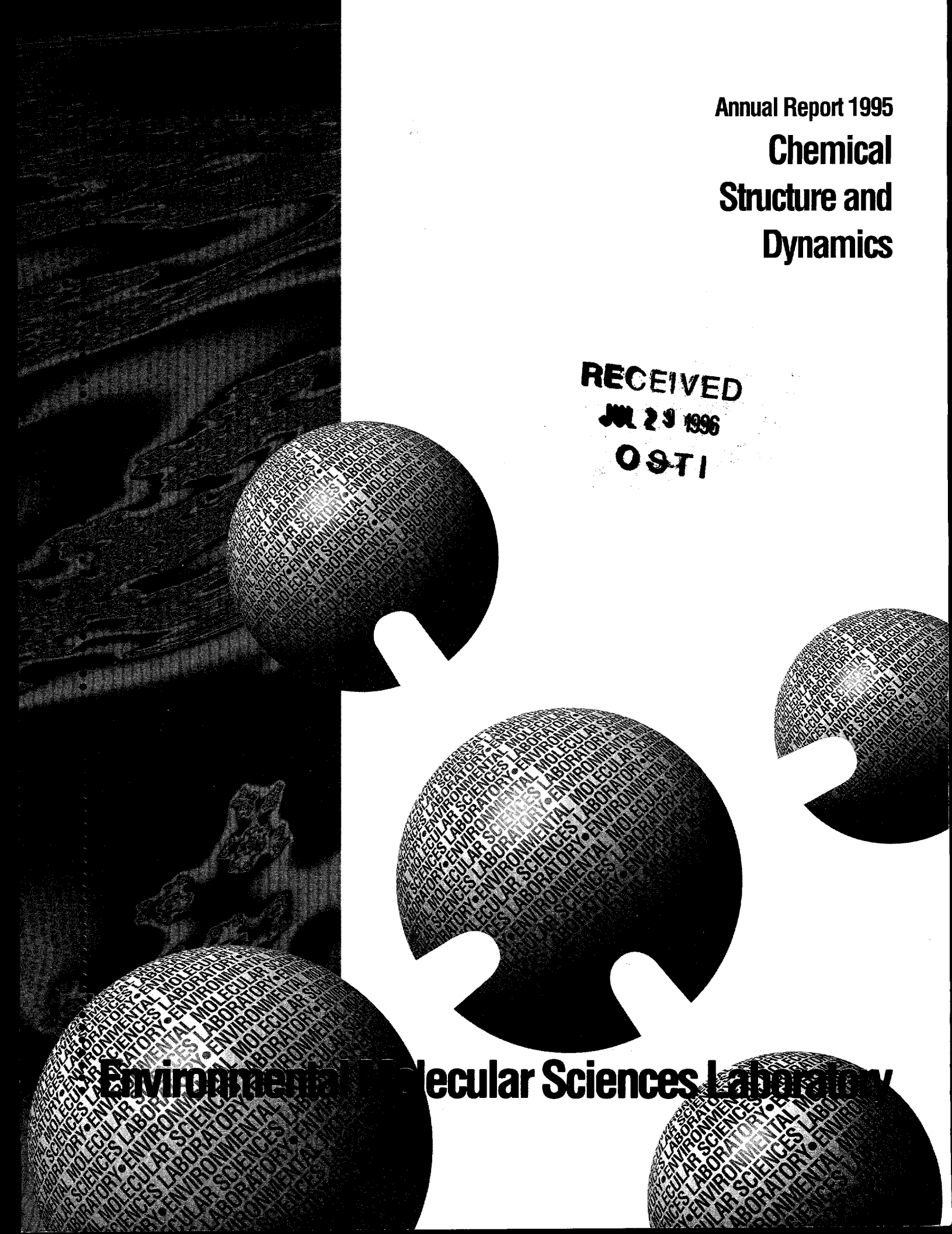


Annual Report 1995
**Chemical
Structure and
Dynamics**

RECEIVED

JUL 29 1996

OSTI



Environmental Molecular Sciences Laboratory

DISCLAIMER

This report was prepared as an account of work sponsored by an agency of the United States Government. Neither the United States Government nor any agency thereof, nor Battelle Memorial Institute, nor any of their employees, makes **any warranty, express or implied, or assumes any legal liability or responsibility for the accuracy, completeness, or usefulness of any information, apparatus, product, or process disclosed, or represents that its use would not infringe privately owned rights.** Reference herein to any specific commercial product, process, or service by trade name, trademark, manufacturer, or otherwise does not necessarily constitute or imply its endorsement, recommendation, or favoring by the United States Government or any agency thereof, or Battelle Memorial Institute. The views and opinions of authors expressed herein do not necessarily state or reflect those of the United States Government or any agency thereof.

PACIFIC NORTHWEST NATIONAL LABORATORY

operated by

BATTELLE

for the

UNITED STATES DEPARTMENT OF ENERGY

under Contract DE-AC06-76RLO 1830

Printed in the United States of America

Available to DOE and DOE contractors from the
Office of Scientific and Technical Information, P.O. Box 62, Oak Ridge, TN 37831;
prices available from (615) 576-8401.

Available to the public from the National Technical Information Service,
U.S. Department of Commerce, 5285 Port Royal Rd., Springfield, VA 22161



This document was printed on recycled paper.

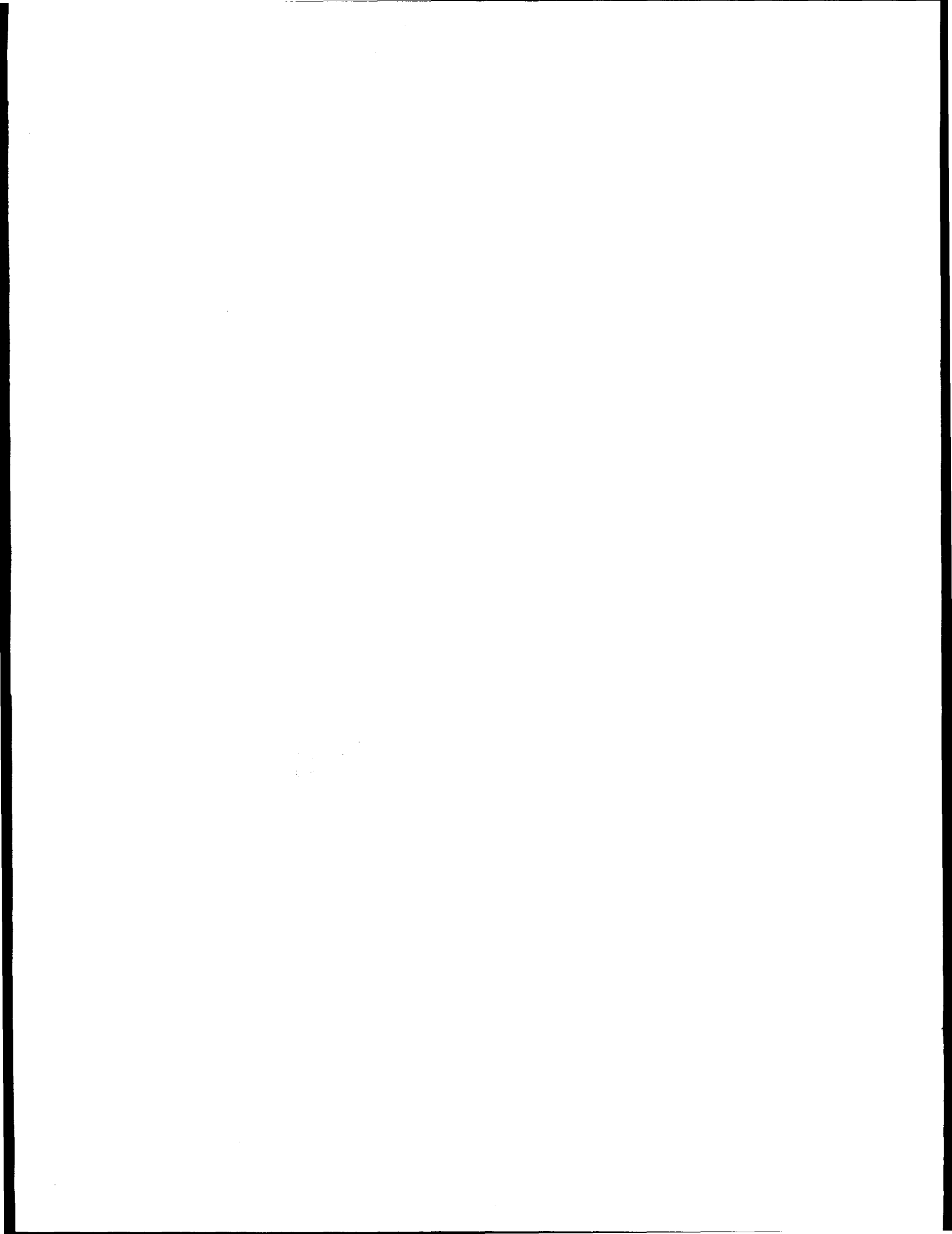
Annual Report 1995 Chemical Structure and Dynamics

Prepared by
Steven D. Colson, Associate Director,
Robin S. McDowell, Program Manager,
and the staff of the Chemical Structure
and Dynamics Program

May 1996

Prepared for the U.S. Department of Energy
under Contract DE-AC06-76RLO 1830

Pacific Northwest National Laboratory
Operated by Battelle for the
U.S. Department of Energy



Contents

1. Introduction	1-1	Low-Temperature Plasma Processing of Chlorinated Hydrocarbons ^c <i>R. G. Tonkyn, S. E. Barlow, and T. M. Orlando</i>	3-6
2. Reaction Mechanisms at Interfaces		Irradiation of Condensed-Phase Acetyl Chloride ^a <i>B. Rowland and W. P. Hess</i>	3-7
Single-Molecule Spectroscopy and Chemical Dynamics ^a <i>H. P. Lu and X. S. Xie</i>	2-1	Electron- and Photon-Stimulated Surface/Interface Chemistry ^a <i>T. M. Orlando, R. G. Tonkyn, G. A. Kimmel, and K. Knutsen</i>	3-9
New Developments in Near-Field Microscopy ^b <i>X. S. Xie, R. X. Bian, R. C. Dunn, P. T. Leung, E. Sanchez, and E. V. Allen</i>	2-2	4. Cluster Models of the Condensed Phase	
Structure and Reactivity of Ice Surfaces and Interfaces ^a <i>C. Huang, R. S. Smith, and B. D. Kay</i>	2-4	Cluster Model Studies of the Structure and Bonding of Environmentally-Important Materials ^a <i>L. S. Wang, J. B. Nicholas, S. D. Colson, and S. R. Desai</i>	4-1
Chemisorption on Oxide Surfaces ^a <i>M. J. Styrniman, C. Huang, R. S. Smith, S. A. Joyce, and B. D. Kay</i>	2-8	Photoelectron Spectroscopy and Electronic Structure of Metal Clusters and Chemisorbed Metal Cluster Complexes ^e <i>L. S. Wang and H. Wu</i>	4-2
Scanning Tunneling Microscopy of Epitaxial Films ^{a,c} <i>S. A. Joyce, J. P. Cowin, M. S. Fyfield, and M. C. Gallagher</i>	2-11	High-Resolution Spectroscopy of Molecules and Clusters ^{a,f} <i>S. W. Sharpe, T. A. Blake, R. L. Sams, and R. S. McDowell</i>	4-6
Synthetic Ionic Interfaces via Ion-Beam and Ice Epitaxy ^a <i>H. Wong, G. B. Ellison, J. P. Cowin, and M. J. Iedema</i>	2-13	Cation-Ether Complexes in the Gas Phase: Bond Dissociation Energies and Equilibrium Structures of Li ⁺ [1,2-dimethoxyethane] _x x = 1-2, and Li ⁺ [12-crown-4] ^a <i>D. Ray, D. F. Feller, M. B. More, E. D. Glendening, and P. B. Armentrout</i>	4-7
Bonding and Structure of Organic Ligands at Oxide/Water Interfaces ^c <i>D. M. Friedrich, A. G. Joly, Z. Wang, C. C. Ainsworth, and P. L. Gassman</i>	2-14	Spectroscopy and Dynamics of Molecular Clusters ^a <i>A. H. Bahnmaier, V. A. Ventura, A. G. Joly, J. M. Price, and D. Ray</i>	4-9
Transport of Molecules Across Liquid Water/Vapor Interfaces Probed by Surface Nonlinear Optical Spectroscopy ^c <i>R. Doolen, J. M. Gaudio, and D. Ray</i>	2-16	5. Miscellaneous	
3. Radiation and Other High-Energy Processes at Environmental Interfaces		Characteristics of a Weakly-Ionized Nonneutral Plasma ^{a,c} <i>A. J. Peurrung and S. E. Barlow</i>	5-1
Thermal Distributions Deduced from (2+1) REMPI of CO Products ^{a,d} <i>K. M. Beck, K. A. H. German, and W. P. Hess</i>	3-1	Ultrafast Infrared Pulse Generation and Measurement of Vibrational Decay in Water ^f <i>G. R. Holtom</i>	5-2
Mechanisms of Radiolytic Decomposition of Complex Nuclear Waste Forms ^c <i>K. Knutsen, K. A. German, Y. Su, K. D. Keefer, W. P. Hess, and T. M. Orlando</i>	3-4	Breath Analysis by Laser-Based Spectroscopy ^g <i>S. W. Sharpe, T. A. Blake, and R. L. Sams</i>	5-3

6. Appendix

Chemical Structure and Dynamics Staff	6-1
Publications and Presentations	
Publications.....	6-5
In Press and Submitted	6-7
Presentations.....	6-8
Awards and Recognition.....	6-12
Collaborations	
Outside Collaborations	6-13
Collaborations within PNNL.....	6-14
Acronyms and Abbreviations	6-15
Where CS&D Fits in PNNL.....	6-15

Funding Support

- a* DOE Office of Basic Energy Sciences, Chemical Sciences Division, Fundamental Interactions Branch.
- b* Cooperative Research and Development Agreement (CRADA).
- c* PNNL Laboratory Directed Research and Development (LDRD).
- d* Strategic Environmental Research and Development Program (SERDP).
- e* National Science Foundation.
- f* Instrument development under the EMSL Project.
- g* Medical Technologies Initiative.

1. Introduction

Purpose

The Chemical Structure and Dynamics program is a major component of Pacific Northwest National Laboratory's Environmental Molecular Sciences Laboratory (EMSL), providing a state-of-the-art collaborative facility for studies of chemical structure and dynamics. We respond to the need for a fundamental, molecular-level understanding of chemistry at a wide variety of environmentally important interfaces by (1) extending the experimental characterization and theoretical description of chemical reactions to encompass the effects of condensed media and interfaces; (2) developing a multidisciplinary capability for describing interfacial chemical processes within which the new knowledge generated can be brought to bear on complex phenomena in environmental chemistry and in nuclear waste processing and storage; and (3) developing state-of-the-art analytical methods for the characterization of waste tanks and pollutant distributions, and for detection and monitoring of trace atmospheric species.

This research effort was initiated in 1989 and will continue to evolve over the next few years into a program of rigorous studies of fundamental molecular processes in model systems, such as well-characterized surfaces, single-component solutions, clusters, and biological molecules; and studies of complex systems found in the environment (multispecies, multiphase solutions; solid/liquid, liquid/liquid, and gas/surface interfaces; colloidal dispersions; ultrafine aerosols; and functioning biological systems).

The success of this program will result in the achievement of a quantitative understanding of chemical reactions at interfaces, and more generally in condensed media, comparable to that currently available for gas-phase reactions. This understanding will form the basis for the development of *a priori* theories for predictions of macroscopic chemical behavior in condensed and heterogeneous media, adding significantly to the value of field-scale environmental models, the prediction of short- and long-term nuclear waste storage stabilities, and other areas related to the primary missions of the United States Department of Energy (DOE).

CS&D has developed research programs in the following areas:

- Chemical structures, reaction dynamics, and kinetics in solution and at interfaces, to support DOE needs for
 - characterization, processing, and storage of mixed wastes
 - remediation of contaminated soils and groundwater
 - understanding global change
 - insuring nuclear nonproliferation.
- Structure/function research on molecular systems, especially on problems associated with
 - surface chemistry and catalysis
 - bioremediation
 - high-energy processes.
- Establishment and operation of a portion of EMSL for the study of
 - surface/interface structure and reactions
 - chemical structure and reaction dynamics (clusters, reactive species, and model systems)
 - time-resolved spectroscopy.
- Development of state-of-the-art analytical methods for the characterization of tanks and plumes, and for detection and monitoring of trace atmospheric species.

Background

Studies of the surface chemistry at interfaces requires measurements of many chemical and physical properties within 5 to 10 Å of the interface boundary. An understanding of the interfacial chemistry can be achieved only by combining measured quantities, such as chemical dynamics, structure, and bonding, with theoretical analysis, to produce models consistent with the observations. This interdisciplinary approach is the heart of the EMSL concept, in which a wide variety of experimental and theoretical approaches are combined to address complex problems of importance to DOE.

We have targeted condensed-phase phenomena that are relevant to chemical processes in natural and contaminated systems, including those related specifically to environmental restoration and waste storage issues at DOE sites. For example,

systems have been selected to model the sorption and abiotic transformations of solutes on mineral surfaces in soil and ground water. Sorption and surface-catalyzed abiotic transformations are widely recognized contributors to the natural filtration capacity of soil and porous aquifers for contaminants, and are therefore of central importance in governing contaminant transport rates and persistence. Mechanistically valid models of such phenomena at the microscopic and macroscopic scales are critically needed to predict contaminant migration on DOE sites, but are unavailable because the responsible surface chemical reactions are not completely understood.

Chemical reactivity at environmental solid-liquid interfaces is controlled by the effects of substrate structure on the interactions between solvent and adsorbate solute molecules. In order to observe chemical changes at these interfaces, experimental methods are required to measure the changes in molecular structure and dynamics that are induced by natural and man-made surfaces. Reactions and thermodynamic properties that are enhanced at environmental interfaces include: (1) proton transfer reactions, such as solute hydrolysis and acid dissociation; (2) electron transfer transformations; and (3) stability constants for adsorbate-substrate complexes. These interfacial phenomena strongly impact contaminant dynamics in soil and groundwater. However, the responsible molecular phenomena are not well understood, thereby precluding development of rigorous descriptive models. We anticipate that targeted experiments, relevant to DOE sites, on model systems containing oxides, carbonates, and silicates in contact with solvent and solute molecules can resolve much of the scientific ambiguity regarding interfacial reactions in geochemical systems. Such studies of interfacial chemistry will also have obvious and perhaps far-reaching consequences for our understanding of processes that affect process waste chemistry and waste form integrity when combined with the specific studies of energetic reaction mechanisms contained in the scope of this work.

A quantitative understanding of chemical reaction dynamics at interfaces in condensed media is an important goal for chemical physics research, and a challenging and demanding scientific problem requiring an understanding of the solid substrate, the solvent, and their combined effect

upon the chemical reaction dynamics. It is now possible to bring together diverse expertise and technology to study complex interfacial chemistry. Such a study requires integration of state-of-the-science experimental capabilities for the study of primary chemical processes, with advances in computational technology and sophisticated new theoretical models for predicting molecular structure and potential energy surfaces. Essential for the success of this program is the creation of a stimulating and interactive intellectual environment, where concepts and ideas from theoretical and experimental disciplines can be integrated to produce a comprehensive approach to the study of complex phenomena. The EMSL organization and laboratory structure are designed to provide the development of this environment through internal and external collaborations.

The CS&D group has particular expertise in the preparation and spectroscopic analysis of molecular clusters (S. D. Colson, W. P. Hess, D. Ray, S. W. Sharpe, and L. S. Wang); ultrafast and nonlinear optical spectroscopies (D. Ray, G. R. Holtom, and X. Xie); ultrahigh resolution spectroscopy for measurements of electronic and geometric structures and dynamics (S. W. Sharpe and R. S. McDowell); surface and interface structure, chemical reaction dynamics, and kinetics (J. P. Cowin, S. A. Joyce, B. D. Kay, and T. M. Orlando); and ion-molecule traps and storage technology (S. E. Barlow).

Approach

Experimental studies of molecular and supra-molecular structures and thermodynamics are key to understanding the nature of matter, and lead to direct comparison with computational results. Kinetic and mechanistic measurements, combined with real-time dynamics measurements of atomic and molecular motions during chemical reactions, provide a molecular-level description of reaction processes. The anticipated results of this work are the achievement of a quantitative understanding of chemical processes at complex interfaces, the development of new techniques for the detection and measurement of species at such interfaces, and the interpretation and extrapolation of the observations in terms of models of interfacial chemistry.

Our methodology dissects complex interfacial problems into components that are subject to quantitative investigation and interpretation. Target solvent-reactant-surface systems have been selected for study because of their theoretical interest and applicability to DOE's environmental problems. The theoretical basis for understanding such systems starts with the literature data base, augmented by new measurements on synthetic interfaces of controlled composition and structure. The interpretations are supported by the understanding of molecular processes obtained by molecular dynamics and structural measurements of gas-phase clusters, of macroscopic solid surfaces, and of solutions.

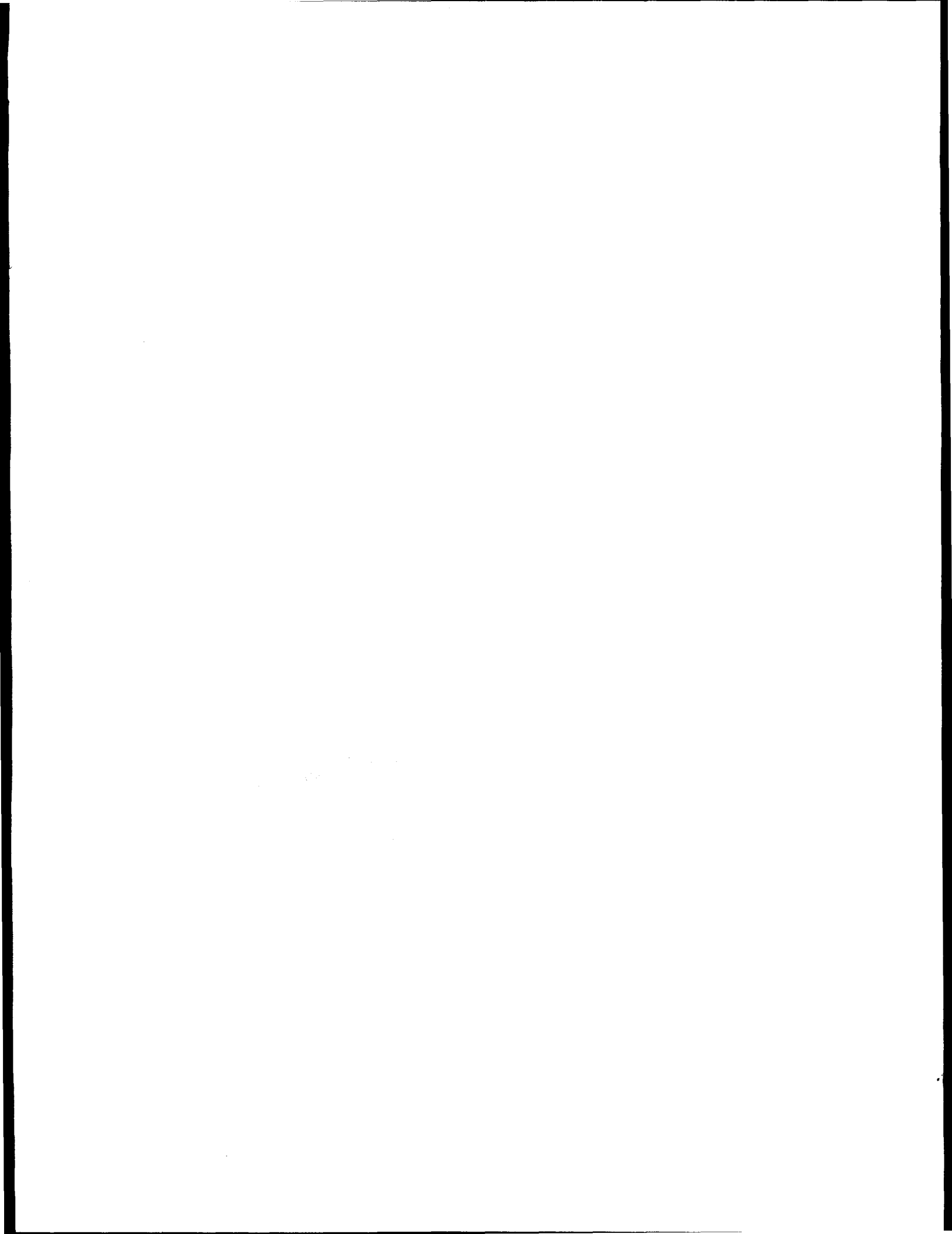
Structural and kinetics studies of phenomena at model oxide surfaces will elucidate mechanisms of the complex interfacial chemistry of the subsurface environment. This work focuses on the epitaxial growth of doped water (as amorphous ice) layers on metal-oxide surfaces, where direct measurements can be made of diffusion, dissolution, bimolecular reactions, and electrochemistry. Extrapolation of these findings to more complex natural systems is facilitated by theoretical models, and through the results of direct liquid-phase and liquid-solid interface measurements. Using the near-field optical microscope, for example, the fate of a single molecule in solution or at an interface can be probed without averaging over spatially- and temporally-inhomogeneous environments of all molecules in the sample.

Many of the interfacial chemistry problems facing the DOE involve mixed organic/inorganic/radioactive materials. Thus, we need to address high-energy processes unique to this type of waste form, including the primary molecular processes of ionization and dissociation, and resulting reactions of high-energy species. Particular attention is given to the complex mechanisms of radiolytic (gamma ray, X ray, and electron)-induced degradation of current and proposed future high-level nuclear waste forms: solidified waste, glasses, and

ceramics. The emphasis here is on understanding the underlying physical and chemical mechanisms responsible for the formation of byproducts and loss of integrity in composite matrix materials.

Studies of the structure and bonding of organic ligands at oxide/water interfaces provides insight into geologically-important mineral surfaces and environmentally-significant ligand/complexant interactions. Isolated, gas-phase clusters of atoms that compose the actual surface are being synthesized to mimic surface structures. Spectroscopic determination of their structures is important to the evaluation of theoretical models of their chemical properties. Solvent-solvent and solvent-surface interactions are studied in a similar manner. Studies of both pure solvent and mixed solvent-substrate clusters help delineate the relative importance of the forces required to model the solvent effects. Likewise, reactant-substrate, reactant-solvent and solvent-reactant-substrate systems can be modeled as isolated clusters. Our approach to these very complex systems is to use the common practice of experimental extrapolation: small, simpler systems are subjected to quantitative theoretical and experimental analysis, which forms the basis for understanding more complex systems. For instance, while it may not be possible to obtain detailed structural data on solvent-reactant-substrate clusters, measurements of chemical reaction dynamics in these clusters can be modeled with approximate theories tested previously by their application to simpler systems. Furthermore, we can deposit selected chemical species (including clusters) designed to mimic reactive sites on inert substrates and study their chemical activity. This work also has the potential for producing *designer surfaces* that may be valuable as chemical sensors, or for development of unique materials for chemical separations.

Our activities in calendar year 1995 are summarized in this report.



2. Reaction Mechanisms at Interfaces

Single-Molecule Spectroscopy and Chemical Dynamics

H. P. Lu* and X. S. Xie

Supported by DOE Office of Basic Energy
Sciences.

*Postdoctoral Research Associate.

Recent developments in fluorescence microscopy enable single-molecule spectroscopy at cryogenic temperature¹ to be extended to the room-temperature regime.²⁻⁴ Time-resolved spectroscopic experiments on single-molecules dynamics on both the 10^{-2} to 10^3 sec time scale and the picosecond to nanosecond time scale have been demonstrated.³

Figure 2.1 shows a typical far-field fluorescence image of single molecules (sulforhodamine 101) dispersed on a glass surface, taken with an epifluorescence microscope.^{5,6} The different intensities of the peaks are due to the different molecular orientations and absorption spectra.

On the 10^{-2} to 10^3 second time scale, we can observe single events, such as orientational motions, spectral diffusion, and photobleaching. Single-molecule events are usually characterized by abrupt jumps in experimental observables. For example, we have observed intensity fluctuations

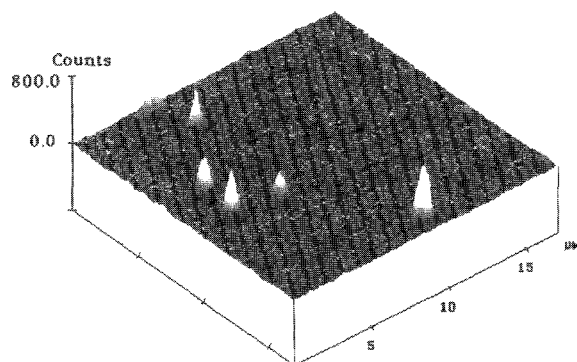


Figure 2.1. Far-field fluorescence image ($17 \mu\text{m} \times 17 \mu\text{m}$) of single sulforhodamine 101 molecules dispersed on a glass surface. The different intensities of the peaks are due to the different molecular orientations and the different excitation spectra.

in the emission from single sulforhodamine 101 molecules that are attributed to the spectral fluctuation (instead of rotational diffusion) of the molecules.³ We have recently conducted a detailed study of this phenomenon. Time-resolved single-molecule emission spectra are acquired with 100-ms time resolution (Fig. 2.2). Time correlation functions of the first moments of single-molecule spectra are obtained, with decay time constants inversely proportional to excitation intensities, demonstrating that the origin of the spectral fluctuation is in photo-induced conformational changes associated with nonradiative relaxations. Understanding the nature of spectral fluctuation is crucial to future single-molecule experiments.

On the picosecond to nanosecond time scale, we can study the dynamics of repetitive processes.

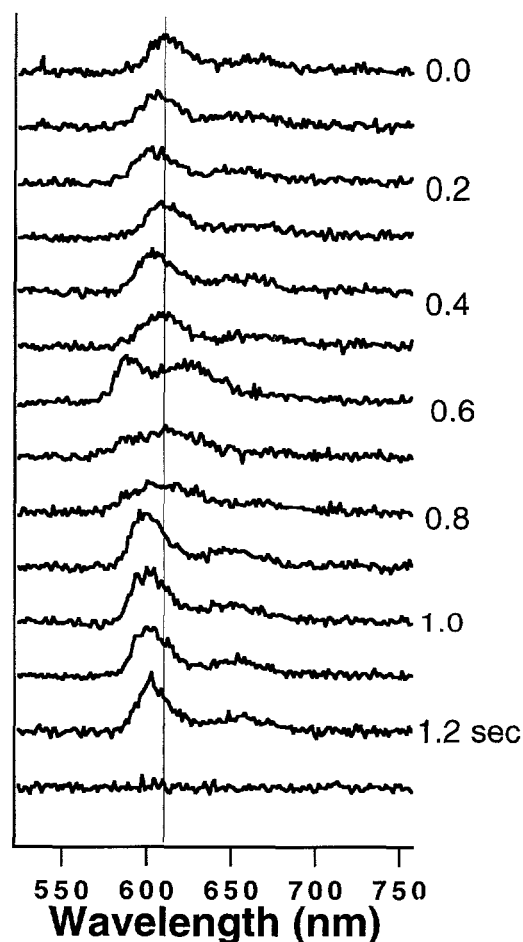


Figure 2.2. The emission spectrum of a single sulforhodamine 101 molecule fluctuates with time. Sequential spectra were taken at 100-ms collection intervals until the photobleaching occurred.

Thus, it is possible to study photoinduced chemical reactions of single molecules in specific local environments. Figure 2.3 shows the fluorescence decay of a single cresyl violet molecule adsorbed on an indium tin oxide (ITO) surface. This molecule undergoes an interfacial electron transfer reaction in its excited state, with a single exponential decay of 480 ps. Interestingly, we find a distribution of electron transfer rates for individual molecules at different sites. While experiments done on a large ensemble of molecules of this system exhibit dispersed kinetics, conducting time-resolved measurements on a single-molecule basis allows us to investigate chemical reactions at interfaces with much greater detail.

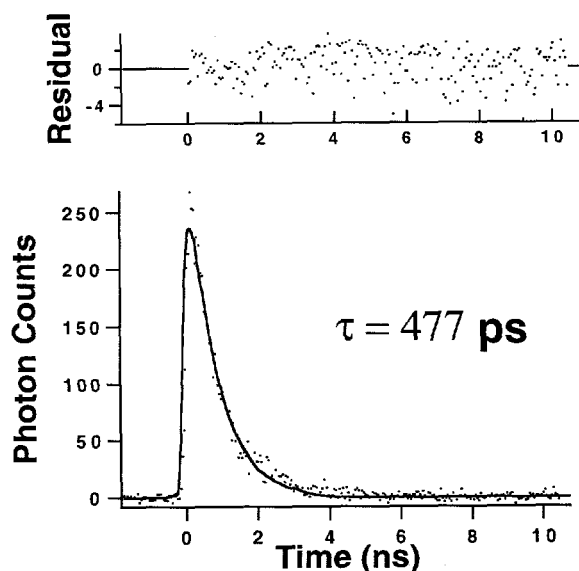


Figure 2.3. Fluorescence decay of a single cresyl violet molecule undergoing a photo-induced electron transfer reaction on an indium tin oxide (ITO) surface.

References

1. W. E. Moerner, *Science* **256**, 46 (1994).
2. J. K. Trautman *et al.*, *Nature* **369**, 40 (1994).
3. X. S. Xie and R. C. Durn, *Science* **265**, 361 (1994).
4. W. P. Ambrose *et al.*, *Science* **265**, 364 (1994).
5. S. Nie, D. T. Chiu, and R. N. Zare, *Science* **266**, 1018 (1995).
6. J. J. Macklin *et al.*, *Science*, in press.

New Developments in Near-Field Microscopy

X. S. Xie, R. X. Bian,* R. C. Dunn,[†]
P. T. Leung,[§] E. Sanchez, and E. V. Allen[‡]

Supported by Cooperative Research and Development Agreement (CRADA).

*EESD Earth Systems Sciences Department, Atmospheric Sciences Section.

[†]Present Address: Department of Chemistry, University of Kansas, Lawrence, Kansas 66045.

[§]Department of Physics, Portland State University, Portland, Oregon 97207.

[‡]PNNL Applied Physics Center.

Recent advances in the near-field scanning optical microscope (NSOM)¹ allow the imaging of single-molecule emission with nanometric resolution² and single-molecule spectroscopy at room temperature. With NSOM, molecular fluorescence can be spectrally³ and temporally⁴⁻⁶ resolved, for detailed studies of molecular interactions and dynamics on a single-molecule basis with a spatial resolution beyond the diffraction limit.

In near-field scanning optical microscopy, the fluorescence lifetime of a single dye molecule can be changed, sensitively dependent on the relative positions of the molecule and the aluminum-coated fiber tip (Fig. 2.4). To extract useful information from NSOM experiments, perturbations to spectroscopic measurements induced by the NSOM tip must be characterized. We have experimentally determined and numerically computed single-molecule fluorescence lifetimes as a function of the relative position of the molecule and the NSOM tip.⁶ In addition, radiative rates, nonradiative rates, emission quantum yields, and spectral shifts are also computed. The computational results shown in Fig. 2.5 provide significant insight into the behavior of fluorescence lifetimes.⁶

This computation was performed by incorporating a phenomenological model and solving the electromagnetic fields using the finite-difference time-domain (FDTD) approach. Our new methodology is capable of predicting molecular emission properties in front of a metal/dielectric interface of arbitrary geometry.

The FDTD computation also provides guidance for nonperturbative NSOM experiments.⁶ It allows us to predict the proper conditions under which spec-

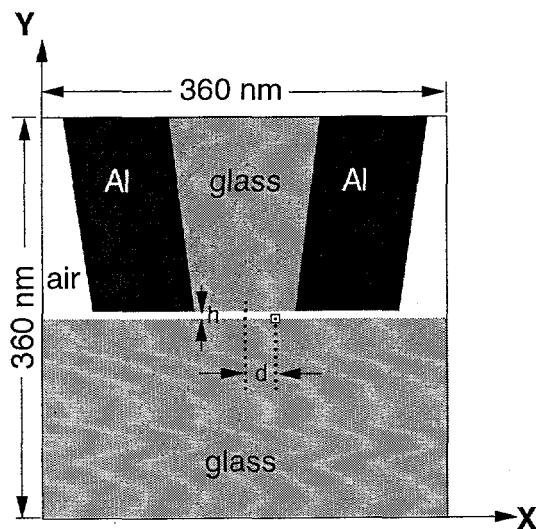


Figure 2.4. Schematic of the NSOM tip with an aperture diameter of 100 nm. Emission properties of a single molecule are calculated as a function of the lateral displacement (d) and tip-molecule gap (h).

Microscopic measurements with NSOM can be done with minimal perturbations. Effects on excitation and emission spectra are negligible at room temperature, given the broad spectral widths. Although radiative and nonradiative rates are significantly affected by the presence of the aluminum-coated tip, and are very sensitive to the tip morphology, for many intrinsically fast dynamical processes, such as photo-induced electron transfer reactions, population lifetimes can be measured essentially free from perturbation.

On the experimental front, we have significantly improved the quality of aluminum coating and developed a liquid cell for biological applications. To continue our effort on spectroscopic mapping of photosynthetic membranes,⁷ we have taken high-quality simultaneous shear-force and near-field images of photosynthetic membrane fragments, as well as of single proteins under water.⁸ Figure 2.6 shows such images of membrane fragments containing light-harvesting complexes provided by Professor Laurens Mets' laboratory at the University of Chicago.

References

1. E. Betzig and J. K. Trautman, *Science* **257**, 189 (1992).

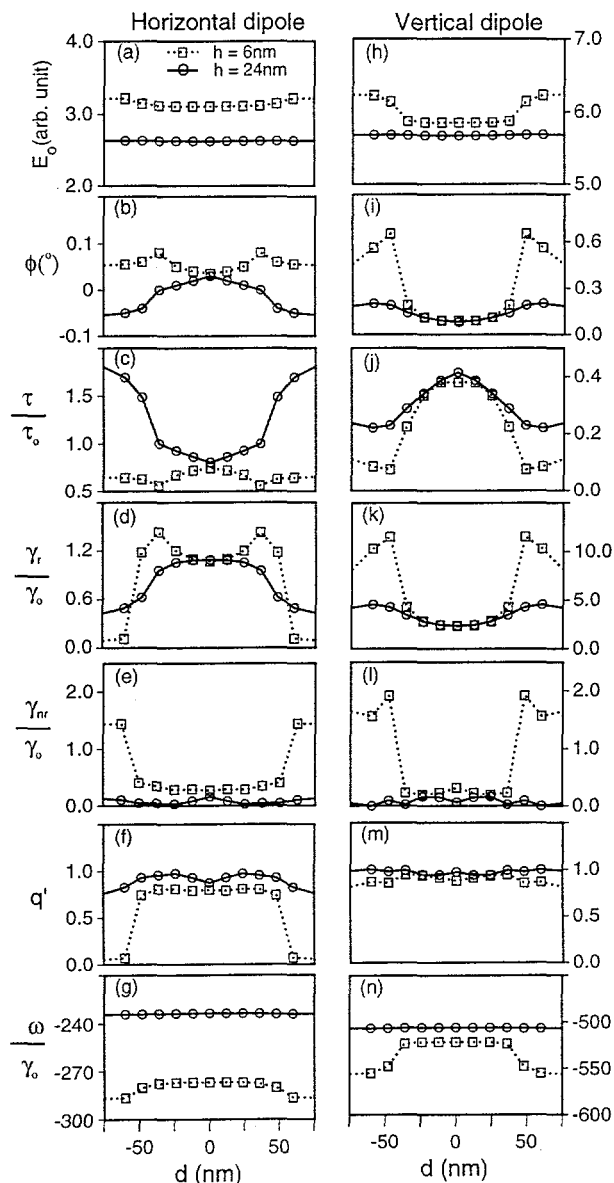


Figure 2.5. Two-dimensional FDTD results for both a horizontal dipole (left column, a-g) and a vertical dipole (right column, h-n) as a function of the lateral displacement, d , evaluated at tip-molecule gaps $h = 6$ and 24 nm. From top to bottom, the quantities simulated are the reflected field amplitude E_0 and phase ϕ , normalized lifetime τ/τ_0 , normalized radiative rate γ_r/γ_0 and nonradiative rate γ_{nr}/γ_0 , apparent quantum yield q' , and spectral shift $\Delta\omega/\gamma_0$. (From Ref. 6.)

2. E. Betzig and R. J. Chichester, *Science* **262**, 1422 (1993).
3. J. K. Trautman *et al.*, *Nature* **369**, 40 (1994).
4. X. S. Xie and R. C. Dunn, *Science* **265**, 361 (1994).
5. W. P. Ambrose *et al.*, *Science* **265**, 364 (1994).

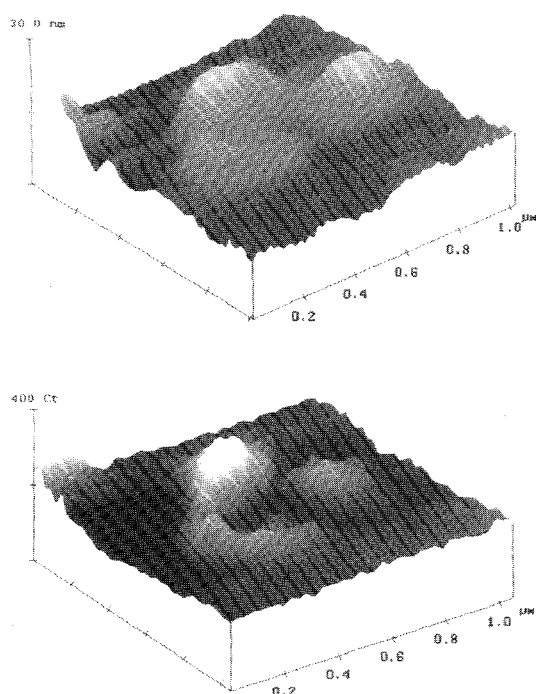


Figure 2.6 Simultaneous shear-force (top) and near-field (bottom) images taken under water for membrane fragments containing closely-packed light-harvesting complexes. Both single- (7–8 nm) and double-stacked (15 nm) membrane fragments are seen in the shear force image.

6. R. X. Bian *et al.*, *Phys. Rev. Lett.* **75**, 4772 (1995).
7. R. C. Dunn *et al.*, *J. Phys. Chem.* **98**, 3094 (1994).
8. X. S. Xie *et al.*, in *Focus on Modern Microscopy*, P. Cheng, ed. (World Scientific Publishing Co.), in press.

Structure and Reactivity of Ice Surfaces and Interfaces

C. Huang,* R. S. Smith, and B. D. Kay

Supported by DOE Office of Basic Energy Sciences.

*Postdoctoral Research Associate.

Molecular-beam scattering from surfaces is a powerful experimental tool for studying the dynamics and kinetics of the interaction of molecules with surfaces. The coupling of surface science, molecular beam, and laser technologies makes possible

the measurement of total energy disposal and redistribution in gas-surface scattering. These experimental methods have been employed to acquire detailed surface kinetics and state-to-state scattering measurements of molecules interacting with metallic substrates. Such experiments have resulted in a fairly detailed understanding of surface chemistry on metals. Unfortunately, we currently do not have a similar understanding of the elementary dynamical and kinetic processes occurring on ice and oxide surfaces. Such interactions are clearly important from an environmental viewpoint, because they form the molecular-level basis for the complex physiochemical processes that occur on the surface of atmospheric aerosols, at the aqueous/mineral geochemical interface, and at the vapor/liquid interface. Our goal is to apply and extend molecular-beam surface scattering techniques to these systems in an effort to elucidate the relevant interactions.

In this project, the chemisorption and solvation kinetics and dynamics of polar molecules on multilayer ice surfaces are studied using molecular-beam-surface scattering, thermal desorption (TPD and isothermal), and laser spectroscopic techniques. These experiments will help unravel the mechanism by which a strongly polar neutral molecule dissolves into an aqueous solvent and ultimately forms solvated ions. Sticking coefficients of prototypical "electrolytes," such as HCl and NH₃, on ice surfaces will be determined as a function of incident energy, angle, and surface temperature. The branching ratio between molecular vs. dissociative ("solvation") chemisorption will be probed via isotope exchange between the hydrogens of the "electrolyte" and the "solvent" substrate. In related experiments, hydrophobic and hydrophilic interactions between water and various other materials will be probed using beam-generated thin films. Interlayer diffusion and phase separation will be probed using thermal desorption and surface analytic techniques.

Amorphous and glassy materials have important applications in many areas of physical, biological, and materials science. In particular, amorphous water ice has been the focus of considerable diverse and interdisciplinary research. The reasons include its applicability as a model for liquid water, its existence as a major component in cometary and interstellar ice, and the current debate over its physical and thermodynamic

properties. The work described here, although germane to all of these areas, is aimed at understanding the structure and molecular-level interactions of nanoscale thin films of water ice with the underlying substrate. A wealth of literature exists on water adsorption on surfaces, but despite its importance, the microscopic details of the structure and energetics are not fully understood. The prevailing interpretation is that water deposited on surfaces forms a smooth ice-like bilayer structure and evaporates with zero-order kinetics suggestive of layer-by-layer desorption. Zero-order kinetics are expected if sublimation occurs from a smooth film of constant exposed surface area. Surprisingly, we find that the desorption kinetics are not consistent with smooth layer-by-layer evaporation, and are strongly dependent on the hydrophilicity of the substrate. The kinetics for the amorphous-to-crystalline ice phase transformation are also studied. Our experimental results are completely explained by a quantitative kinetic model, and provide information about water-substrate interactions and fundamental data about phase transformation mechanisms in glasses and amorphous materials.

An effusive molecular beam was used to grow precise thicknesses of amorphous ice films on both Ru(001) and Au(111) single-crystal substrates at 85 K. After ice film growth, the substrates were resistively heated at a linear ramp rate of 0.6 K/s from 85 K to the desired desorption temperature, after which the temperature was held constant. A quadrupole mass spectrometer was used to measure the angle-integrated desorption rate as a function of time. Isothermal desorption spectra for D₂O ice thin films grown on Ru(001) and Au(111) are shown in Fig. 2.7. The dose on both substrates was 56 layers (1 layer = $\sim 10^{15}$ molecules/cm²). Similar experiments with H₂O gave analogous results. The desorption rate exhibits an initial rapid increase due to ramping the temperature from 85 to 160 K. At 160 K, the desorption rate decreases rapidly to a value approximately half the initial rate, followed by a much slower decrease. The small oscillations in the experimental spectra are due to small fluctuations (± 0.05 K) in the isothermal temperature control.

Initially, desorption is from ice that is completely amorphous, but as the phase transition proceeds, the desorption rate rapidly decreases because the amorphous ice is being converted to the more stable crystalline phase. After the phase transition is

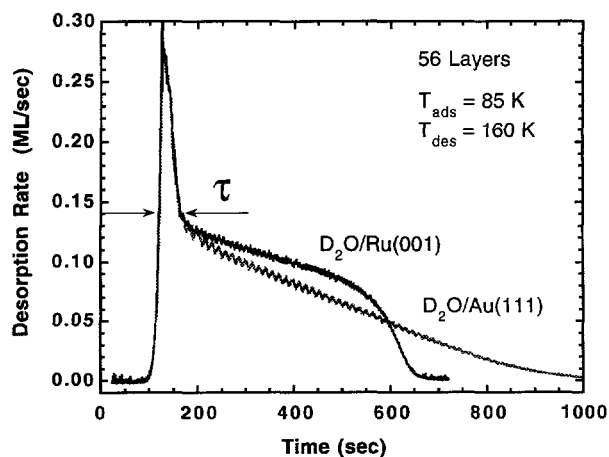


Figure 2.7. Isothermal desorption spectra for amorphous D₂O ice grown at 85 K on Ru(001) and Au(111). The initial time-dependence of the desorption rate is the result of the conversion from amorphous to crystalline ice. The late-time difference in the desorption kinetics is believed to reflect the morphologies of the ice films on the two substrates.

complete, the decrease in the desorption rate slows. The time to complete the phase transition is labeled τ . Although τ is the same for both the Ru(001) and Au(111) substrates, clear differences are seen in the slopes of the desorption rate after the phase transition. The non-zero slopes indicate that the desorption kinetics are non-zero order and suggest that the morphologies of films grown on the two substrates are different. These differences in the slopes persist for film thicknesses up to 150 layers (~ 500 Å). Above 150 layers, the Au(111) spectra begin to appear more like that of Ru(001). These differences can be understood by considering the strength of the water-substrate interaction. Water is known to wet the hydrophilic Ru(001) surface and form an ice-like bilayer structure. The water-Au(111) interaction is weaker than the water-water interaction, and leads to hydrophobic non-wetting. As a consequence, ice films grown on Ru(001) are expected to be smoother and the desorption kinetics will be closer to zero-order, whereas ice films grown on Au(111) may tend to form sphere-like, 3-dimensional nanoclusters, and the desorption kinetics will be markedly non-zero order.

Isothermal desorption spectra for various initial thicknesses of D₂O on Au(111) are displayed in Fig. 2.8, and clearly indicate that the crystallization kinetics are thickness-dependent; similar behavior

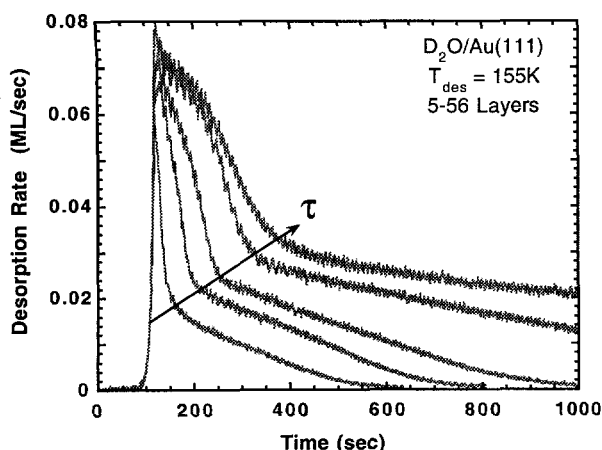


Figure 2.8. Isothermal desorption spectra for various thickness D_2O ice films deposited on Au(111). The crystallization time τ increases with increasing film thickness.

is observed for films grown on Ru(001). Figure 2.9A shows the observed crystallization time τ as a function of film thickness for Ru(001) and Au(111). The data show that τ increases with thickness to a saturation value independent of the substrate. Figure 2.9B shows the observed crystallization time τ as a function of substrate temperature for both Ru(001) and Au(111). The observed temperature dependence shows Arrhenius-like behavior, with a substrate-independent apparent activation energy of 20 kcal/mole.

The substrate-independent, nonlinear, saturable thickness dependence of τ argues against substrate-catalyzed crystallization. If the crystallization were catalyzed at the substrate/ice interface, τ would increase linearly with film thickness and be substrate-dependent. Our data can be described by the equation shown in the caption to Fig. 2.9. L^* can be interpreted as the average distance between embryos in the amorphous ice. When the thickness of the film is small compared to L^* , τ will increase linearly with thickness because the volume of material a given nucleation embryo must crystallize increases linearly with thickness. When the films are thick compared to L^* , then the volume of material a given nucleation embryo must crystallize is constant, and, as such, τ becomes independent of thickness. The thickness dependence data from both substrates give a similar value for L . Our interpretation that L is a measure of the spacing between nucleation embryos is consistent

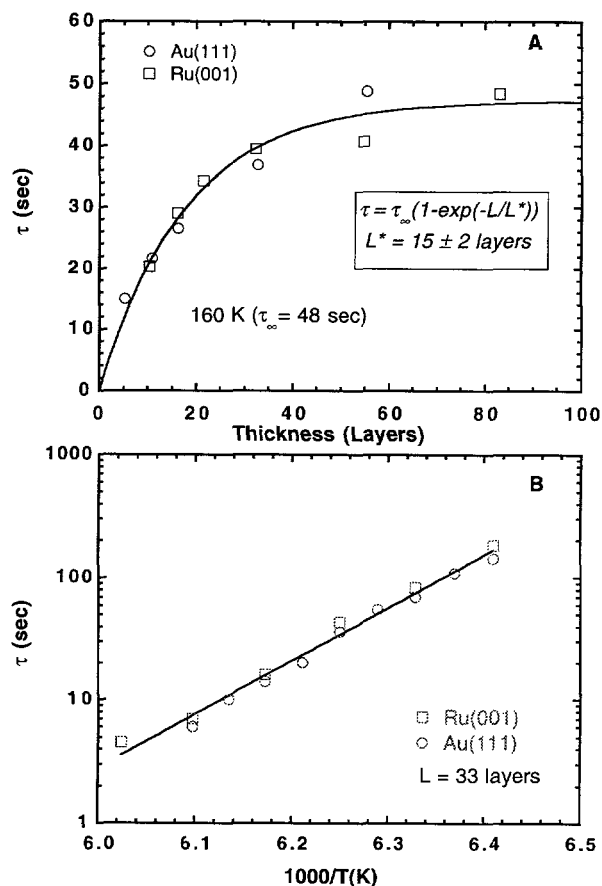


Figure 2.9. (A) The dependence of the crystallization time τ upon initial ice film thickness for D_2O films deposited on both Ru(001) and Au(111) substrates. The solid line is a fit to the equation $\tau = \tau_{\infty}(1 - \exp(-L/L^*))$, where τ_{∞} and L^* are fit parameters and L is the thickness in molecular layers. The same parameters describe the τ vs. thickness dependence for films grown on both Ru(001) and Au(111) substrates. The L^* parameter is related to the average distance between nucleation embryos, and corresponds to a distance of about 15 molecular layers ($\sim 50 \text{ \AA}$). (B) Arrhenius plot of τ versus substrate desorption temperature for 33-layer-thick films grown on Ru(001) and Au(111) substrates. The observed temperature dependence shows Arrhenius-like behavior with a substrate-independent apparent activation energy of 20 kcal/mole.

with these embryos located within the ice and independent of substrate.

The desorption time dependence can be simulated by a kinetic model that assumes the total desorp-

tion rate is the sum of the amorphous and crystalline desorption rates, weighted by their respective volume mole fractions. Because desorption occurs from the surface, this assumption means the surface mole fraction must equal the volume mole fraction. Such a situation can arise if the amorphous phase exhibits mobility on a length scale exceeding L^* during crystallization. Experimental evidence for such mobility was presented in the CS&D 1994 *Annual Report*. The crystallization kinetics are contained in the time-dependence of the crystalline mole fraction, which is best described using a classical nucleation and growth kinetic model. The time-dependence of the crystalline mole fraction is given by the Avrami equation,

$$\chi(t) = (1 - \exp((-kt)^n)),$$

where χ is the mole fraction, k is a phenomenological rate constant, and n is a parameter dependent on the nucleation and growth mechanism of the crystalline phase. The best fit to the experimental data yields $n = 4$, which corresponds to a spatially-random constant nucleation rate and spatially-isotropic 3-dimensional growth. The kinetic parameters are all obtained directly from the experimental data.

Figure 2.10 shows a comparison of the experimental results and the kinetic model for three different desorption temperatures. The total desorption rate and the component desorption rates from the amorphous and crystalline phases are displayed. The results indicate that the model accurately describes the time- and temperature-dependence of the crystallization and desorption kinetics. The simulation provides a clear explanation for the overall time dependence of the desorption rate. The initial rapid decay in the desorption rate is the result of the transformation of the amorphous phase into the crystalline phase. The autocatalytic crystallization kinetics are clearly evident from the time evolution of the crystalline component, and reflect the increasing crystalline grain surface area as a function of time. Fitting the experimental data to the kinetic model yields 16 kcal/mole for the apparent crystallization activation energy, which is consistent with a prior infrared spectroscopic study on hyperquenched glassy water. The simulations show the higher value of 20 kcal/mole obtained from Fig. 2.9B arises from partial crystallization that occurs during the temperature ramp up to the isothermal desorption temperature.

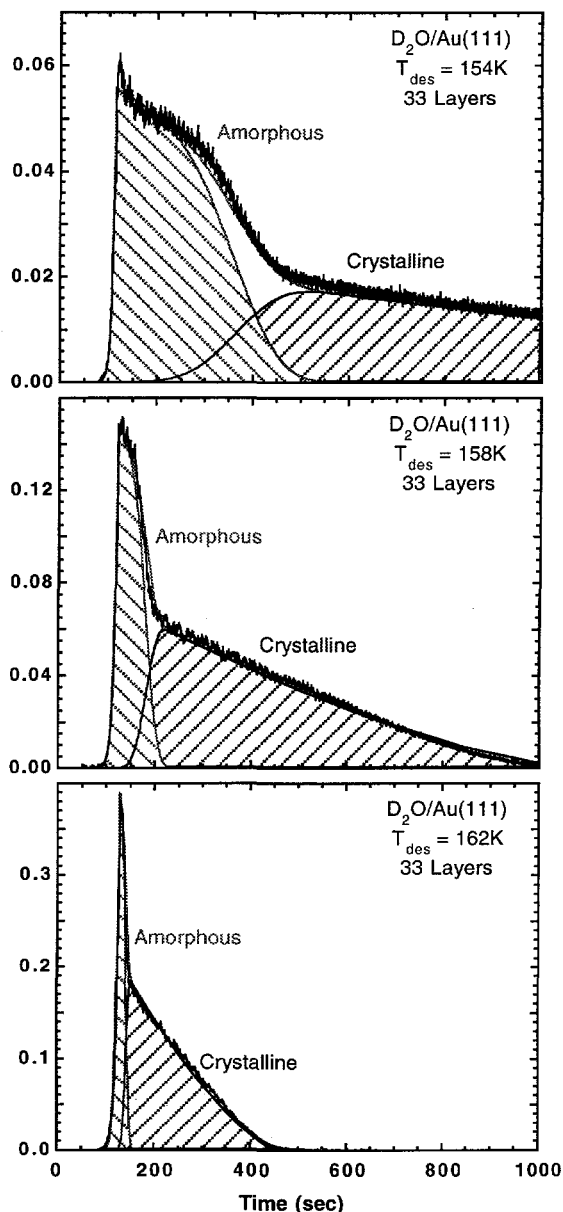


Figure 2.10. Comparison of the experimental isothermal desorption spectra with model simulations for various temperatures. The smooth line through the experimental data is the simulated total desorption rate. The contribution to the total rate from amorphous ice is shaded \\\ and from crystalline ice is shaded //. The decomposition of the total desorption rate into the amorphous and crystalline contributions clearly indicates the autocatalytic nature of the crystallization kinetics.

The crystallization kinetics are substrate-independent, and consistent with a random nucleation and isotropic growth model in which the mean distance between nucleation embryos, L^* , is about

50 Å. The substrate dependence of the desorption kinetics can be understood by considering the hydrophilic (Ru(001)) versus hydrophobic (Au(111)) nature of the substrate. The hydrophilic substrate yields smoother extended films, while the hydrophobic substrate yields 3-dimensional nanoclusters. The substrate-independence of the crystallization kinetics indicate that morphological differences responsible for the substrate-dependent desorption occur on length scales exceeding L^* , the mean distance between nucleation embryos. These findings reveal that interfacial ice-substrate interaction plays a critical role in determining the nanoscale morphology and macroscopic evaporation kinetics of ice films. These findings should have important applications in the diverse areas of astrophysics, atmospheric science, materials science, wetting phenomena, and the physics and chemistry of liquids.

Based upon the progress to date, we are now able to begin a detailed study of the interaction of various molecules with well-characterized ice substrates. Initial efforts will focus on the adsorption, desorption, and reaction kinetics of CH_3OH , NH_3 , and HCl with ultra-thin ice films. Concurrent with these studies of model hydrophilic interactions, we will continue to explore hydrophobic interactions by extending our studies of the interaction of chlorinated hydrocarbons with the ice substrates. After we demonstrate the utility of our approach to understanding solvation phenomena, we will extend the experiments to include quantum-resolved measurements of the nascent rovibrational distributions of the products which are scattered from the ice substrates. In related experiments, we will explore the applicability of using this *thin-film chemistry* to create chemically-tailored substrates that mimic the aqueous-mineral geochemical interface.

Chemisorption on Oxide Surfaces

M. J. Stirniman,* C. Huang,*

R. S. Smith, S. A. Joyce, and B. D. Kay

Supported by DOE Office of Basic Energy Sciences.

*Postdoctoral Research Associate.

We are examining chemical phenomena occurring at model oxide surfaces. Oxide interfaces are important in the subsurface environment. Specifically, molecular-level interactions at mineral surfaces are responsible for the transport and reactivity of subsurface contaminants at Hanford. Unfortunately, our molecular-level understanding of oxide surface chemistry is severely lacking. Initial experiments will focus on the dissociative chemisorption dynamics of halogenated hydrocarbons (e.g., CCl_4 , CHCl_3 , CH_2Cl_2 , CH_3Cl), H_2O , CH_3OH , NH_3 , and HCl on model oxide surfaces (e.g., MgO , SiO_2 , Al_2O_3). These studies will employ variable-energy supersonic molecular beams to determine energy-, angle-, and coverage-dependent trapping or dissociation probabilities. In addition to using bulk single-crystal samples, a variety of techniques, such as molecular beam epitaxy or chemical vapor deposition, will be explored to grow epitaxial thin oxide films on single-crystal metallic substrates. The successful synthesis of such crystalline thin oxide films will enable the entire arsenal of electron-based surface analytical techniques to be applied to the characterization of these nonconducting materials.

Magnesium oxide is often described as a model basic oxide, having a simple rocksalt structure, a single valence state, and only one stable low-index, {100}, surface orientation. As such, it is well-suited to fundamental studies of adsorption and catalysis at oxide surfaces. The interaction of water with the surface of MgO has itself been the subject of many recent investigations, both experimental and theoretical. Despite considerable efforts, several important issues remain unresolved experimentally. For example, the adsorption mechanism (Langmuirian versus precursor-mediated), the saturation coverage, the chemical nature of the adsorbate, and the desorption kinetics are presently not fully understood. Equally germane and quantitatively unresolved is the effect surface morphology has on these questions, specifically the role of 5-fold coordinate terrace sites versus lower-coordinate defects, such as

steps, kinks, vacancies, and adatom sites. At present the general consensus experimentally is that MgO adsorbs water dissociatively to form surface hydroxyl groups, and, theoretically, that dissociation occurs at select defect sites. However, the nature of the water-terrace interaction is less certain. This uncertainty is partly due to the use of a wide variety of MgO samples in the previous experimental studies: MgO smokes, powdered MgO, thin films of MgO grown on a variety of substrates, and single-crystal MgO subjected to various cleaning procedures, all of which make direct comparison of the previous results difficult.

The interaction of water with single-crystal MgO(100) was studied by employing a combination of molecular-beam reflection and temperature-programmed desorption (TPD) techniques. Surface contamination and long-range surface order were monitored with Auger electron spectroscopy (AES) and low-energy electron diffraction (LEED), respectively. Surface defects were systematically controlled by a combination of Ar⁺ sputtering and thermal annealing in O₂. Water, typically D₂O, was dosed from a triply-differentially-pumped, quasi-effusive molecular beam source. The angle-integrated incident, scattered, and desorbed water fluxes were monitored with a quadrupole mass spectrometer situated to avoid line-of-sight detection.

Apparent sticking coefficients as a function of surface coverage and temperature were determined using the beam reflectivity method of King and Wells, and are displayed in Fig. 2.11. The data clearly demonstrate that the adsorption kinetics on this surface are markedly non-Langmuirian. The apparent sticking coefficient remains near unity up to the temperature-dependent saturation coverage, consistent with precursor-mediated adsorption. At temperatures below 150 K, extended dosing results in the formation of a non-saturable multilayer ice film. Above 170 K, it is not possible to form multilayer ice with the beam fluxes employed. The maximum water coverage prior to the onset of ice formation is 1.3 ± 0.1 monolayers (ML), where we define 1 ML as the coverage necessary to occupy every surface unit cell on MgO(100) with a single water molecule ($1.13 \times 10^{15} \text{ cm}^{-2}$). At temperatures above 300 K, the apparent sticking coefficient is close to zero. However, it has been shown that an apparent sticking coefficient that decreases with increasing surface temperature can result from the competi-

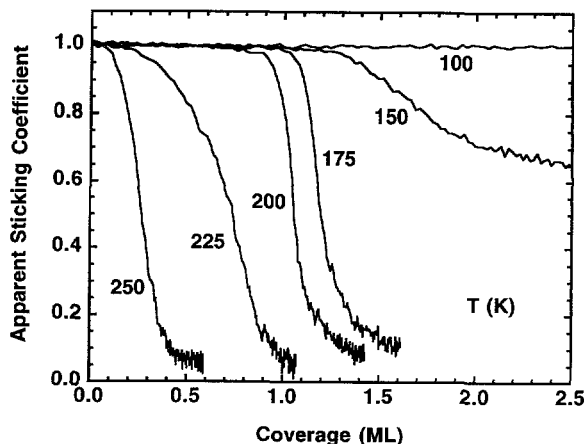


Figure 2.11. Apparent sticking coefficient versus coverage from beam reflectivity experiments on the sample that had been sputtered and annealed at 1100 K. The sample was dosed at each temperature for 60 seconds at a flux of ca. 6×10^{13} molecules/cm²/sec.

tion between adsorption and desorption, and we believe this to be the case in the present study. Note that at 175 K and above, the apparent sticking coefficients displayed in Fig. 2.11, while decreasing rapidly, do not go to zero. We believe this is due to the incipient stage of the hydration of bulk MgO (periclase) to form the thermodynamically-favored Mg(OH)₂ (brucite). We are currently engaged in an examination of this phenomenon, and our results will be presented in the 1996 *Annual Report*. Finally, we note that the adsorption behavior is qualitatively similar for both sputtered and unsputtered samples: i.e., precursor-mediated adsorption, maximum surface coverages of 1.3 ± 0.1 ML, and small, but non-zero (~ 0.07 at 250 K) apparent sticking coefficients after surface saturation.

The results of the TPD experiments are shown in Fig. 2.12. Figure 2.12 (top) shows the TPD of varying initial coverages of D₂O from the unsputtered surface. This surface was annealed in oxygen at 1100 K, contaminant-free (via AES), and exhibited a sharp (1×1) LEED pattern. The low-temperature desorption feature peaking near 160 K is due to the non-saturable adsorption of multilayer ice. The sharp, high-temperature feature near 235 K exhibits a peak whose temperature is nearly invariant with increasing initial coverage, and has a high-temperature tail that decays slowly with increasing temperature. This peak saturates

at a coverage of 1 ML ($\pm 10\%$). The broad feature between the multilayer and monolayer peaks has a saturable coverage of ~ 0.3 ML, and we postulate that it is due to a partial second layer adsorbed on top of the first monolayer. This intermediate layer could serve to bring the hexagonal multilayer ice into registry with the presumably square monolayer structure adsorbed directly on the oxide sur-

face. The TPD from a surface sputtered and then annealed at 600 K is shown in Fig. 2.12 (middle). While free from contamination, no LEED pattern was observed for this surface. The ice peak and the broad feature between 170 and 220 K are similar to the unspattered surface, but significant differences are apparent in the high-temperature feature. The sputtered sample exhibits a much broader high-temperature desorption, with a peak that shifts from 300 K to 240 K as the initial coverage is increased. This high-temperature feature also saturates at 1 ML ($\pm 10\%$), as in the unspattered sample, Fig. 2.12 (top). The sputtered sample was then annealed in oxygen at 1100 K, yielding a contaminant-free surface exhibiting a sharp (1×1) LEED pattern visually indistinguishable from that of the unspattered surface shown in Fig. 2.12 (top). The TPD for this surface is shown in Fig. 2.12 (bottom). The high-temperature feature appears to be essentially a linear combination of both the unspattered and sputtered surfaces. Again, this feature has a saturation coverage of 1 ML ($\pm 10\%$). Both the TPD and LEED features of this sample remained essentially unchanged with repeated and prolonged high-temperature annealing cycles. We also examined thin-film MgO grown on a hexagonal Ru(0001) substrate by codeposition of Mg and O₂ vapors. The TPD, although not shown here, were essentially identical to those displayed in Fig. 2.12 (middle).

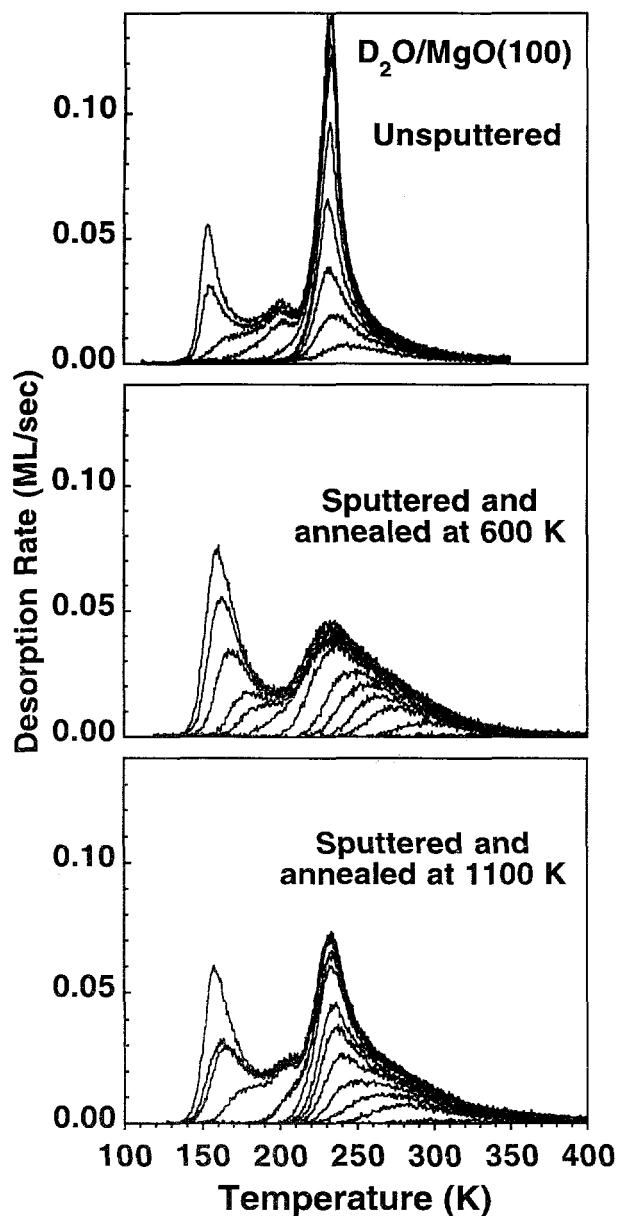


Figure 2.12. Desorption spectra of varying initial coverages of D₂O from Mg(100) for three different sample preparation procedures described in the text.

These TPD results show that the overall coverage of adsorbed water remains fairly constant as the concentration of surface defects is systematically varied. The line shape of the TPD spectrum and how the peak temperature shifts with increasing coverage are often used to infer the molecular nature of the adsorbate. TPD peaks yielding coverage-independent maxima are consistent with first-order kinetics, and suggest molecular adsorption. TPD peaks that shift to lower temperature with increasing coverage are often indicative of second-order kinetics, and are consistent with dissociative chemisorption. Based on these concepts, one could naively interpret the data presented in Figs. 2.12 as follows: water adsorption on the unspattered surface, Fig. 2.12 (top), is predominately molecular in nature, while sputtering produces a highly-defective surface upon which water is predominately dissociated. Simple kinetic analyses based on the Polanyi-Wigner equation and using first- and second-order kinetics with normal prefactors [10^{13} sec⁻¹ (1st order) and 10^{13} (ML-sec)⁻¹ (2nd order)], yield a

desorption activation energy of ~63 kJ/mole for both states. For all the surfaces described, the extent of isotopic exchange with the predominately Mg¹⁶O substrate was below the sensitivity limit of the experiment (less than 10% exchange), determined by exchange with the chamber walls. The lack of isotopic exchange is expected for molecular chemisorption, and further indicates that dissociative chemisorption, if present, produces oxygen-containing fragments chemically distinct from the lattice oxygen.

Although this interpretation is intuitively appealing, it is difficult to rationalize all of the data presented in Fig. 2.12 in this framework. Deconvolving the monolayer desorption feature into molecular and dissociated fractions yields dissociated fractions of ~0.25, 1.0, and 0.75 for the unsputtered, sputtered damaged, and thermally annealed surfaces displayed in Figs. 2.12, respectively. Such levels of defect mole fractions seem physically improbable, and are inconsistent with the sharp and visually indistinguishable LEED patterns observed for the unsputtered (Fig. 2.12 (top)) and thoroughly annealed sample (Fig. 2.12 (bottom)). Additionally, it is physically unpalatable to contemplate a fully defected surface as required to fit the data in Fig. 2.12 (middle). On the other hand, a strong kinetic coupling between the terrace, defect, and bulk hydroxide sites could cause the desorption kinetics to be very sensitive to a relatively small concentration of defects, provided the defects are the kinetic pathway leading to bulk hydroxylation. We are presently engaged in an investigation of the nature of the kinetic coupling between the various sites.

Scanning Tunneling Microscopy of Epitaxial Films

S. A. Joyce, J. P. Cowin,
M. S. Fyfield,* and M. C. Gallagher[†]

Supported by Laboratory Directed
Research and Development (LDRD),
and DOE Office of Basic Energy Sciences.

*Graduate student, Portland State University.

[†]Postdoctoral Research Associate.

The scanning tunneling microscope (STM) is capable of imaging solid surfaces and molecular adsorbates with atomic-scale resolution. As a real space probe, the STM can directly determine the role of surface structure, especially at defects such as steps, vacancies, etc., in the adsorption and heterogeneous chemistry of molecules on surfaces. Many surfaces of relevance to environmental chemistry are unsuitable for detailed studies due to the insulating nature of many materials; the lack of large, single-phase crystals; or difficulties associated with surface preparation. Our approach has been to use thin-film epitaxy to overcome these problems. In addition, thin films have the advantage that structures not stable in the bulk samples can be either kinetically or thermodynamically stabilized in thin films. We have previously studied the growth and structure of several oxide thin films, such as MgO on molybdenum and TiO on tungsten. The metal-oxide films were grown by vapor deposition of the metallic species either in an oxidizing ambient or by post-deposition oxidation. To gain a better understanding of these film growth processes, we have investigated the pure metal film system, specifically the growth of pure Mg metal on Mo(001).

The epitaxy of Mg, a hexagonal close-packed (hcp) metal in the bulk, onto a room-temperature body-centered cubic (bcc) Mo(001) substrate has been investigated by STM and low-energy electron diffraction (LEED). Growth initiates with the nucleation of two-dimensional Mg islands on the substrate terraces. Growth via island nucleation, as opposed to nucleation at substrate step edges, indicates that the diffusion of Mg on the molybdenum surface is relatively slow, i.e., Mg adatoms nucleate islands on the terraces before the individual adatoms can diffuse to the more highly-coordinated step edges. Following the completion of the initial layer, subsequent growth does proceed by nucleation at step edges (step flow), sug-

gesting that Mg adatom diffusion is faster on Mg-covered surfaces. Figure 2.13 shows an STM image of the 3.5-layer-thick film. The growth of new terraces from existing step edges is clear. Low-energy electron diffraction measurements show that the Mg film has adopted a square lattice with a primitive in-plane lattice constant a of ~ 3.2 Å. The strong interaction of the film with the underlying substrate has stabilized a pseudomorphic form with respect to the normally hexagonal symmetry of bulk Mg. The step heights in the film as measured by STM are 2.1 Å. This is in contrast to 1.6-Å steps in the underlying Mo substrate. This difference indicates that the Mg film has adopted a face-centered cubic (fcc) structure. Single atomic steps on bcc(100) surfaces are $a/2$, whereas for fcc(100) surfaces they are $\sqrt{2}a/2$. We believe the Mg films adopt a fcc lattice to maintain the bulk coordination number. Both fcc and hcp lattices are 12-fold coordinated; bcc lattices are only 8-fold coordinated.

Layer-by-layer growth persists up to 4 monolayers (ML), after which a transition to 3-dimensional island growth occurs. The island shape as observed by STM and the evolution of new diffraction features observed by LEED are consistent with the growth of 3-dimensional hexagonal structures. LEED measurements show the presence of two domains, rotated by 30 degrees. These

domains result from the two sets of inequivalent high-symmetry alignments of a hexagonal lattice on a square lattice. Above 12 equivalent layers of Mg, only the hexagonal symmetry is observed. Figure 2.14 shows an image of a thick Mg film. Highlighted in the image are emergent screw dislocations. Screw dislocations are extended bulk defects that intersect the surface and generate steps that emerge from an otherwise flat surface. In all cases, only two atomic-height steps emerge from the screws, allowing us to unambiguously determine the bulk structure for the thick films. From symmetry arguments, screw dislocations in a hcp material must result in steps in multiples of two atomic heights; fcc materials require steps in multiples of three atomic heights. The thick films are therefore hexagonal close-packed, as in bulk Mg.

The growth modes of magnesium on molybdenum surfaces can be explained in terms of the relative interactions of successive layers. Zhou and Cowin have previously shown in thermal desorption experiments that binding of Mg atoms to a molybdenum surface is nearly twice as strong as the interaction of magnesium with itself. This strong interfacial interaction leads to Mg adopting a cubic symmetry similar to the molybdenum, as well as a reduced mobility leading to 2-dimen-



Figure 2.13. A 900×900 -Å STM image of 3.5 layers of magnesium on Mo(001). Four step edges are seen running diagonally from the upper right to the lower left.

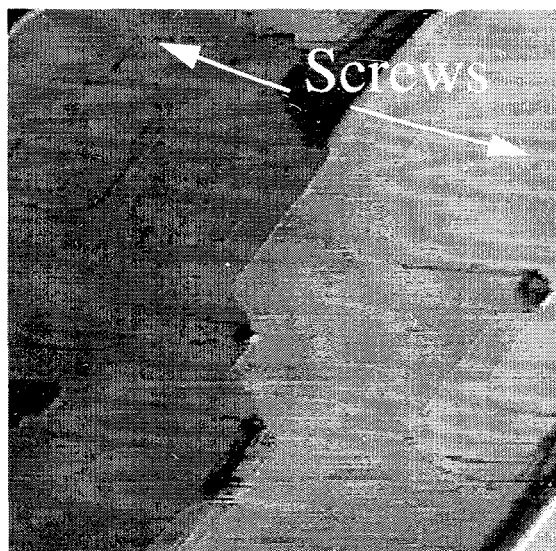


Figure 2.14. A 2000×2000 -Å STM image of 12 layers of magnesium on Mo(001). Note the 120° intersection of the step edges, as expected for a hexagonal lattice.

sional island growth in the first layer. For the next several layers, the interaction weakens to allow for more rapid diffusion and step-edge nucleation and growth. Above five layers, the Mg film converts to its bulk hcp structure.

Synthetic Ionic Interfaces via Ion-Beam and Ice Epitaxy

H. Wong,* G. B. Ellison,[†]

J. P. Cowin, and M. J. Iedema

Supported by DOE Office of Basic Energy Sciences.

*Postdoctoral Research Associate.

[†]Professor of Chemistry, University of Colorado.

The majority of contaminants at DOE sites are in ionic form, i.e., as "salts," and their transport in soils, separations from tanks, or remediation, involve ionic reactions at surfaces of minerals or other materials. An approach has been developed to recreate these interfaces under laboratory control, to elucidate reaction mechanisms. A very-low-energy ion beam, with high brightness, mass selection, and capability for both positive and negative molecular ions, has been built in collaboration with the University of Colorado. This, combined with ice-epitaxial methods now in wide use at PNNL, allows tailor-making water-solid interfaces with ions.

Ice interfaces have been demonstrated to be a good model for liquid water reactions, as most of the chemical interactions are much stronger than the melting/freezing energies of water, and transport is not a problem for the 10- to 1000-nm ice films used in these studies. The ion source must deliver 10 nA or more of ions at no more than a few eV of kinetic energy, to prevent high-energy damage to the ions or to the aqueous interface under construction. It must be mass-selected to pick out just the ions or isotopes desired for study. It must also supply important aqueous-type ions, such as hydronium (H_3O^+), ammonium (NH_4^+), simple metal ions such as cesium or sodium, anions like OH^- , Cl^- , OCl^- , HCO_3^- , NO_3^- , and similar ions with waters of hydration attached. The ion source was developed in collaboration with Professor G. B. Ellison of the University of Colorado. A Wein mass filter was coupled to a novel short

ion decelerator, and to a versatile supersonic jet electron-impact ion source, and provided with superb differential pumping. We have demonstrated hydronium and ammonium ions, and a similar source at the University of Colorado has produced bright molecular anion beams, including several of those previously listed.

Figure 2.15 shows the ion output at the sample at about 4 eV as the Wein mass filter selects ions produced for a pure D_2O feed gas. The 12 nA at D_3O^+ provides ample hydronium ions for study (isotopically labeled here), while OD^+ and D_2O^+ are important radical ions for reactive studies. Figure 2.16 shows the result of a test of delivering the very reactive radical ion D_2O^+ to a reactive, bare Pt surface. The solid curve gives the probability of the ion adsorbing intact instead of simply bouncing, and the dashed curve gives the probability of the ion dissociating on impact to eventually produce deuterium molecules. At 3 eV the probability of intact adsorption is 0.14, and the impact-induced damage is zero. By 10 eV, the ion intact adsorption probability drops dramatically, and damage (dissociation) commences. This simple demonstration shows that for controlled ion deposition, ion beams with at most a few eV of kinetic energy are crucial, and are delivered with this new apparatus.

The impact-induced dissociation of the water ion at the surface commencing above 10 eV is *not* accompanied by oxygen adsorption. We understand this in terms of an impulsive collision with the surface, whereby the oxygen atom bounces off

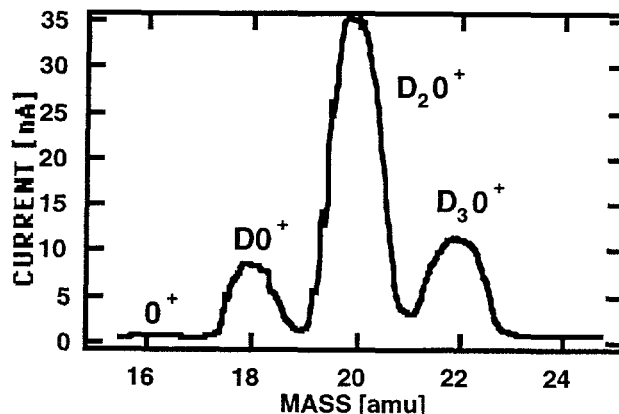


Figure 2.15. Sample ion-beam outputs of hydronium and radical ions.

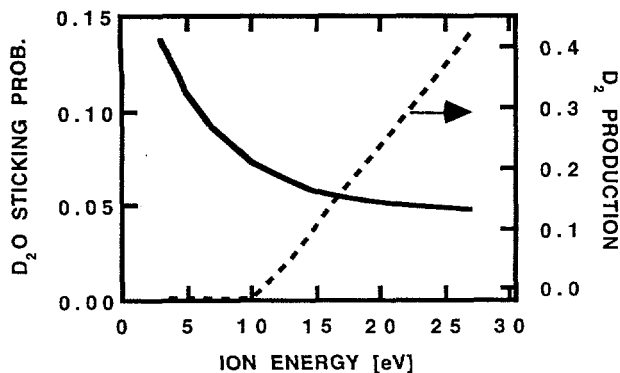


Figure 2.16. D_2O^+ deposition and D_2 production vs. beam energy.

the stiff Pt lattice with high probability, oblivious to the fate of the light deuteriums. Above 10 eV, enough internal energy is produced in the impulsive collision to break the deuterium-oxygen bonds and form new ones with the surface.

Studies in progress involve adding ions into and onto water ice films, to simulate the aqueous-ion interface. Projects include establishing absolute scales of surface acidity and potential, and studies of ion hydration and diffusion, using probes of contact potential, temperature-programmed desorption, and vibrational spectroscopy of adsorbed ions.

Bonding and Structure of Organic Ligands at Oxide/Water Interfaces

D. M. Friedrich, A. G. Joly, Z. Wang,
C. C. Ainsworth,† and P. L. Gassman†*

Supported by Laboratory Directed Research and Development (LDRD).

*Postdoctoral Research Associate.

†Earth Systems Sciences Department

The adsorption process for natural and anthropogenic organic ligands at the mineral-water interface is integral to many subsequent processes occurring in soil and subsurface environments, including contaminant transport, mineral formation and dissolution, and surface catalysis. Crucial to the influence of organic compound adsorption in these processes is the surface concentration of the adsorbed ligand and the molecular structure of

the surface species. The molecular structures of inner-sphere complexes have been correlated to ligand-enhanced rates of mineral dissolution.

Often, structures of surface complexes have been inferred from macroscopic adsorption and potentiometric titration data, and the application of surface complexation models that characterize the sorbate-sorbent interaction as the formation of inner- and outer-sphere complexes. Inner-sphere ligand-exchange complexes result from the formation of polar-covalent bonds between oxide surface metals, exchanging structural OH, and sorbate ligands, e.g., organic acids. The formation of an outer-sphere complex is considered to be a purely electrostatic interaction between sorbate and oppositely-charged surface groups. Typically, the sorbate and surface metal of such an outer-sphere, ion-associated surface complex are separated by one or more waters of hydration. The sorbate may also accumulate in the ion swarm of the double layer.

Predictive relationships arising from the application of surface complexation models result from hypothesized molecular surface structures whose sole criterion for accuracy is goodness-of-fit to macroscopic data (titration, pH-dependent adsorption envelopes, etc.). Under these conditions, modeling efforts are little more than exercises in curve fitting. Models with vastly different and contradictory molecular hypotheses describe sorption data equally well, and therefore cannot yield an unambiguous description of adsorption. Hence, the ability of a model to simulate such experimental data does not guarantee insight into the physical nature of the interfacial molecular structure of a sorbate. In order to better understand and simulate important aqueous-mineral interfacial phenomena, it is crucial to obtain spectroscopic data concerning speciation, structures, and dynamics of organic ligands at the aqueous-mineral interface under controlled conditions that are still relevant to the natural environment.

The current investigations are performed using sodium salicylate as the organic acid anion sorbate and colloidal alumina as the mineral interface. Salicylate was chosen because it is a fluorophore and is reported in the literature as a model compound for the study of organic ligand-surface speciation, bonding, and structure as a function of important geochemical variables (pH, ionic strength, surface loading). Alumina was chosen

because of its spectroscopically benign nature (IR and UV transmittance, weak Raman interference).

Fluorescence spectra of sodium salicylate is routinely measured in this study at levels of 10^{-8} M in 1 g/l alumina suspensions (70-nm particle size) using polarized UV laser excitation. At this low concentration, over 90% of the salicylate is sorbed to the alumina colloidal particles at a surface coverage of less than 2% of maximum (i.e., ~ 40 nm² per sorbed salicylate anion). Three types of surface complexes have been identified by fluorescence techniques: a bidentate ligand-exchange complex (the majority species), a monodentate ligand-exchange complex, and a small amount of ion-associated surface complex. Fluorescence polarization anisotropy demonstrates that all three types of surface complex are hindered from orientational diffusion.

Crucial to identifying these three surface complexes are (1) the assignment of the fluorescence band of free salicylate to emission from an excited-state intramolecular proton transfer (IPT) tautomer; (2) the recognition that the weak, temperature-dependent absorption band in the Stokes gap arises from a ground-state IPT tautomer; and (3) successful measurement of emission polarization anisotropy from turbid (light-scattering) suspensions. The majority species is a bidentate (ligand-exchanged) Al:salicylate complex (315 nm absorption). A somewhat smaller concentration of monodentate Al:salicylate complex at the surface (326 nm absorption) seems to have no intramolecular hydrogen bond (IHB) and spectroscopically resembles the ground-state IPT tautomer. Excited-state IPT (ESIPT) emission (415 nm) can occur only if the phenolic hydroxyl is protonated and H-bonded to the salicylate carboxyl group. In water the IHB is easily broken when the carboxylate negative charge is neutralized by binding to Al³⁺ cation. Therefore, the very small amount of polarized ESIPT emission seen in some suspensions is assigned to an ion-associated, outer-sphere complex that is structurally hindered from rotational diffusion on the time scale of fluorescence (4.5 ns). These results are the first direct spectroscopic evidence of an equilibrium between bidentate, monodentate, and outer-sphere alumina-salicylate complexes, and, for speciation studies, demonstrates the utility of combining polarized emission spectroscopy with knowledge of the photochemical properties of the organic ligand.

Time-resolved streak camera measurements of emission anisotropies of salicylate:alumina suspensions prove that sorbed salicylate ligands do not diffuse orientationally on the time scale of the fluorescence. Figure 2.17 illustrates how time-resolved anisotropy is used to distinguish free and sorbed salicylate. In suspensions containing $\leq 10^{-6}$ M total salicylate, no fast component of the anisotropy decay is observed, indicating that the majority of salicylate is bound to the alumina particles. This is consistent with radiolabel measurements that placed an upper limit on the concentration of free, solution-phase species of less than 10% of the 10^{-7} M total salicylate in suspension. Direct optical absorbance measurements indicate less than 2% of 10^{-6} M total salicylate is free.

A simple phenomenological model of extinction by light scattering was used to fit the decrease of fluorescence anisotropy with increasing suspension turbidity (Fig. 2.18). Small sample loadings of narrow size distribution (< 1 g/l) result in a small degree of depolarization caused by light scattering. This indicates that the measured anisotropies can be extrapolated to the zero-scattering limit, and can be interpreted in terms of sorbate/solute distribution and rotational mobility of sorbed species. From the low-scattering, upper-limit anisotropy of ~ 0.3 , we conclude that 95% of the excitation transition dipole moment is parallel to the molecular emission transition moment in the

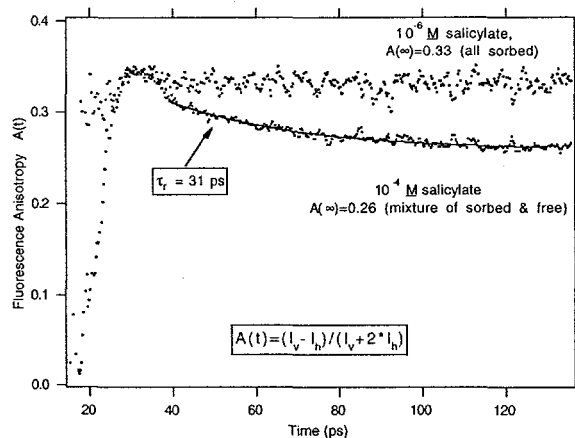


Figure 2.17. Decay of fluorescence anisotropy vs. time for aqueous suspensions consisting of 10^{-4} and 10^{-6} M sodium salicylate and 1 g/l alumina colloid (70-nm average diameter). At the higher concentration, the decay of anisotropy is due to rotational diffusion of the free salicylate fraction.

salicylate-alumina complex. This same relationship of transition moment directions is observed in free salicylate in rigid ethanol glass at 80 K, confirming that excitation and emission bands originate in the same electronic excited state ($S_1, \pi\pi^* \ ^1L_a$) in both the normal and proton-transferred tautomers of salicylate.

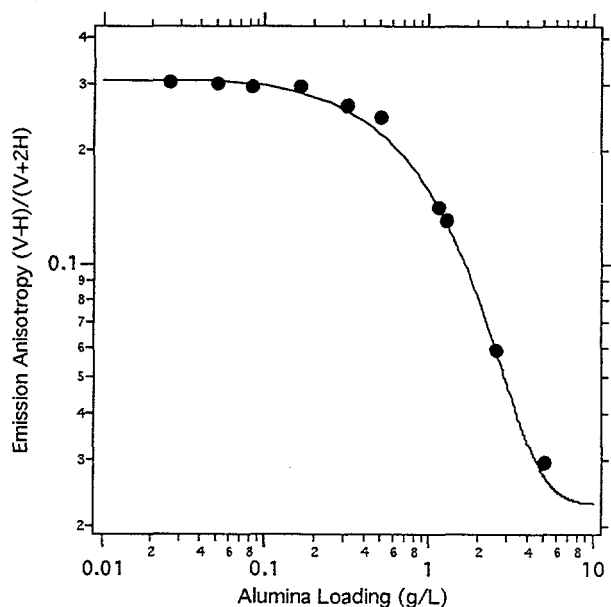


Figure 2.18. Effect of alumina suspension loading on observed emission polarization anisotropy. Observed anisotropy values (dots) are fit to a simple phenomenological scattering model (solid line) in which turbidity τ randomizes a fraction of the intrinsically polarized fluorescence components V_0 (vertical) and H_0 (horizontal).

$$V = V_0 \exp(-\tau) + k(V_0 + H_0)[1 - \exp(-\tau)]$$

$$H = H_0 \exp(-\tau) + k(V_0 + H_0)[1 - \exp(-\tau)]$$

For each polarization component, V and H , the randomization coefficient k (here 0.4) is the fraction of scattered light that exits the cell in the direction of the detector. The amount of undetected (lost) scattered light is $(1 - 2k)$.

Transport of Molecules Across Liquid Water/Vapor Interfaces Probed by Surface Nonlinear Optical Spectroscopy

R. Doolen,* J. M. Gaudioso,[†] and D. Ray

Supported by Laboratory Directed Research and Development (LDRD).

*Postdoctoral Research Associate.

[†]Science and Engineering Research Semester (SERS) student.

The goal of this project is the direct spectroscopic measurement of the thermochemistry and kinetics of mass transfer across liquid water/vapor interfaces. The detailed, molecular-level data obtained from these experiments, along with molecular-scale simulations performed by staff in the PNNL Theory, Modeling, and Simulation program, will provide improved understanding of the uptake of gases by aqueous solutions, and may provide an alternative method to measure mass accommodation coefficients of atmospherically-important species.

The basic experimental approach is to measure the orientation, the adsorption isotherm, and the solvation kinetics of selected adsorbates on liquid water surfaces by surface second-harmonic-generation spectroscopy, using a high-repetition-rate femtosecond laser and a photon counting detection system.

The measured adsorption isotherm for dimethyl sulfoxide (DMSO) on DMSO/water solutions is shown in Fig. 2.19. DMSO was selected for these experiments because it plays a significant role in tropospheric chemistry (DMSO is an intermediate in the oxidation of dimethyl sulfide to methanesulfonic acid and H_2SO_4),¹ and because accurate values for the mass accommodation coefficient² and Henry's Law constant³ of DMSO in water are available.

The measured adsorption isotherm can be fit to a Langmuir model, and a value of $-18(3)$ kJ/mol determined for ΔG_{ads}^0 at 298 K. This value, in conjunction with data obtained from the literature,^{2,3} provides the first complete set of thermodynamic data for the mechanism proposed for the uptake of nonreactive solutes by dilute aqueous solutions. A schematic potential energy surface, constructed from these thermodynamic data, describing the

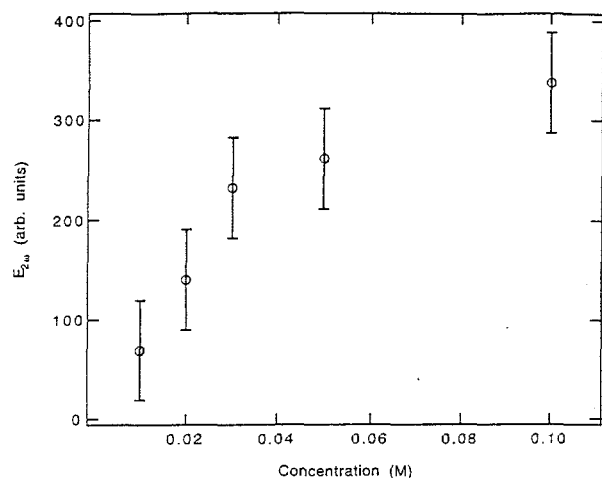


Figure 2.19. DMSO(aq) adsorption isotherm.

uptake of DMSO by aqueous solutions is shown in Fig. 2.20.

At equilibrium (e.g., in the closed static cell used in these experiments), the partitioning of DMSO between the gas phase, the liquid phase, and the liquid/vapor interface is completely determined by the solvation energy and the adsorption energy. The kinetics of the transport of DMSO across the liquid/vapor interface is currently under study. Additional interface-specific measurements are also in progress that will allow critical examination of models proposed for the uptake of gases by liquid surfaces.

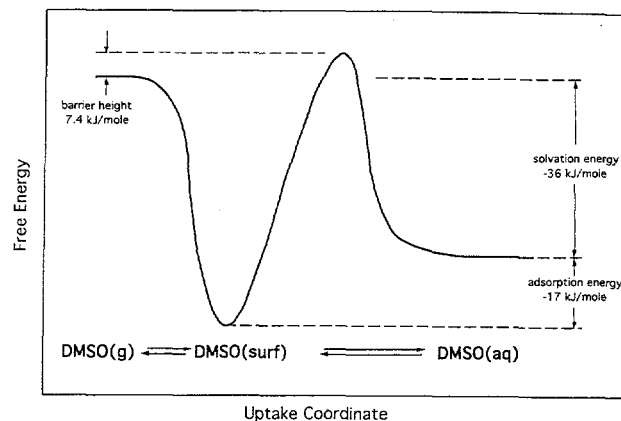
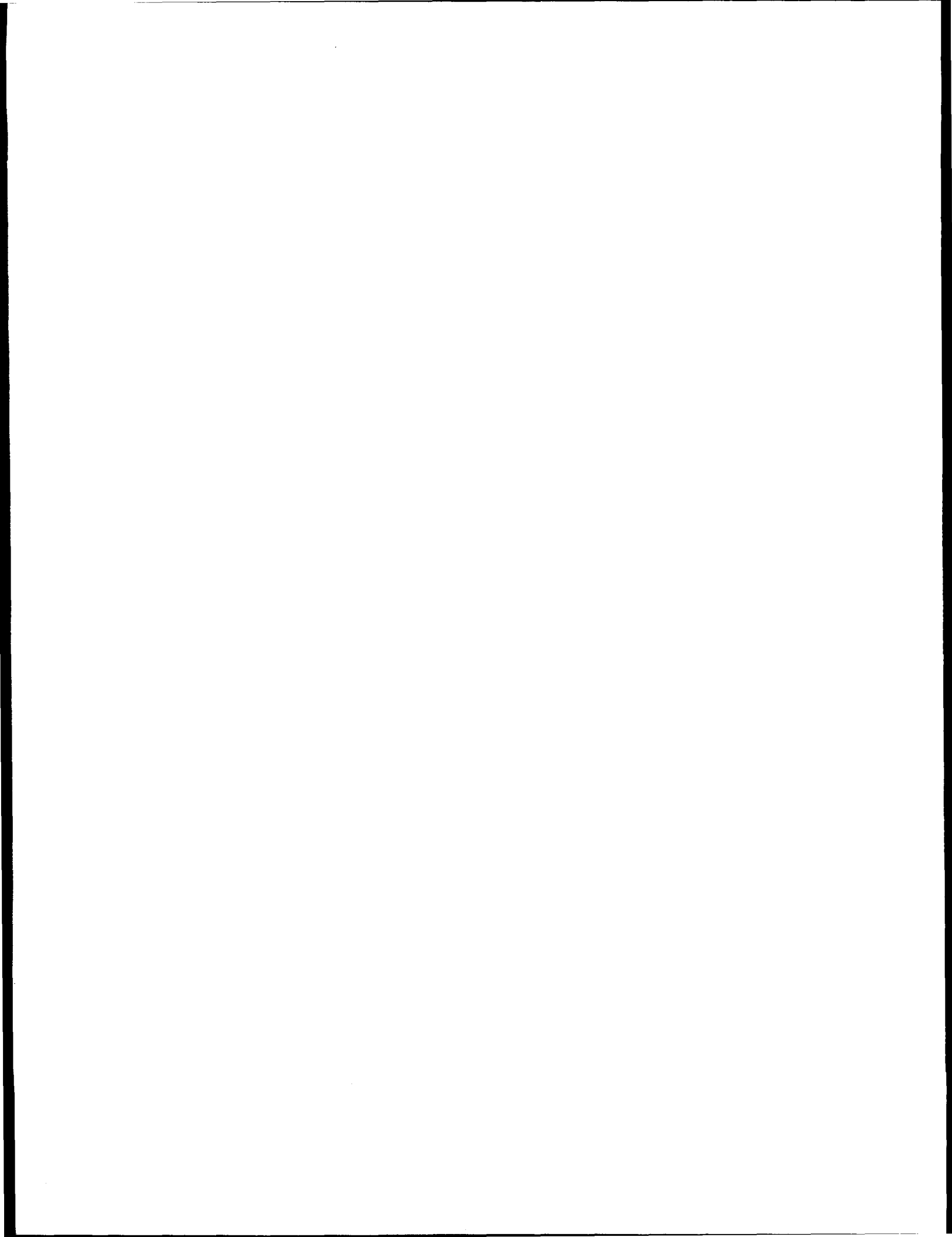


Figure 2.20. Schematic potential energy surface for the uptake of DMSO by liquid water.

References

1. F. Yin, D. Grosjean, and J. H. Seinfeld, "Photo-oxidation of dimethyl sulfide and dimethyl disulfide. I. Mechanism development," *J. Atmos. Chem.* **11**, 309-364 (1990); X. Lin and W. L. Chameides, "CCN formation from DMS oxidation without SO_2 acting as an intermediate," *Geophys. Res. Lett.* **20**, 579-582 (1993).
2. W. J. De Bruyn, J. A. Shorter, P. Davidovits, D. R. Worsnop, M. S. Zahniser, and C. E. Kolb, "Uptake of gas-phase sulfur species methane-sulfonic acid, dimethylsulfoxide, and dimethyl sulfone by aqueous surfaces," *J. Geophys. Res.* **99**, 16927-16932 (1994).
3. S. F. Watts and P. Brimblecombe, "The Henry's Law constant of dimethyl sulphoxide," *Environ. Tech. Lett.* **8**, 483-486 (1987).



3. Radiation and Other High-Energy Processes at Environmental Interfaces

Thermal Distributions Deduced from (2+1) REMPI of CO Products

K. M. Beck,* K. A. H. German,[†] and W. P. Hess

Supported by DOE Office of Basic Energy Sciences and the Strategic Environmental Research and Development Program.

*Associated Western Universities Senior Research Fellow.

[†]Postdoctoral Research Associate.

Pulsed laser irradiation of solid samples produces plumes of gaseous material suitable for mass or chemical analysis. The combination of laser ablation and mass spectrometry techniques (LAMS) offers a method by which solid micro-samples can be analyzed for elemental and chemical composition. Such techniques are being developed to characterize a variety of solid samples, including soil and hazardous mixed wastes. The LAMS analysis of mixed wastes (radionuclide/chemical mixtures) involving molecular ionic compounds requires a detailed knowledge of the desorption properties of these components.¹ Calcium carbonate (CaCO_3) is of particular interest because it is a major constituent of the earth's crust, often appears in routine soil sample analysis, and is a component in waste storage tanks at the Hanford site. In an attempt to develop LAMS as an analysis tool, we have initiated a study of pulsed ultraviolet (UV) laser desorption of carbon monoxide (CO) from the geologic calcite form of CaCO_3 .

A sensitive method utilized by numerous researchers for the detection of final product-state CO in photochemical processes is (2+1) resonance enhanced multiphoton ionization (REMPI).²⁻⁶ The (2+1) process involves two-photon excitation of the $\text{B}^1\Sigma \leftarrow \leftarrow \text{X}^1\Sigma$ transition followed by one-photon ionization from the B state to the ion ground electronic state. Subsequent profile-fitting of the rotational bandhead then affords insight into the product state distribution.

We have recently compared the CO $\text{B} \leftarrow \leftarrow \text{X}(0,0)$ Q-band spectra of neutral CO products desorbed

from CaCO_3 following pulsed UV excitation with those obtained from bulk CO under similar conditions. As a result of this investigation, we have concluded that fitting the unresolved Q-band from CO may lead to consistently spurious results with "hotter" temperatures $\Delta T > 60$ K assigned for product-state distributions. On the other hand, Doppler-limited spectra allow temperature assignments to within 10 K. This discrepancy may arise from line strength perturbation phenomena.

The experimental apparatus consists of an ultra-high vacuum (UHV) chamber (base pressure 10^{-10} Torr) equipped with a time-of-flight mass spectrometer. Geologic samples of calcium carbonate are cleaved and the resulting chips are mounted with spring clips on the vacuum manipulator. The CaCO_3 crystals are irradiated with 5-ns pulses of 193-nm excimer light, incident on the sample at 40° to the crystal face. The desorbed CO is then probed 4 mm above the crystal surface by a second, tunable laser delayed by ~ 15 μs from the excitation pulse.

We measure state population distributions using probe laser powers of < 35 $\mu\text{J}/\text{pulse}$ in a focused beam ($f = 20$ cm), or an estimated fluence of $< 3 \times 10^5$ W/cm^2 . To test the suitability of the 2+1 REMPI technique for determining product-state distributions, we obtained and analyzed REMPI spectra from gas-phase samples of room-temperature CO under chamber and probe laser conditions similar to those used for desorption studies of CaCO_3 .

Figure 3.1 displays the partially-resolved Q-band spectra for CO obtained following pulsed laser desorption from CaCO_3 . Although previously published spectra do not resolve and identify individual J -state transitions,²⁻⁷ the appearance of such structure is not unexpected because the difference between the X- and B-state rotational constant causes a splitting of Q-branch transitions that increases with J .⁸ This splitting is greater than the combined Doppler and laser bandwidths for $J > 7$ and approaches 1.0 cm^{-1} for $J = 20$. The unresolved spectra reported to date have been attributed to both the broad bandwidth of the excitation laser used in some studies, or, for the case of a relatively narrow-band excitation laser, to the lifetime broadening of the B state due to rapid ionization. As individual J -state transitions could not be resolved, fitting routines were developed to fit unresolved CO $\text{B} \leftarrow \leftarrow \text{X}$ Q-branch spectra to a

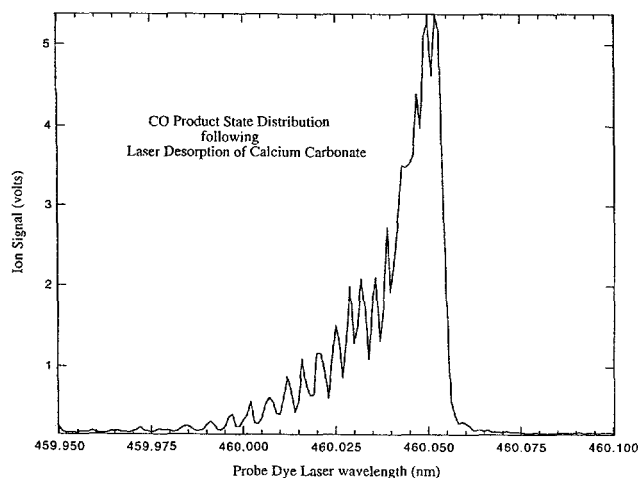


Figure 3.1. Partly-resolved Q-branch $B \leftarrow \leftarrow X$ spectrum of CO following laser desorption of freshly-cleaved CaCO_3 . The (2+1) REMPI scheme through the B-state covers a range of only 20 cm^{-1} . Wavelengths shown are of the dye fundamental, which is subsequently doubled to $\sim 230 \text{ nm}$. Laser power at 230 nm is 2.0 mW ; the background chamber pressure is $10\text{--}120 \text{ Torr}$ at 295 K . Note that a number of high-energy J -level transitions are completely resolved.

temperature, using line shape functions dominated by the laser bandwidth and line strengths based on the $(2J + 1)$ degeneracy.⁴ This method is still used today.⁷ Until now, no Doppler-limited and resolved spectrum of the Q-branch under UHV conditions has been available to explore the approximate nature of this approach. The spectra presented here are sufficiently well-resolved that such assumptions are not necessary, and individual rotational-state populations can be obtained directly for $J > 7$.

To aid the analysis of the CO product-state distributions, we obtained spectra of room-temperature (295 K) gas-phase CO samples at low pressure. We then fit the spectra using standard routines to determine the accuracy of the (2+1) REMPI approach. Figure 3.2 displays the Q-band spectrum of CO ($B^1\Sigma \leftarrow \leftarrow X^1\Sigma$) obtained using the relatively low laser power of 0.64 mW . Superimposed upon this scan is a simulated spectrum calculated up to the $J = 23$ level. At higher laser powers, we find that presence or lack of Q-branch structure in the room-temperature gas-phase samples is quite sensitive to laser fluence, and hence we have explicitly included a Lorentzian term in our simulation and fitting program to account for the inten-

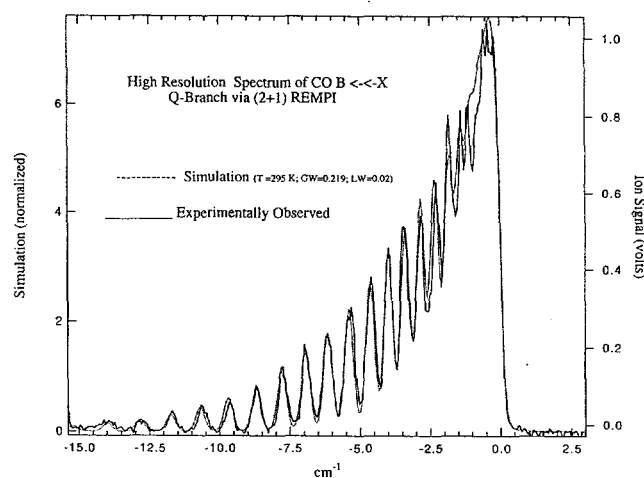


Figure 3.2. Doppler-limited CO spectrum at 10^{-8} Torr at 295 K . Dye laser power is 0.64 mW at 230 nm , with averaging of 10 shots/point at 20 Hz . The solid line is the recorded spectrum, with the simulated fit (dashed) superimposed. The plots are scaled against wavenumbers (0.0 cm^{-1} at $J = 0$). The beam width of the doubled dye laser is 0.085 cm^{-1} . The Gaussian full-width-half-maximum (FWHM) is 0.219 cm^{-1} under these conditions; the Lorentzian line width (a variable parameter) gives a best fit at 0.02 cm^{-1} . Higher-energy J levels are well-modeled, with some discrepancy occurring near the bandhead.

sity-dependent lifetime broadening. We fit the CO spectra without constraining the Voigt profiles generated from the measured laser bandwidth and Doppler components.

The parameters used to simulate the low-power spectra of Fig. 3.2 are a temperature of $T = 295 \text{ K}$, a two-photon bandwidth of 0.095 cm^{-1} , and a Doppler width of 0.20 cm^{-1} . The total Gaussian width (GW) is then 0.22 cm^{-1} , which is effectively Doppler-limited. The Lorentzian width of 0.02 cm^{-1} is consistent with the known lifetime of the B state, although it is negligible relative to the precision of the calculations. We consider the simulation in Fig. 3.2 to be a good fit to the spectrum; indeed, if this had been a CO product-state distribution, such fitting routines would have been serviceable enough to extract a rotational temperature, or to indicate the lack thereof. At the same time, we note that the simulation does not accurately model transitions nearer the bandhead. Specifically, the $J = 4\text{--}7$ peaks appear stronger than anticipated. Higher- J transitions appear to be much more

cleanly fit and in keeping with the degeneracy-based $(2J+1)$ -ordered transition strength.

Figure 3.3 displays the Q-band spectrum of the CO ($B^1\Sigma \leftarrow X^1\Sigma(0,0)$) transition obtained under the same chamber conditions as Fig. 3.2, but at a laser intensity of 10 mW ($\sim 5 \times 10^6$ W/cm²). This clearly exhibits the effects of power broadening on the unresolved bandhead region. Simulation of this spectrum requires a 10-fold increase in the Lorentzian linewidth, as expected for a shortened excited-state lifetime. Unexpectedly, a temperature of 295 K cannot be made to fit this feature under any Lorentzian linewidth variations. The best fit occurs with a 20% increase in this effective temperature ($T = 355$ K in Fig. 3.3). The greatest difficulty in fitting the unresolved spectrum appears in the vicinity of the $J = 4-7$ transitions. In producing unexpectedly large lifetime-broadened signals, they have dramatically pushed out the Q bandhead by a wavenumber or more.

Under these conditions, the ionization step is completely decoupled from the 2-photon process, and rotational transition strengths are unaffected by whether the ionization rate is greater than other

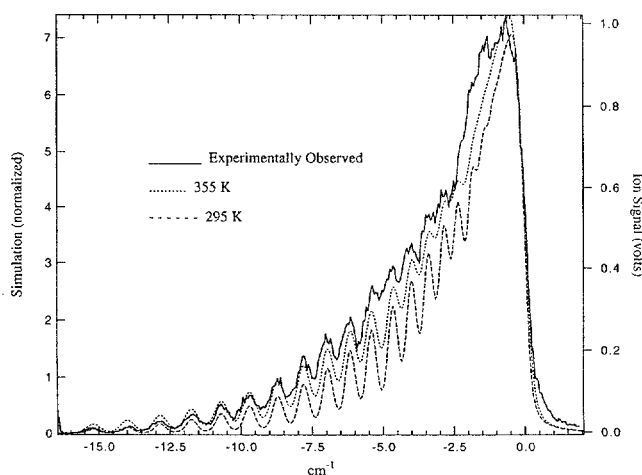


Figure 3.3. CO spectrum (solid line) recorded under chamber conditions identical to Fig. 3.2, except that laser power has been increased to 10.0 mW. Two simulations are shown, for temperatures of 295 K (short dashes) and 355 K (long dashes). The Lorentzian linewidth was 0.2 cm⁻¹ for both simulations (10 times that used in Fig. 3.2). Note the difficulty in fitting the bandhead region near $J = 4-7$. While the "fit" at $T = 355$ K is better, neither simulation gives the accuracy seen in Fig. 3.2.

B-state loss rates. Discrepancies between the simulation and the observed spectra must reflect subtleties in the 2-photon absorption transitions, and not statistics derived from kinetic decay processes.

Smyth *et al.*⁵ suggested that at 230 nm, the (2+1) REMPI technique utilizes a very non-resonant 2-photon absorption, which is dominated by molecular overlap integrals through the combination of at least two electronic states: $A^1\Pi$ and $C^1\Sigma^+$. Other intermediate states must be involved, such as $E^1\Pi$ and $I^1\Delta$, but also virtual vibrational (i.e., $\Delta v = \pm 1$) and rotational (i.e., $\Delta J = \pm 1, \pm 2$) levels within the initial and final states.

Halpern *et al.*⁹ deduced approximate equations to determine the relative importance of transition rates, K , for 2-photon absorption pathways in NO and CO with integrated band averages that can be related to measured and calculated band f numbers. Using their approach, we estimate that the contribution to the total 2-photon transition rate from the final-state rotational intermediates, for example, is on the same order as that for the electronic intermediate state $C^1\Sigma$. So, in part, these virtual rotational levels account for the impressive strength of Q-band transitions, which the very nonresonant electronic intermediates alone cannot explain.

Compounding this situation, perturbation involving the low-energy rotational transitions in the R and P branches give rise to line shifts and possibly abnormal lifetime broadening behavior. For the R branch of the $B - X(0,0)$ transition, the energy spacings of $J = 0$ and $J = 1$ are ~ 0.1 cm⁻¹ further apart than predicted, while those of $J = 3$ and $J = 4$ are ~ 0.1 cm⁻¹ closer together.¹⁰ This phenomenon also appears in the P branch with ~ 0.15 cm⁻¹ further separation than expected for $J = 1-3$ levels.

Within the Q branch, this pattern of 2-photon absorption and perturbation might appear as a weaker than $(2J + 1)$ transition strength for $J = 0-3$, and a stronger than $(2J + 1)$ transition strength for $J = 4-5$. This transition strength variation then obviously leads to an intensity-dependent perturbation of the spectra.

Despite taking full account of power broadening behavior, fitting the unresolved Q branch generally leads to higher temperature assignments at laser fluences greater than 10^6 W/cm². On the

other hand, Doppler-limited spectra of CO allow temperature assignments within 10 K. The precision of future LAMS microsample analysis will be favorably impacted by application of this rigor to desorption studies of CO chemical product.

References

1. R. A. Bradley, E. Lanzendorf, M. I. McCarthy, T. M. Orlando, and W. P. Hess, *J. Phys. Chem.* **99**, 11715–11721 (1995).
2. G. W. Loge, J. J. Tiee, and F. B. Wampler, *J. Chem. Phys.* **79**, 196–202 (1986).
3. L. F. DiMauro, *Chem. Phys. Lett.* **138**, 175–179 (1987).
4. T. A. Spiglanin, R. A. Perry, and D. W. Chandler, *J. Chem. Phys.* **87**, 1568–1576 (1987).
5. P. J. H. Tjossem and K. C. Smyth, *J. Chem. Phys.* **91**, 2041–2048 (1989).
6. J. P. Looney, J. E. Harrington, K. C. Smyth, T. R. O'Brien, and T. B. Lucatoro, *J. Vac. Sci. Technol. A* **11**, 3111–3120 (1993).
7. C. J. S. M. Simpson, P. T. Griffiths, R. L. Lovegrove, P. Matousek, and M. Towrie, *Chem. Phys. Lett.* **246**, 269–274 (1995).
8. K. P. Huber and G. Herzberg, *Constants of Diatomic Molecules* (Van Nostrand Reinhold, New York, 1979).
9. J. B. Halpern, H. Zacharias, and R. Wallenstein, *J. Mol. Spectrosc.* **79**, 1–30 (1980).
10. M. Eidelsberg, J.-Y. Roncin, A. LeFloch, F. Launay, C. Letzelter, and J. Rostas, *J. Mol. Spectrosc.* **121**, 309–336 (1987).

Mechanisms of Radiolytic Decomposition of Complex Nuclear Waste Forms

K. Knutsen,* K. A. German,*
Y. Su,* K. D. Keefer,[†] W. P. Hess,
and T. M. Orlando

Supported by Laboratory Directed Research and Development (LDRD).

* Postdoctoral Research Associate.

[†] Environmental Technology Division,
Tank Focus Area

Nuclear waste glasses are subject to large radiation doses due to the beta and gamma decay of the embedded ¹³⁷Cs and ⁹⁰Sr. For a glass containing 1.25 weight percent ¹³⁷Cs, the energy released is on the order of 20 W/l, which translates to a self-dose rate of approximately 800 rad/s or about 10¹⁰ rad/year. This large rate of irradiation could produce a significant steady-state concentration of highly-reactive, albeit short-lived, species that could react with water, air, or container materials, during waste processing and waste storage. Though there seem to be no official long-term performance criteria established for glass waste forms, fundamental research on the mechanisms of radiolytic degradation of complex nuclear waste is clearly needed to insure this storage option is implemented in a safe manner. Glass compositions containing relatively large loadings of Na and borosilicates have been proposed as final waste forms, and immobilization via the use of phosphate glasses is currently under consideration.

We have conducted a series of experiments designed specifically to probe the effects of radiation- and ionization-driven chemistry on/in composite solids (i.e., ionic materials, glasses, and ceramics). Our current emphasis is on understanding the underlying physical and chemical mechanisms responsible for radiation-induced damage and loss of composite integrity. It is known that damage from beta (β) and gamma (γ) radiation occurs via ionization-driven events and not displacement-driven processes typically observed during neutron irradiation.^{1,2} In fact, the damage caused by high-energy electrons (Compton electrons), X rays, and gamma rays results from both the primary particle and the copious number of low-energy (1–100 eV) second-

dary electrons. We note that the primary electron energy-loss mechanisms involve inelastic scattering and coupling to the electron density (i.e., the electronic bands) of the amorphous target materials. Therefore, we determine which electronic excitations are involved in surface degradation via detailed quantum-state-resolved electron-stimulated desorption (ESD) studies and atomic-force surface microscopy (AFM) of nominally pristine and irradiated glasses.

In the ESD studies, we monitor cation, anion, and neutral desorption yields and velocity distributions as a function of incident electron energy. These experiments point to the importance of Auger-stimulated processes³⁻⁷ in electron-stimulated degradation, and show that damage cross-sections can be quite high. For example, we have demonstrated large electron-induced degradation cross sections ($\sim 10^{-15}$ – 10^{-16} cm²) in NaNO₃, a wide-band-gap material typically found in Hanford wastes.^{4,5} The degradation involves primarily dissociation of the nitrate group via intermolecular Auger decay of Na excitons or holes in the Na 2*p* band. Intramolecular Auger decay of holes in the nitrate valence band, shallow valence excitations, and dissociative electron attachment processes also result in efficient destruction of the nitrate group. These energetic processes lead to efficient energy localization at the interface/surface, and are expected to contribute significantly to surface degradation. In the case of adsorbate-covered surfaces, which are typical of interfaces in waste containment environments, nonthermal reactions will occur in the overlayer. These reactions can easily produce some of the hazardous byproducts typically observed in underground waste storage tanks.

Although we expect smaller damage cross-sections (10^{-18} – 10^{-20} cm²) for the radiolytic degradation of soda glasses, iron phosphate glasses, and silicotitanates, we fully expect the general mechanisms to be similar to those leading to the degradation of ionic materials such as NaNO₃. It has been pointed out that material susceptibility to radiation-induced degradation scales with the strength of the effective hole correlation energies.³ Thus, damage cross-sections are expected to decrease as one progresses from salts → glasses → ceramics. We have begun quantitative studies of these electron-induced damage trends. Because it is likely the glasses used for the storage or immobilization of wastes will contain high concentra-

tions of Na, we have begun studies on low-flux, low-energy (5–500 eV) electron-beam-induced damage of glasses that contain varying amounts of Na. Previous work has shown that dominant thresholds for the desorption of Na⁺, Si⁺, and O⁺ from soda glass occurred near the Si 2*p* band.⁶ This clearly indicates that damage involves Auger decay, probably from the O 2*p* band. Note that Auger decay leads to a reversal of the attractive Madelung potential, and efficient expulsion of charged species. This is very similar to the well-known Knotek-Feibelman mechanism⁷ which was developed to explain the ESD of cations from full-valency compounds, such as TiO₂. We are currently measuring the thresholds and quantum state-distributions of the O(³P_{2,1,0}) and O(¹D) fragments using laser resonance-enhanced multiphoton ionization spectroscopy. It is relevant to note that these are very reactive species that can contribute significantly to corrosion of surrounding wall materials.

Surface damage induced by irradiating a 5×5×5-mm sample of soda glass (20% Na) with a 3-keV electron beam has been studied using AFM. The clean, unirradiated sample surfaces were imaged in room air, and the images indicated the surfaces were fairly smooth with several 200-nm-high columns. The sample was then placed in a high-vacuum chamber and irradiated with a low-flux 3-keV electron beam for approximately 10 minutes. The resulting surface damage was then probed in air by AFM. The AFM image clearly shows that surface damage was rather severe. Pits, craters, and canyons several microns deep were obvious. Stress release and damage were observed several minutes after irradiation, which suggests the buildup of charge, exciton transport, and possibly some local heating. These preliminary results clearly indicate that soda glass is susceptible to electron-induced degradation. The details of the damage mechanisms are systematically evaluated as a function of the amount of Na present. Damage cross sections will be reported and the question of the stability of glass over time scales necessary for long-term storage of nuclear wastes will be addressed.

References

1. J. F. DeNatale and D. G. Howitt, "A mechanism for radiation damage of silicate glasses," *Nucl. Instr. and Meth.* **B1**, 489 (1984).

2. W. J. Weber, "The effect of radiation on nuclear waste forms," *J. Min. Metals Mat. Soc.* **43**, 35 (1991).
3. B. I. Dunlap, F. L. Hutson, and D. E. Ramaker, "Auger lineshapes of solid surfaces—atomic, bandlike, or something else?" *J. Vac. Sci. Tech. A* **18**, 556 (1981).
4. K. Knutsen and T. M. Orlando, "Low-energy (5–80 eV) electron-stimulated desorption of H⁺, (D⁺), OH⁺ (OD⁺), O⁺, and NO⁺ from solution-grown NaNO₃ crystals," *Surf. Sci.* **348**, 143 (1996).
5. K. Knutsen, G. A. Kimmel, and T. M. Orlando, "A state-resolved study of low-energy (5–120 eV) electron-stimulated degradation of NaNO₃ crystals," to be submitted, *Phys. Rev. B*.
6. Y. X. Wang, F. Ohuchi, and P. H. Holloway, "Mechanisms of electron-stimulated desorption of soda silica glass surfaces," *J. Vac. Sci. Tech. A2*, 732 (1984).
7. M. Knotek and P. Feibelman, *Phys. Rev. Lett.* **40**, 964 (1978).

Low-Temperature Plasma Processing of Chlorinated Hydrocarbons

R. G. Tonkyn, S. E. Barlow,
and T. M. Orlando

Supported by Laboratory Directed Research and Development (LDRD).

Over the past several years, workers at PNNL have demonstrated the utility of atmospheric-pressure packed-bed corona reactors in the treatment of gaseous waste streams containing ≤ 1000 ppm of various contaminants. A main goal of this LDRD project was to improve our understanding of various fundamental chemical and physical processes important in low-temperature plasma destruction. Such an understanding is critical to improving the efficiency of the process technologies in a time- and cost-effective manner. We have therefore developed an atmospheric-pressure sampling mass spectrometer that was used to study the PNNL-designed dielectric-barrier packed-bed corona reactor. In particular, we have studied how the efficiency depends upon various parameters, such as carrier gas composition, humidity, packing material, input power, etc. We

directly monitor in real time the gas delivered to and coming from the reactor, as well as the power input to the reactor. We provide enough control to present reproducible measurements that can be reliably compared with other work both at PNNL and elsewhere. Our investigations have given us insight into the characteristics of these types of reactors, chemical mechanisms in the discharge, information vital to accurate modeling of the discharge, and the scaling parameters.

We have developed a phenomenological model that incorporates the known, broad features of discharge chemistry. This model provides a consistent way of reporting results, and also allows us to express destruction efficiencies in universal terms that can be quantitatively compared to competing technologies.

The model led to experiments yielding the first measurements of electron (and by extension) ion densities in the discharge. (Standard techniques of plasma diagnostics are not suitable here.) We find the mean electron density averaged over the length of the discharge tube and over many cycles of the discharge (at 60 Hz) is $\sim 2\text{--}10 \times 10^6 \text{ cm}^{-3}$. Estimating the electron energy ~ 3 eV, we find the Debye shielding length to be on the order of 1 mm, meaning the concentration of charged species is too low to provide effective shielding anywhere in the system. These results also place limits on the extent that ion- (or electron-)molecule chemistry plays in the observed chemistry.

Experiments with pure N₂ as the carrier gas allowed us to investigate the role of the surface oxide as a possible *chemical* catalyst. We studied several packing materials such as glass, Cr₂O₃, ZrO₂, etc., and did not observe incorporation of surface oxygen into the gas-phase products. However, other quasi- or non-traditional catalytic effects, e.g., enhanced secondary electron emission, may be important.

We have investigated a test matrix by examining the destruction of trichloroethylene (TCE) and carbon tetrachloride (CCl₄) as functions of power, flow rate, carrier gas composition, humidity and packing material.¹ Figure 3.4 shows a portion of the results for TCE, and Fig. 3.5 shows similar results for CCl₄. Several trends are apparent from these figures: notably, TCE is far easier to destroy than CCl₄. The rate of CCl₄ loss is proportional to

the electron density, while TCE can be attacked by a variety of ions and radicals.

Reference

1. R. G. Tonkyn, S. E. Barlow, and T. M. Orlando, "Destruction of CCl_4 in a dielectric barrier/packed bed corona reactor," *J. Appl. Phys.*, accepted.

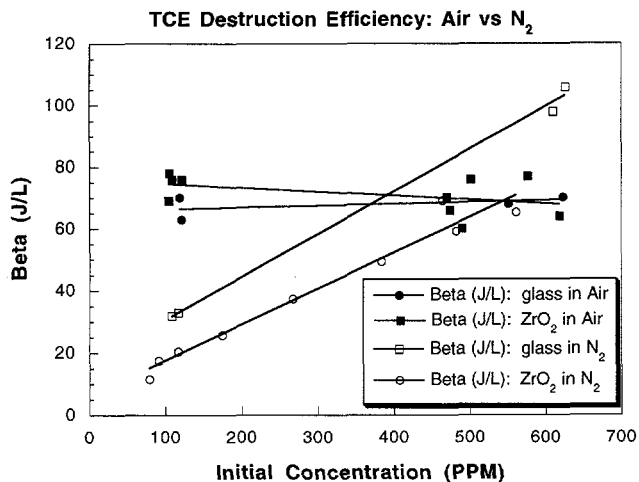


Figure 3.4. Destruction efficiency of trichloroethylene (TCE) under various conditions; β is the energy per liter required to reduce a concentration to $1/e$ of its initial value.

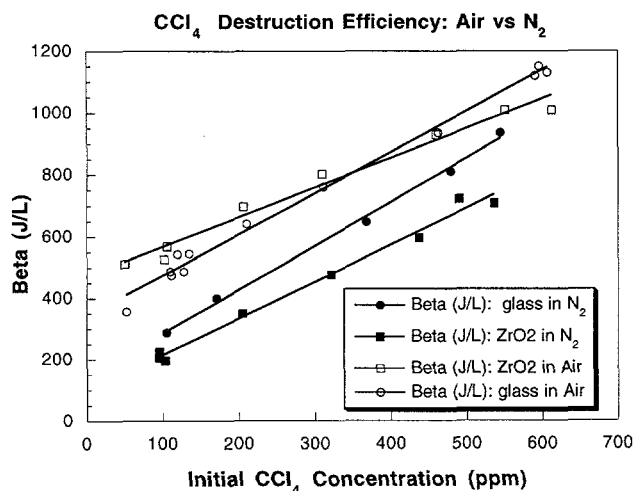


Figure 3.5. Destruction of carbon tetrachloride (CCl_4) under various conditions; β is the energy per liter required to reduce a concentration to $1/e$ of its initial value.

Irradiation of Condensed-Phase Acetyl Chloride

B. Rowland* and W. P. Hess

Supported by DOE Office of Basic Energy Sciences.

*Postdoctoral Research Associate.

The release of chlorinated hydrocarbons into the environment is a potential threat to terrestrial ecosystems and ground water supplies.¹ Chlorocompounds are present in the Hanford-site defense waste and in the soil subsurface, so energetic processes in chlorine-containing compounds impact the storage and processing of mixed waste and the disposition of contaminated soils. We have studied the photodissociation of acetyl chloride molecules within a molecular beam,^{2,3} and found that gas-phase photodissociation is described by sequential reactions



The initial step, following ultraviolet (UV) excitation, produces chlorine atoms with a near unity quantum yield (1). The present study of UV-irradiated condensed-phase amorphous and crystalline acetyl chloride samples extends the previous gas-phase work, and is more closely related to condensed-phase processes occurring in mixed-waste storage tanks.

Although few studies report the condensed-phase photochemistry of acetyl chloride, Kogure *et al.* have studied UV photolysis of matrix-isolated acetyl chloride molecules.⁴ Their results show the photolysis products are ketene and HCl molecules in a 1:1 dimer complex. The reason given for complex formation is that the chlorine radical, which is formed upon photolysis, cannot diffuse through the argon matrix, and therefore reacts with the geminate acetyl radical to produce the ketene+HCl complex.⁴ No concerted elimination reaction channel is proposed. In a related study, the dimer complex of ketene and HBr molecules was studied by *ab initio* calculations.⁵ The theoretical results showed that the elimination reaction of acetyl bromide to produce ketene and HBr is endothermic, with an enthalpy of 21.3 kcal/mol and an activation energy of 93.4 kcal/mol.⁵ Here we study the reactions of thin films of amorphous and crystalline acetyl chloride by Fourier transform infrared (FTIR) analysis of the trapped pho-

toproducts that are formed following UV irradiation.

Samples of acetyl chloride are deposited on an IR-transparent substrate held at 20 K by a closed-cycle cryocooler, to a thickness of $\sim 4 \mu\text{m}$ within an ultra-high vacuum chamber. Amorphous samples are prepared by warming the freshly-deposited films to 100 K for 5 minutes (creating an amorphous sample of high density), and then cooling to 10 K. Crystalline samples are prepared by warming films to 100 K for ~ 1 hour and then recooling to 10 K. The longer warming period completely anneals the amorphous film.

Crystallization of acetyl chloride is monitored by FTIR spectroscopy. Figure 3.6 displays the IR spectra of amorphous and crystalline acetyl chloride samples. The IR bands of the crystalline sample are much sharper than the amorphous sample. The full-width-half-maximum of all the IR bands decreases by a average factor of ~ 2 , and distinct doublets are observed for several IR bands. The relative IR peak heights also change drastically. Following the creation of crystalline and amorphous films, we irradiate the sample using the 4th harmonic of a Nd:YAG laser at 266 nm, collecting infrared spectra before and after irradiation.

By subtracting an IR spectrum of an irradiated sample from the spectrum of a non-irradiated

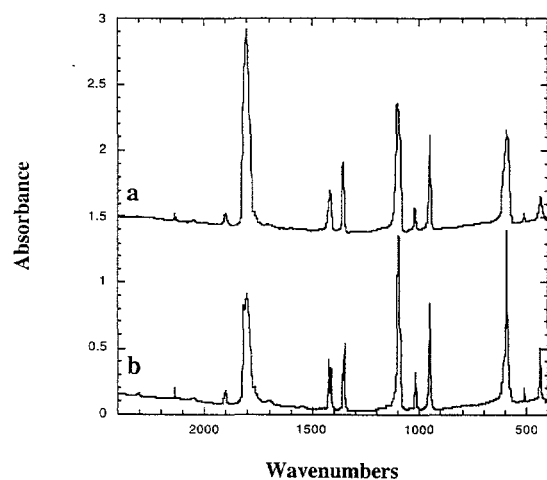


Figure 3.6. The IR spectra of amorphous (a) and crystalline (b) acetyl chloride samples. The IR bands of the crystalline spectrum are much sharper than bands in the amorphous spectrum, and splitting can be observed in some of the higher-frequency bands.

sample, the reaction products that are formed by irradiation are exposed in the resulting difference spectra. An example of a difference spectrum is shown in Fig. 3.7. The HCl and ketene products are readily identified by the strong IR bands in the $\sim 2750\text{--}2350 \text{ cm}^{-1}$ and 2130 cm^{-1} regions of the difference spectrum. Other positive IR bands displayed in Fig. 3.7 are attributed to the vibrational modes of ketene. The negative IR bands are attributed to the vibrational modes of unperturbed acetyl chloride molecules, and the positive IR bands that are not assigned to the vibrational modes of HCl or ketene are attributed to the red-shifted IR bands of acetyl chloride. The red shift of the vibrational modes of perturbed acetyl chloride molecules is caused by intermolecular coupling of acetyl chloride with neighboring ketene+HCl complexes.

The formation of the ketene+HCl complex from a parent acetyl chloride molecule is produced exclusively by an elimination reaction. We observe no evidence for intermolecular reaction channels, i.e., no irradiation products other than the ketene+HCl complexes are observed in the difference spectra. In addition, secondary products, which could be attributed to the reaction of UV-irradiated ketene molecules with HCl molecules, are not observed in our FTIR analysis of irradiated amorphous and crystalline samples.

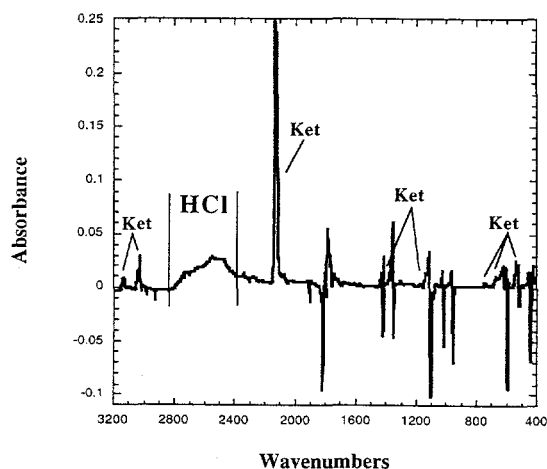


Figure 3.7. The difference spectrum of an irradiated crystalline acetyl chloride sample. The positive IR bands that are attributed to vibrational modes of ketene and HCl are marked. Negative bands are due to the loss of acetyl chloride.

The IR bands associated with HCl and ketene disappear as the temperature of the sample is increased. Because the irradiated spectra approach the pre-irradiation spectra upon warming, we conclude that acetyl chloride molecules are reformed upon warming irradiated samples. Figure 3.8 displays the loss of the IR band intensities of the complex as an amorphous sample is heated from 10 K to 90 K. The reverse reaction of the ketene+HCl complexes to produce acetyl chloride molecules is also observed in the difference spectra of a crystalline sample. These observations are supported by the thermodynamics: the elimination reaction of acetyl chloride molecules to form ketene+HCl complexes is endothermic.

We are currently studying the intermolecular interactions within the ketene+HCl complex by FTIR observations and *ab initio* calculations. Kinetic information and the activation energy of the reverse reaction are being derived from time- and temperature-dependent spectra. The crystallization activation energy of acetyl chloride will also be obtained.

References

1. U. S. Congress, Office of Technology Assessment, *Complex Cleanup: The Environmental Legacy of Nuclear Weapons Production, OTA-O-484* (U. S. Government Printing Office, Washington, DC, 1991), p. 150.
2. S. Deshmukh and W. P. Hess, *J. Chem. Phys.*

100, 6429 (1994).

3. S. Deshmukh, J. D. Myers, S. Xantheas, and W. P. Hess, *J. Phys. Chem.* **98**, 12535 (1994).
4. N. Kogure, T. Ono, and F. Watari, *J. Mol. Struct.* **296**, 1 (1993).
5. Y. Su, T. S. Dibble, J. S. Francisco, and Z. Li, *Chem. Phys.* **196**, 59 (1995).

Electron- and Photon-Stimulated Surface/Interface Chemistry

T. M. Orlando, R. G. Tonkyn,
G. A. Kimmel,* and K. Knutsen*

Supported by Office of Basic Energy Sciences.
*Postdoctoral Research Associate.

1. Low-Energy Electron-Stimulated Reactions in Amorphous Ice

The formation of negative-ion resonances during scattering of low-energy electrons with atoms, molecules, surfaces, and interfaces is a process of fundamental importance in physics, materials science, chemistry, and radiation biology. In general, electron collisions with isolated molecules lead to negative-ion resonances via either dipole scattering, single-electron shape resonances, or multi-electron core-excited resonances. The core-excited resonances generally consist of an excess electron temporarily bound by attractive interactions with the excited (typically Rydberg) target molecule. These negative-ion resonances, which are generally 2-electron, 1-hole configurations (Feshbach or core-excited shape resonances), decay primarily via dissociative electron attachment (DEA) or electron autodetachment. The DEA process for simple diatomic or small polyatomic species consists of resonant electron capture into a relatively short-lived ($\sim 10^{-14}$ sec) anion state that is dissociative in the Frank-Condon region. Because DEA leads to the production of both anion and neutral fragments, DEA is typically studied by measuring anion fragment yields as a function of incident electron energy (E_i). Resonances that decay via electron autodetachment produce excited (rotational, vibrational, and electronic) neutral states and are therefore often observed as intermediates in high-resolution, electron-energy loss and electron-transmission spectroscopy. Though extensive information concerning gas-phase shape

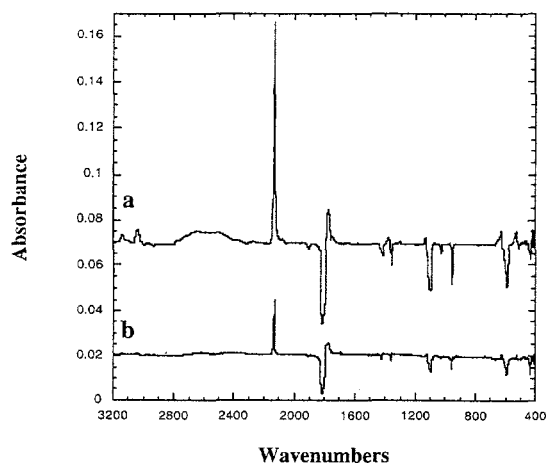


Figure 3.8. The difference spectra of an irradiated amorphous acetyl chloride film at 10 K (a) and 90 K (b). The intensity of the strong positive IR band of ketene at 2130 cm^{-1} decreases by a factor of 4.

resonances exists, there is much less information on the formation and dissociation of negative-ion resonances in the condensed phase or at surfaces and interfaces.

We have studied core-excited negative-ion resonances in thin films of ice by time-of-flight (TOF) laser resonance-enhanced multiphoton ionization (REMPI) detection of the $D_2(^1\Sigma_g^+)$ desorbates produced during low-energy (5–50 eV) electron-beam irradiation of amorphous ice (Fig. 3.9). The REMPI detection scheme allows us to monitor the vibrational and rotational states of the departing D_2 reaction product as a function of incident electron energy (E_i). Structure in the D_2 yield is observed for incident electron energies 8–16 eV and $18 < E_i < 32$ eV. We attribute this structure to 1-hole, 2-electron, core-excited shape resonances. The low-energy structure is assigned to excitation of the $3a_1$ and $1b_2$ bands, whereas the higher-energy feature is associated with excitation of the $2a_1$ level. These resonances, or the excited states produced after electron autodetachment, decay via molecular elimination to yield $D_2(^1\Sigma_g^+)$ directly. D_2 is observed with $v = 0, 2$ and *not* $v = 1$, suggesting a symmetry propensity in the excited-state production probability and decay dynamics.

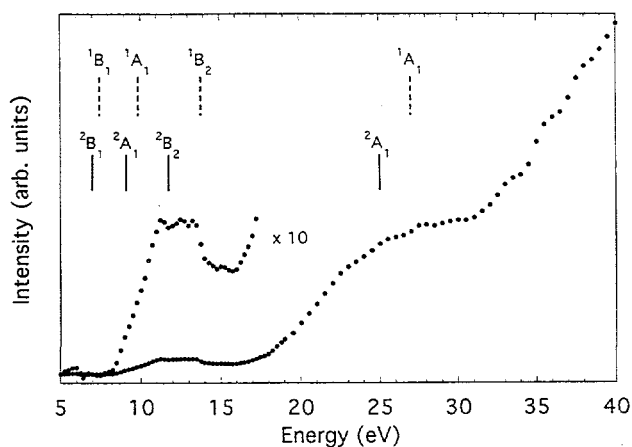


Figure 3.9. The $D_2(^1\Sigma_g^+, v = 0, J = 0)$ yield from a 100-Å film of D_2O ice as a function of incident electron energy. Note the structure between 8–16 eV and 18–32 eV. The assignments indicated by dotted lines represent the known gas-phase Rydberg transitions. The assignments shown by solid lines represent the positions of condensed-phase dissociative electron-attachment resonances.

The onset of ionization of condensed water is believed to be at ~ 6.5 eV. We have determined that the excitons, which are energetically near the bottom of the conduction band, either autoionize or dissociate to yield $H(^2S) + OH(X,^2\Pi)$ or $H_2(^1\Sigma_g^+) + O(^3P,^1D)$. The threshold for exciton production is 6.5 ± 0.3 eV, and the state distributions of the dissociation products indicate the exciton has triplet and singlet character.¹ We have therefore begun studies to optically pump the $1b_2 \rightarrow 3s:4a_1$ transition directly with vacuum ultraviolet (VUV) photons. We generate VUV photons via nonlinear third harmonic generation in rare gas mixtures. Measurements of dissociation yields and product state distributions resulting from direct *photoexcitation* of this exciton are currently underway.

2. Production of $O(^3P_j)$ and $NO(X^2\Pi)$ from Low-Energy (5–100 eV) Electron Impact on Solution-Grown $NaNO_3$ Single Crystals

Neutral products of the low-energy (5–100 eV) electron-stimulated degradation of solution-grown $NaNO_3$ single crystals are identified via quadrupole and laser resonance enhanced multiphoton ionization (REMPI) spectroscopy. The yields, threshold energies, velocity distributions, and internal-state distributions are determined for the $O(^3P_j)$ and $NO(X^2\Pi_{3/2,1/2})$ products that result directly from electron impact. Other neutrals detected include O_2 and NO_2 . These products are primarily produced from recombination of O atoms with O and NO. This work complements our earlier study² of the ionic products of electron-stimulated degradation of $NaNO_3$, and provides an important step in establishing the role of radiolysis of $NaNO_3$ in the production of N_2O in the Hanford mixed (radioactive/chemical) waste tanks.

The $NaNO_3$ crystal is heated to 423 K to maintain the surface stoichiometry and prevent charging during electron irradiation. A pulsed electron beam of well-defined energy strikes the $NaNO_3$ surface, releasing a plume of neutral products into the ultra-high-vacuum chamber. A few millimeters from the surface, a UV laser pulse crosses the plume, selectively ionizing the neutrals via resonance-enhanced multi-photon ionization. The resulting ions are then detected with a time-of-flight mass spectrometer.

The electron energy thresholds for O and NO production are both at ~ 8 eV. This energy corre-

sponds to a charge-transfer band in NaNO_3 . Removal of an electron from the NO_3^- valence band to the $3s$ orbital of Na^+ results in the production of NO_3^* , which then dissociates to the neutral products detected. The increase in the O and NO yields at ~ 15 eV corresponds to ionization of the $4a_1'$ level in NO_3^* , but is also approximately the energy at which 2-hole states in the valence band can form. The velocity distributions of both $\text{O}(^3\text{P}_j)$ and $\text{NO}(^2\Pi)$ correspond well to Maxwell-Boltzmann distributions at 423 K, so both of these products are translationally thermalized to the NaNO_3 surface temperature. The other J states of O, however, have non-thermal components, and the J -state distribution of $\text{O}(^3\text{P}_j)$ is 5:2:1 for $J = 2, 1, 0$, respectively. This is somewhat hotter than the thermal (423 K) distribution of 5:1.75:0.46. The NO product appears to be rotationally thermalized to the surface temperature, but is vibrationally very hot, with vibrational bands detected out to $v = 5$.

This experiment confirms that large amounts of O and NO are produced directly by low-energy electron impact on NaNO_3 . Gas-phase reactions of NO with H atoms and organic radicals are known to produce HNO. Although ion yields from ESD of NaNO_3 are two to three orders of magnitude smaller than neutral yields, NO^+ reacts at near the collision rate to produce HNO as well. In turn, HNO reacts with HNO to produce N_2O . Thus, radiolysis of NaNO_3 produces reactive radicals and ions that can react with organics at the solid/liquid interface to produce a precursor to N_2O . Future experiments involving electron-beam irradiation of NaNO_3 /organic interfaces will determine the importance of this interfacial radiolysis to N_2O production in the waste tanks.

3. Photo-Induced Dissociation of NaNO_3
Interfaces: Production of $\text{O}(^3\text{P}_j)$,
 $\text{O}(^1\text{D})$, and $\text{NO}(^2\Pi)$ at 193 nm

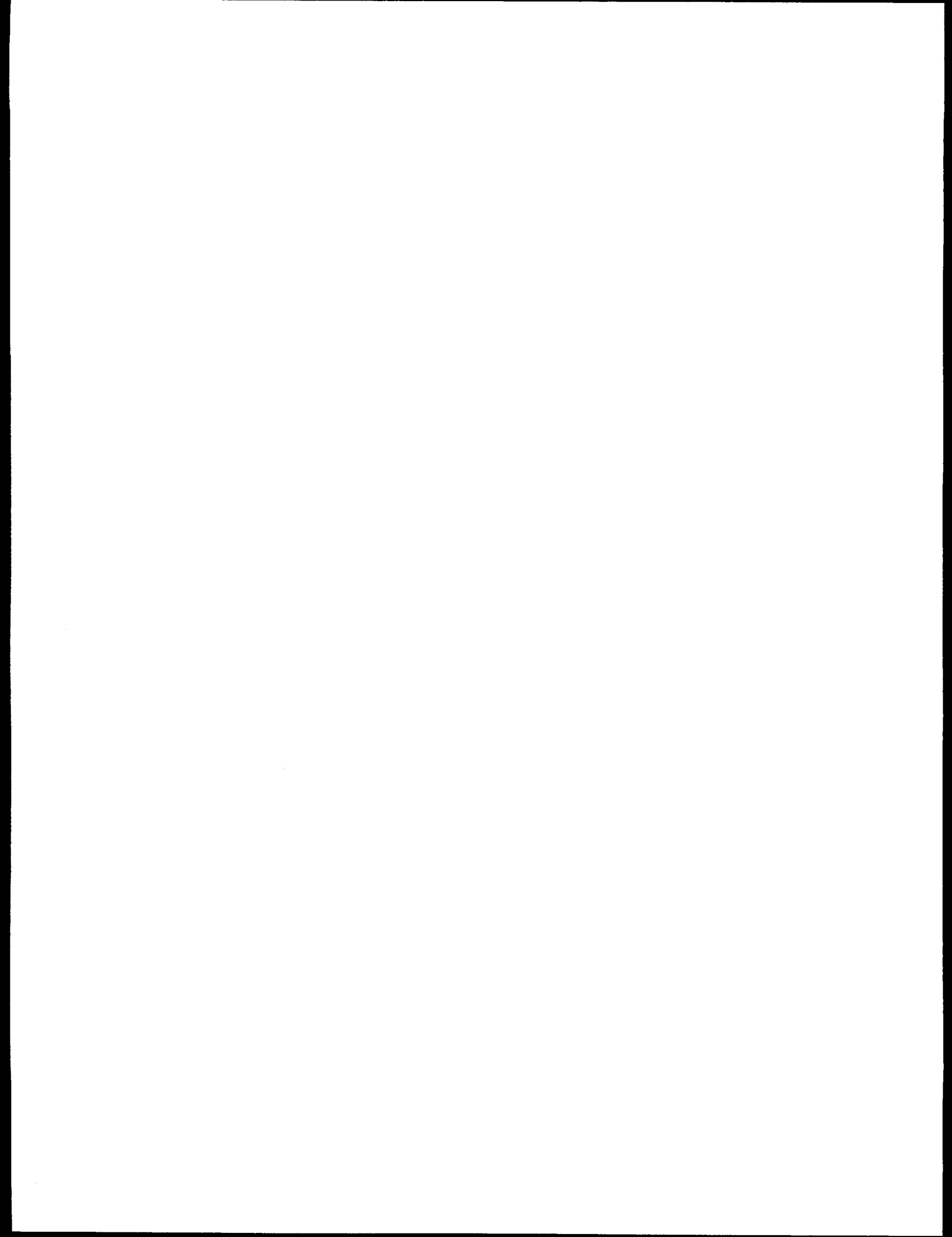
The laser-induced degradation of solution-grown NaNO_3 single crystals is studied at 193 nm. The

yields, velocity distributions, and 193-nm laser power dependence of the O and NO products of photon impact are measured via REMPI and time-of-flight mass spectrometry. The J -state distributions of the $\text{O}(^3\text{P}_j)$ are measured at the peak of the O velocity distribution.

The velocity distributions for the $\text{O}(^3\text{P}_j)$ and NO products again agree well with a 423-K Maxwell-Boltzmann distribution, which shows that the neutral fragments are translationally thermalized to the NaNO_3 surface temperature. In addition, at the peak of the velocity distribution, the O atom J -state populations are also thermalized. $\text{O}(^1\text{D})$ is a minor product, and appears to be translationally hot, suggesting that it is produced with little or no interaction with the NaNO_3 surface. The $\text{O}(^3\text{P}_j)$ and NO signals show a linear (1-photon) dependence upon the 193-nm laser power, at laser powers between 0.3 and $16 \mu\text{J}/\text{cm}^2$. This result is many orders of magnitude less than previous reported studies³ on laser ablation of NaNO_3 , and suggests that degradation involves a self-trapped exciton. Self-trapped excitons are well-known to cause desorption in alkali-halide systems, and the mechanisms leading to desorption in more complex molecular crystals seem to be quite similar. The extremely low fluence supports the notion of dissociation (desorption) by exciton decay, as the yield is expected to depend on energy density with no observable threshold.

References

1. G. A. Kimmel and T. M. Orlando, *Phys. Rev. Lett.* **75**, 2606 (1995).
2. K. Knutsen and T. M. Orlando, *Surf. Sci.* **348**, 143 (1996).
3. R. L. Web, S. C. Langford, and J. T. Dickinson, *Nucl. Inst. Methods Phys. Res. B* **103**, 297 (1995).



4. Cluster Models of the Condensed Phase

Cluster Model Studies of the Structure and Bonding of Environmentally-Important Materials

L. S. Wang, J. B. Nicholas,*
S. D. Colson, and S. R. Desai†

Supported by DOE Office of Basic Energy Sciences.

*Theory, Modeling and Simulation.

†Postdoctoral Research Associate.

Oxides of Si, Al, Mg, and Ti are predominant components of the earth and are important environmental materials. Their surface chemistries play important roles in the storage and underground transport of wastes. At EMSL, a major effort is being directed to understanding their surface and interface properties. We have begun to study the structure and bonding of these oxide clusters with a combined experimental and theoretical approach using anion photoelectron spectroscopy (PES) and quantum calculations. The smaller, controlled sizes of these cluster systems provide atomic-level models to better understand the bulk surfaces and defect sites, and are also an excellent testing ground to validate theories that are intended for large and real-world systems.

A magnetic-bottle time-of-flight PES spectrometer with a laser vaporization cluster source has been used for these studies. This apparatus has a mass resolution ($M/\Delta M$) of about 500 and an electron energy resolution of better than 30 meV at 1 eV kinetic energy, making it a powerful apparatus for the study of clusters. Several initial experiments have been completed on small silicon oxide clusters, germanium oxide clusters, and aluminum oxide clusters. Preliminary studies on titanium clusters have also been performed.

1. A Photoelectron Spectroscopic Study of Small Silicon Oxide Clusters: SiO_2^- , Si_2O_3^- , and Si_2O_4^-

We obtained the photoelectron spectra of SiO_2^- , Si_2O_3^- , and Si_2O_4^- anion clusters at 4.66-eV photon energy. All the spectra show broad photodetachment features, suggesting considerable geometry

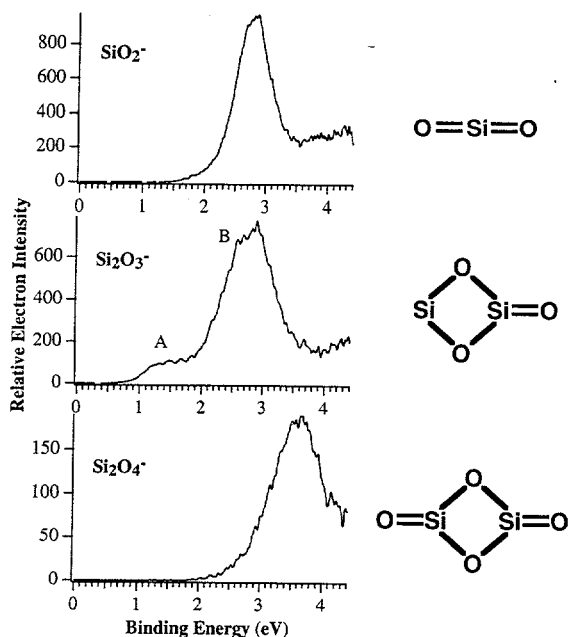


Figure 4.1. Photoelectron spectra of SiO_2^- , Si_2O_3^- , and Si_2O_4^- , at 266-nm photon energy. The neutral cluster structures are also shown.

change between the anion and the neutral. The vertical detachment energies are 2.76(10), 2.75(10), and 3.63(10) eV for SiO_2^- , Si_2O_3^- , and Si_2O_4^- , respectively (Fig. 4.1). The spectrum of Si_2O_3^- shows a weak feature at lower binding energy, suggesting existence of another isomer. The spectra of GeO_2^- and Ge_2O_3^- were also obtained and compared to the silicon analogs. They are similar to the silicon oxide species, but both have higher detachment energies, 2.93(7) for GeO_2^- and 3.01(7) for Ge_2O_3^- . The Ge_2O_3^- spectrum is consistent with only one isomer. The structure and bonding information for these small oxide clusters have been obtained.

2. Vibrationally-Resolved Photoelectron Spectroscopy of AlO^- and AlO_2^-

Vibrationally-resolved photoelectron spectra of AlO^- and AlO_2^- have been obtained at two photon energies, 3.49 and 4.66 eV (Fig. 4.2). Both the ground and first excited states are observed for AlO . The spectrum of AlO_2^- can be obtained only at the higher photon energy due to the high electron affinity (EA) of AlO_2 . The electron affinities of AlO and AlO_2 are 2.60(1) and 4.23(1) eV, respectively. The rather high EAs for both molecules are consistent with the fact that AlO^- and AlO_2^- anions are closed-shell, isoelectronic with SiO and SiO_2 , respectively. The vibrational frequency of the

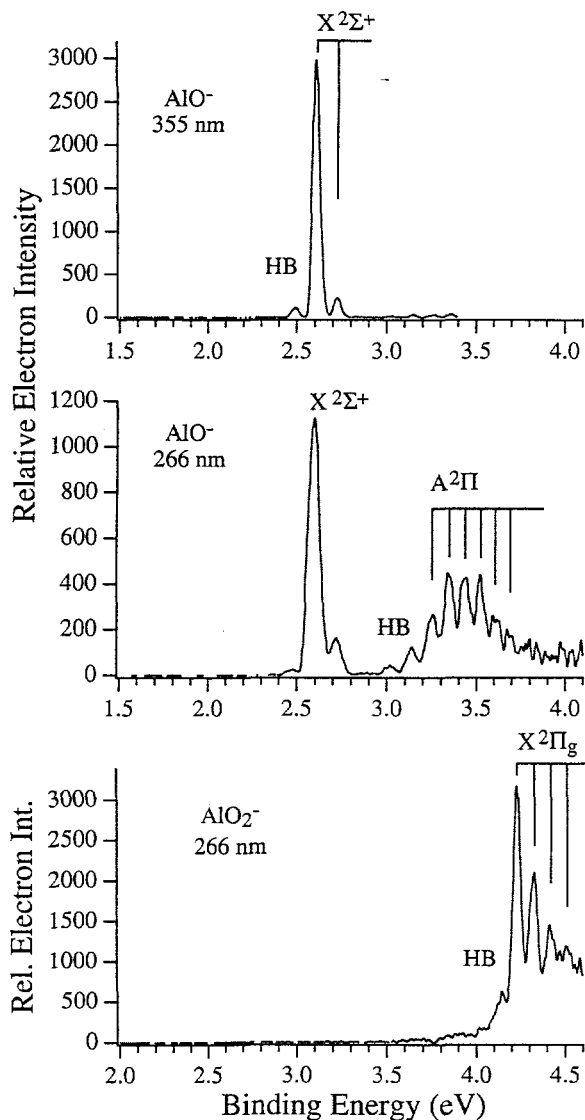


Figure 4.2. Vibrationally-resolved photoelectron spectra of AlO^- and AlO_2^- . Vibrational features are indicated by the vertical lines. HB stands for hot-band transitions.

AlO^- anion is $900(50) \text{ cm}^{-1}$. The vibrational frequencies and excitation energy obtained for AlO agree with previous optical measurements. The totally-symmetric vibrational frequency is $750(40) \text{ cm}^{-1}$ for AlO_2 and $680(60) \text{ cm}^{-1}$ for AlO_2^- . We conclude the AlO_2 molecule, as well as AlO_2^- , have linear O-Al-O structures.

3. Small Silicon Oxide Clusters, Si_3O_y^- : Models for Oxidation of Silicon Surfaces

A series of silicon oxide clusters, Si_3O_y ($y = 1-6$), are studied by anion photoelectron spectroscopy

(PES) and *ab initio* calculations. The PES spectra of Si_3O_y^- are taken at 3.49 and 4.66 eV photon energies (Fig. 4.3). The electron detachment energies (DE) and low-lying excited states are measured. The cluster structures are determined through *ab initio* calculations by comparing the calculated and observed DEs of each cluster. Starting from the triangular Si_3 cluster, each Si_3O_y cluster with increasing y can be viewed as a sequential oxidation. Each O atom is added to bridge two Si atoms from Si_3O to Si_3O_4 . From Si_3O to Si_3O_3 , each O atom is added to the edge of the Si_3 cluster, resulting in ring-type cluster structures. At Si_3O_4 , the cluster begins to assume a more 3-dimensional type of structure. One Si atom in Si_3O_4 is coordinated by the four O atoms in a distorted

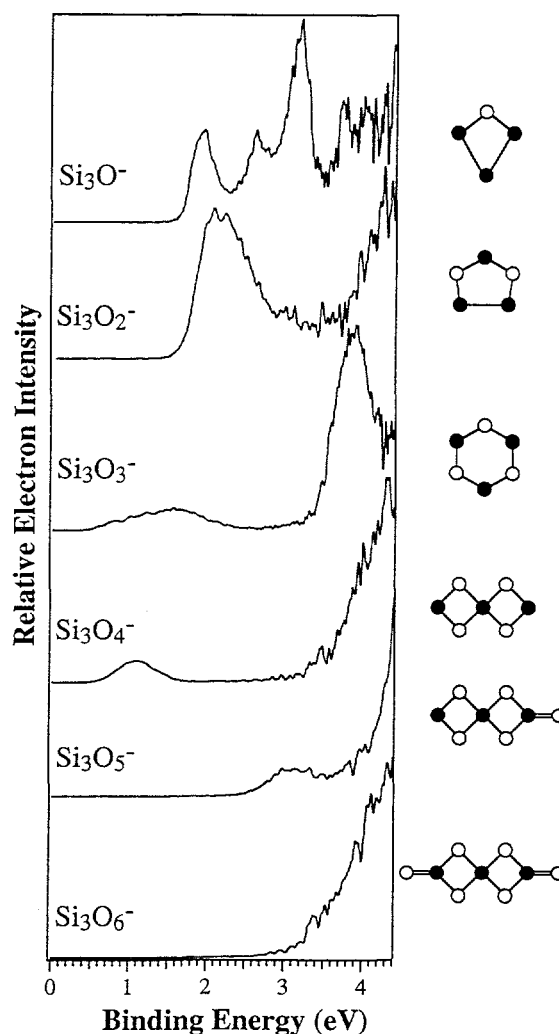


Figure 4.3. Photoelectron spectra of Si_3O_y^- (for $y = 1-6$) at 266 nm. The cluster structures are also shown.

tetrahedral geometry. The other two Si atoms each bind to two O atoms, giving an overall D_{2d} symmetry for Si_3O_4 . For Si_3O_5 and Si_3O_6 , each O atom is successively bonded to the two 2-coordinated Si atoms. At an atomic level, this sequence of structures is quite similar to the structural models for the oxidation of bulk silicon surfaces by O atoms.

Photoelectron Spectroscopy and Electronic Structure of Metal Clusters and Chemisorbed Metal Cluster Complexes

L. S. Wang and H. Wu*

Supported by the National Science Foundation.

*Department of Physics, Washington State University.

1. Two Isomers of CuO_2^- : The $\text{Cu}(\text{O}_2)$ Complex and the Copper Dioxide

Photoelectron spectroscopy of CuO_2^- has been studied at three detachment wavelengths: 532 nm, 355 nm, and 266 nm. Vibrationally-resolved spectra for two distinct isomers are observed: the $\text{Cu}(\text{O}_2)$ complex and the copper dioxide molecule. The $\text{Cu}(\text{O}_2)$ complex has an electron affinity (EA) of 1.503(10) eV with a ground-state vibrational frequency of 530(50) cm^{-1} . Its first electronic excited state is 7,400(300) cm^{-1} above the ground state. The $\text{Cu}(\text{O}_2)^-$ anion is also observed to undergo photodissociation to $\text{Cu}^- + \text{O}_2$ at both 532-nm and 355-nm detachment wavelengths. The copper dioxide molecule is found to have a high EA of 3.46(4) eV. Three low-lying excited states are observed within 1 eV above the ground state. The first two excited states of the copper dioxide molecule both possess a totally-symmetric vibrational frequency of 640(60) cm^{-1} .

2. Electronic Structure of Small Titanium Clusters: Emergence and Evolution of the 3d Band

The electronic structure of titanium clusters (Ti_n , for $n = 3-65$) is probed by size-selected anion photoelectron spectroscopy (Fig. 4.4). It is observed that the 3d band emerges at the 8-atom cluster, beyond which the d -band broadens and

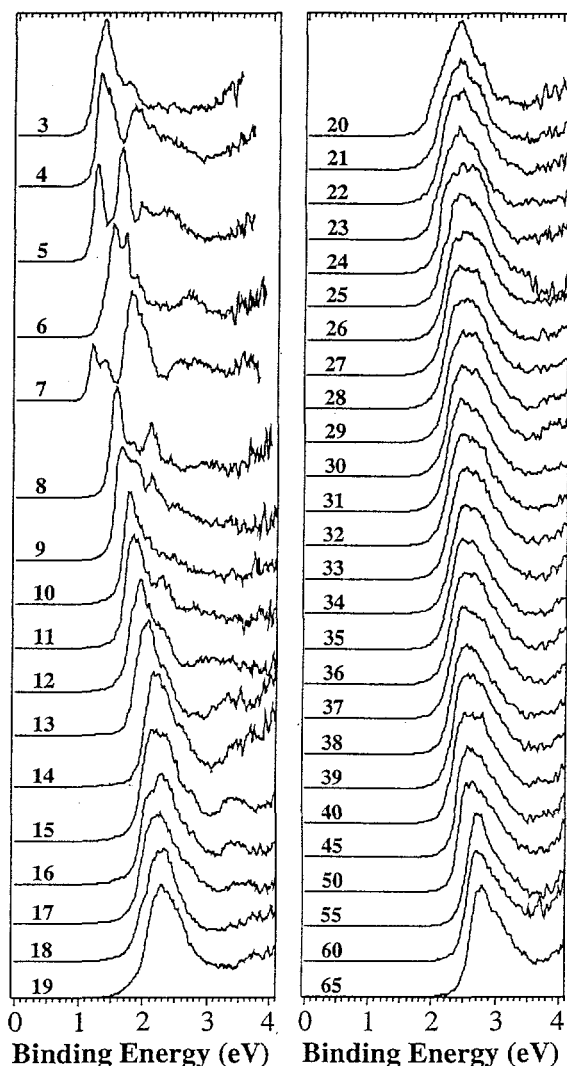


Figure 4.4. Photoelectron spectra of titanium clusters, Ti_n^- ($n = 3-65$) at 266 nm. Notice the spectral similarity above the 8-atom cluster. The broad feature is already quite similar to that of bulk photoemission from titanium surfaces.

evolves toward that of the bulk. The electronic structure of the titanium clusters is found to become bulk-like at relatively small cluster sizes. This point is discussed in terms of the delocalization of the titanium 3d orbitals and the implications for the cluster structures.

3. Electronic Structure of Small Copper Oxide Clusters: From Cu_2O to Cu_2O_4

We have studied the electronic structure of copper oxide clusters, Cu_2O_x ($x = 1-4$), using anion photoelectron spectroscopy and density functional calculations. The experiment is used to success-

fully guide a computational search for the cluster geometries. The predicted electron affinities at the obtained cluster structures reproduce exactly the trend observed experimentally. The definitive determination of the cluster structures enables a detailed analysis of the chemical bonding and electronic structure involving Cu atoms in different oxidation states exhibited by these clusters.

4. Observation and Photoelectron Spectroscopic Study of Novel Mono- and Di-Iron Oxide Molecules: FeO_y^- ($y = 1-4$) and Fe_2O_y^- ($y = 1-5$)

We have studied novel iron oxide molecules involving one and two iron atoms by anion photoelectron spectroscopy at 3.49 and 4.66 eV photon energies. Vibrationally-resolved photoelectron spectra and low-lying excited states are obtained for FeO_y^- ($y = 1-4$) (Fig. 4.5) and Fe_2O_y^- ($y = 1-5$). In both series, the photoelectron spectra become particularly sharp and better resolved for the higher oxides, FeO_3^- , FeO_4^- , Fe_2O_4^- , and Fe_2O_5^- . The electron affinity of the neutral oxide molecules is observed to increase almost linearly with the number of oxygen atoms, suggesting a sequential oxidation behavior. For the mono-iron oxide series, an oxidation saturation is evidenced by the leveling-off of the electron affinity from FeO_3 to FeO_4 . The structures and chemical bonding of these oxide molecules are discussed based on the sequential oxidation behavior. Isomers involving possibly O_2 or O_3 complexes are also observed for the di-iron oxides above Fe_2O .

5 Dimer Growth, Structural Transition, and Antiferromagnetic Ordering of Small Chromium Clusters

The evolution of structural and magnetic properties of small chromium clusters towards the bulk is elucidated through a systematic density-functional study. A tightly-bound Cr_2 dimer is found to play a key role in determining the cluster structures. A unique dimer growth route is discovered for clusters up to Cr_{11} , where a structural transition occurs from the dimer growth to a bulk-like body-centered-cubic structure (Fig. 4.6). All the clusters exhibit antiferromagnetic ordering with size-dependent magnetic moments.

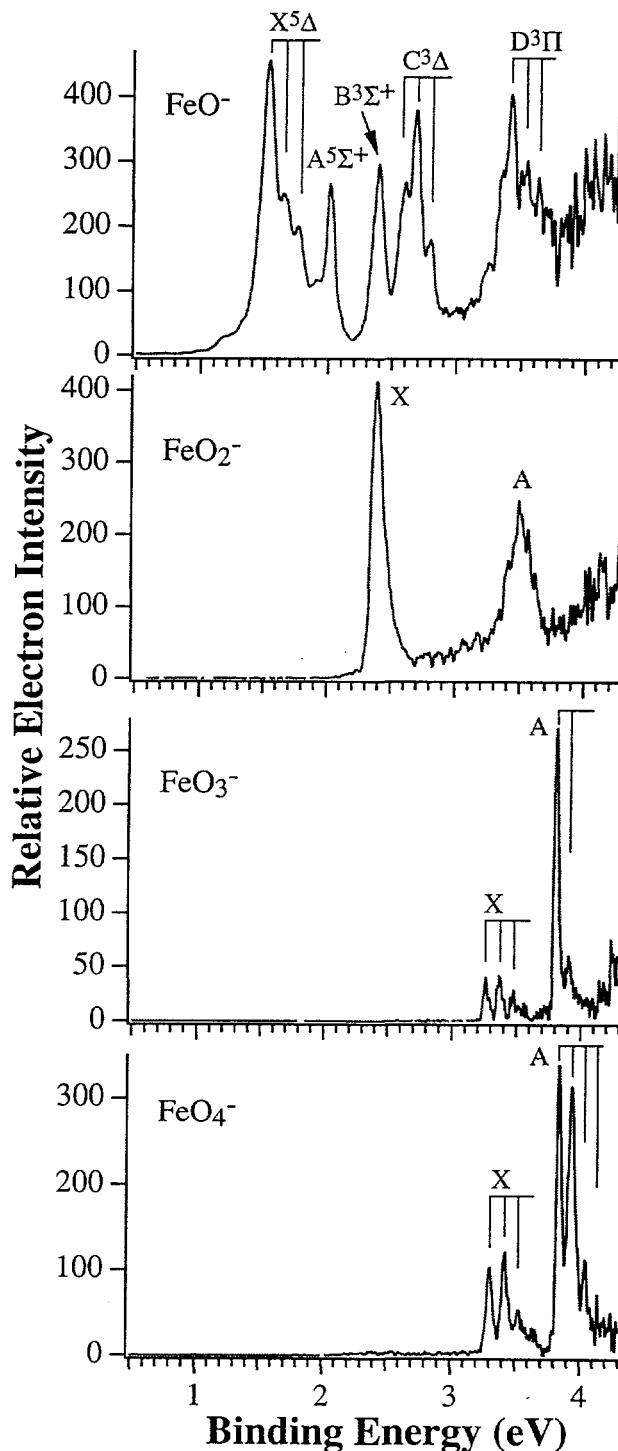


Figure 4.5. Vibrationally-resolved photoelectron spectra of FeO_y^- ($y = 1-4$) at 266 nm. Notice the increase of the electron affinity from FeO to FeO_3 and the spectral similarity between FeO_3 and FeO_4 .

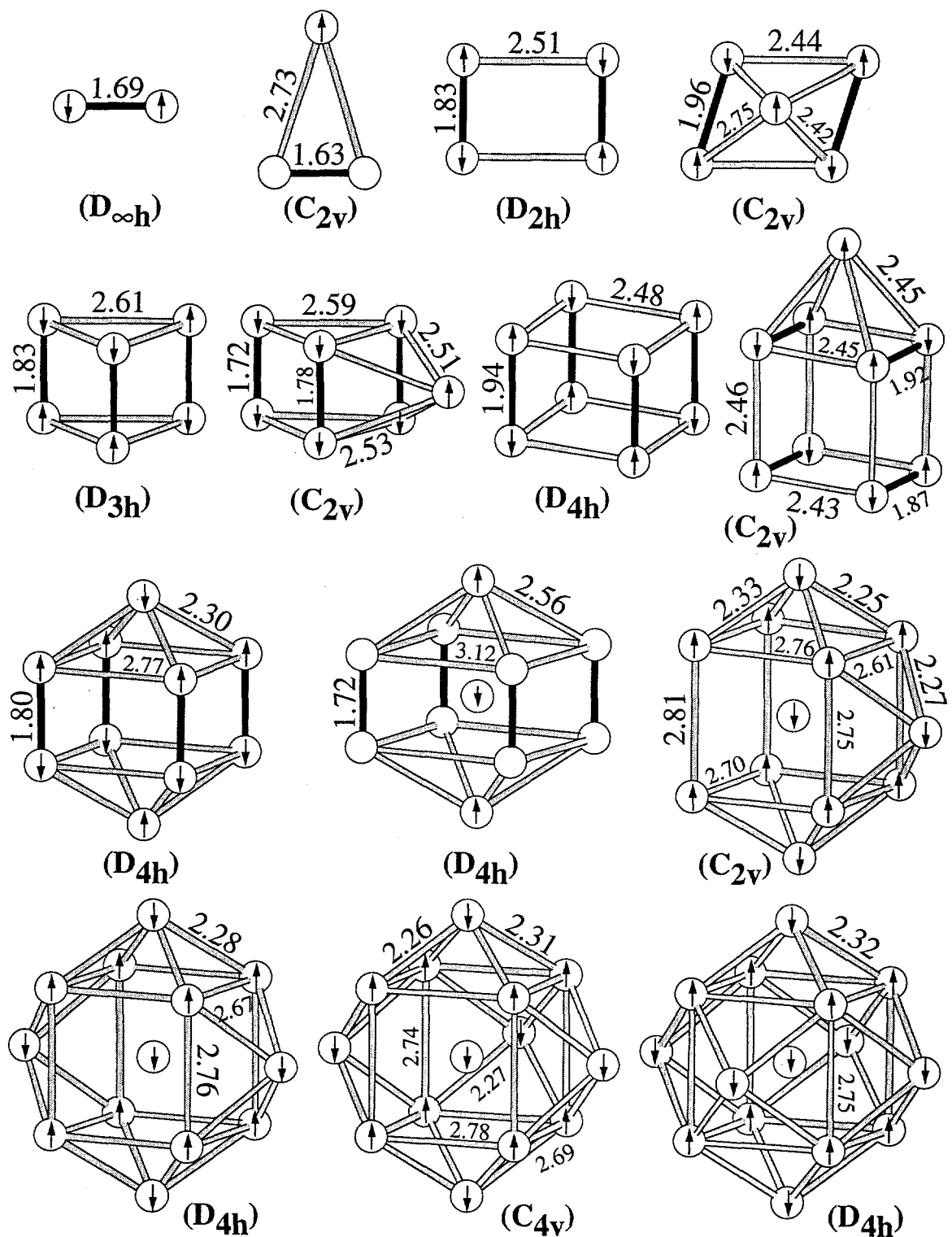


Figure 4.6. The lowest-energy structures of small chromium clusters, Cr_n ($n = 2-15$). The bond length is in Å. Note the dimer growth pattern from Cr_2 to Cr_{11} and the structure change from the dimer growth to bulk-like body-centered cubic structures at Cr_{12} . The dark bonds are the dimer-like bonds. The arrows represent the direction of the local atomic spin.

High-Resolution Spectroscopy of Molecules and Clusters

S. W. Sharpe, T. A. Blake,
R. L. Sams,* and R. S. McDowell

Supported by DOE Office of Basic Energy Sciences, and instrument development by Environmental Molecular Sciences Laboratory (EMSL).

*Associated Western Universities Fellow.

With the exception of homonuclear diatomics such as O₂, N₂, and Cl₂, all molecules possess infrared (IR)-active vibrational modes. Infrared spectroscopy is one of several powerful techniques the physical chemist can call upon for studying the behavior of matter on an atomic scale. In addition, infrared spectroscopy forms the basis for a suite of analytical techniques that are highly specific and extremely sensitive, and can be directly applied to monitoring problems.

High-resolution gas-phase infrared spectroscopic techniques have traditionally been plagued by several problems, including spectral congestion, Doppler broadening, and pressure broadening. Spectral congestion is related to the number of quantum states populated at a given temperature, and is dictated by Maxwell-Boltzmann statistics. Doppler broadening is related to temperature through the kinetic energy relationship, but also involves the random 3-dimensional motion of the gas molecules. Pressure broadening is related to the collisional frequency of the molecules, which in turn depends upon the density and temperature of the sample. By cooling and reducing the pressure of a gas in specially-designed cells, these three effects can be minimized, but at the expense of greatly reduced signal strength.

A technique that takes advantage of rapidly expanding a gaseous sample into a moderate vacuum has been used in our laboratory for the last 5 years. A gas sample is expanded through a slit orifice that measures 12 cm in length by 50 μm wide. The resulting ribbon of gas expands at supersonic velocities, and in the process molecules entrained in the gas are cooled to a few degrees above absolute zero. Also, the random 3-dimensional motion of the gas molecules is changed to a 2-dimensional flow with little velocity component transverse to the mass flow. If infrared light is used to interrogate the gas molecules through the

plane of expansion, spectral congestion, Doppler broadening, and pressure broadening are reduced significantly.

In the past, we have made extensive use of tunable infrared lead-salt diode lasers to interrogate the expanding gas. While infrared lasers make ideal light sources in many respects (i.e., extremely high spectral brightness, low noise, narrow bandwidth, and rapid tunability), they are severely limited by narrow spectral coverage. Often an experiment will be determined by what laser coverage is available. Recently, we have succeeded in interfacing a high-resolution Fourier-transform infrared spectrometer (FTIRS) with a continuous slit expansion source. Fourier-transform infrared spectroscopy is an alternative to laser sources, and offers continuous spectral coverage from the near to far infrared (~15,000 to 10 cm⁻¹). Although FTIRS has been used by others to interrogate molecular beams, these setups utilized a round expansion orifice at moderate spectral resolution. The PNNL FTIRS/beam machine is capable of recording high resolution ($\Delta\nu < 0.0015$ cm⁻¹) spectra at rotational temperatures of 15 K anywhere in the near- to far-infrared spectral region. As a first test case, 5% nitrous oxide in argon:helium was studied in the new spectrometer, and the results are shown in Fig. 4.7. Note the broad spectral coverage and high signal-to-noise ratio. The features to the red of the prominent ν_3 fundamental are due to combination difference bands with one and two quanta of energy in the ν_2 bending modes. A Boltzmann temperature analysis of these three bands indicates a vibrational temperature of 773 K and a rotational temperature of 15 K. We are currently investigating the origin of the apparent vibrational heating.

This unique instrument has recently been used to complete an infrared spectral investigation of perfluoroethane, a Freon™ substitute. Diode lasers and the FTIRS spectrometer were used in this study. The laser study was of slightly higher resolution and had approximately 10 times the signal-to-noise of the FTIRS results, but despite this problem the FTIRS data are comprehensive, covering two entire bands and requiring a fraction of the time required by the diode lasers to acquire; this comparison is shown in Fig. 4.8. Analysis of these data is currently in progress.

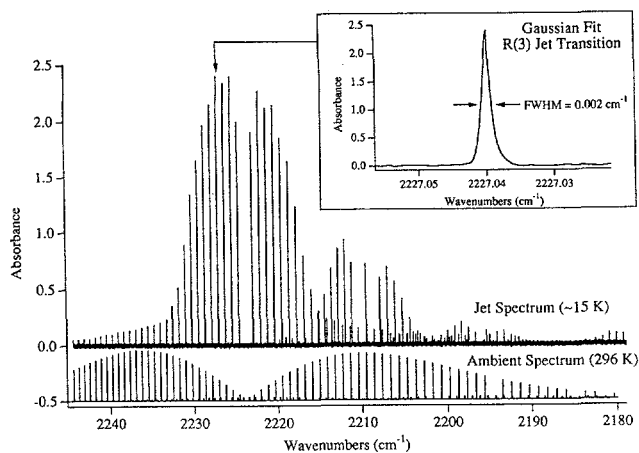


Figure 4.7. Preliminary data taken on the new PNNL FTIRS/beam machine. The most intense features correspond to individual rotational-vibrational lines of the ν_3 transition of N_2O .

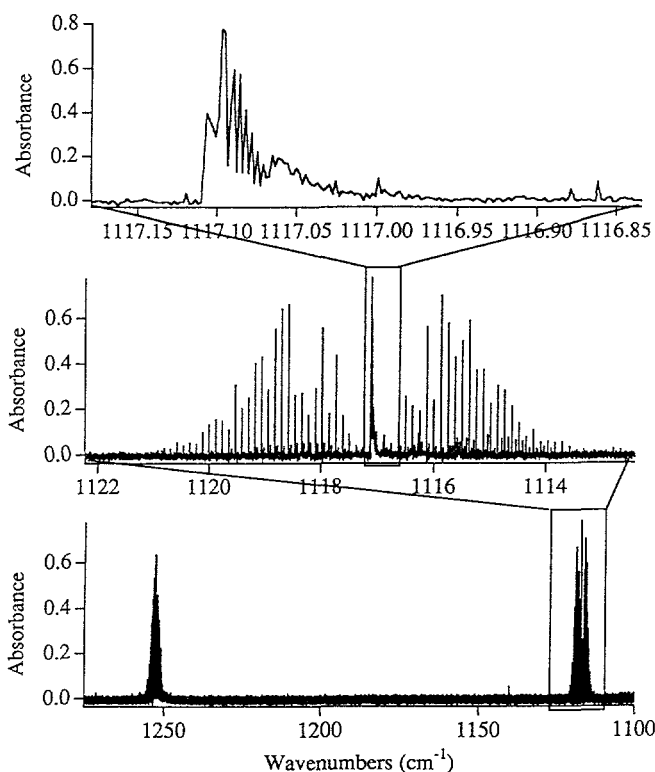


Figure 4.8. FTIRS/beam spectrum of C_2F_6 , taken by averaging 50 interferograms. Elapsed time for data acquisition was approximately 2.5 hours. Note the extensive spectral coverage.

Cation-Ether Complexes in the Gas Phase: Bond Dissociation Energies and Equilibrium Structures of $Li^+[1,2\text{-dimethoxyethane}]_x$, $x = 1-2$, and $Li^+[12\text{-crown-4}]$

D. Ray, D. F. Feller,
M. B. More,† E. D. Glendening,*
and P. B. Armentrout†*

Supported by DOE Office of Basic Energy Sciences.

*Theory, Modeling, and Simulation.

†Department of Chemistry, University of Utah.

Non-covalent interactions between ions and neutral molecules are of fundamental importance in molecular recognition phenomena occurring in complex chemical and biochemical systems.¹ The study of a series of cation/ether complexes composed of different metal cations, and a selection of ligands ranging from simple, monodentate ethers to cyclic polyethers, provides an opportunity to examine the non-covalent interactions operative in simple ion-molecule complexes. Cation/ether complexes are also interesting from a practical point of view. Crown ethers have been proposed for use in new chemical separations technologies² and in the development of advanced analytical methods.³ Computational models capable of reliably predicting ligand selectivity in a variety of condensed-phase environments would be valuable tools for the advancement of separations technologies. Such methods are currently under development; however, the development is hindered by a lack of suitable experimental data. One goal of the present work is to provide accurate experimental data to address this deficiency.

The principal challenge to quantitative theoretical descriptions of ion-molecule interactions arises from the need to reproduce accurately both the dominant classical electrostatic and quantum mechanical contributions to the interaction. The relative importance of these two effects varies from system to system, but two recent studies^{4,5} of Li^+ /ether complexes have demonstrated that both contributions are essential. Treating relatively large chemical systems with the requisite level of theory is technically very challenging. In general, small-basis-set Hartree-Fock (HF) theory is inca-

pable of accurately describing such interactions. Because theory is ultimately called upon to model a wide variety of molecular systems, a successful method must exhibit a certain degree of balance in its treatment of possibly competitive interactions. For example, the selectivity of macrocyclic ligands, such as 18-crown-6, toward alkali cations in aqueous solution hinges on a subtle balance between ion-ligand, ion-water, ligand-water, and water-water interactions. We have previously^{5,6} identified second-order perturbation theory coupled with polarized basis sets as a good entry-level theoretical approach for cation/neutral systems.

Accurate measurement of the intrinsic properties of cation/ether complexes is the principal challenge from the experimental perspective. Studies of ion-molecule complexes in the gas phase can provide insight into the intrinsic aspects of the interactions, because the isolated complexes are unperturbed by solvent-induced phenomena. In the present study, collision-induced dissociation (CID) cross-section measurements are made with a guided-ion-beam mass spectrometer, an instrument specifically designed for measurements of the kinetic energy dependence of collision induced phenomena. For $\text{Li}^+[\text{DXE}]_x$, $x = 1-2$, the primary and lowest-energy dissociation channel observed experimentally is endothermic loss of one dimethoxyethane molecule. For $\text{Li}^+[\text{12-crown-4}]$, the primary dissociation channel is endothermic loss of the intact crown ether, although ligand fragmentation is also observed. The cross-section thresholds are interpreted to yield 0- and 298-K bond energies after accounting for the effects of multiple ion-molecule collisions, internal energy of the complexes, and unimolecular decay rates. The calculated and experimentally-derived bond energies are in good agreement for $\text{Li}^+[\text{DXE}]$, reasonable agreement for $\text{Li}^+[\text{12-crown-4}]$, and differ by 32 ± 12 kJ/mol for $\text{Li}^+[\text{DXE}]_2$. On average, the experimental bond dissociation energies differ from theory by 9 ± 6 kJ/mol per metal-oxygen interaction. These results and the bond dissociation energies of Li^+ complexes with dimethyl ether (DME) from our previous work are shown in Fig. 4.9.

The equilibrium structures are determined primarily by strong electrostatic and polarization interactions between Li^+ and the ligands. Charge-transfer interactions are also important, as indicated by a natural energy decomposition analysis. Correlations between the bond dissociation ener-

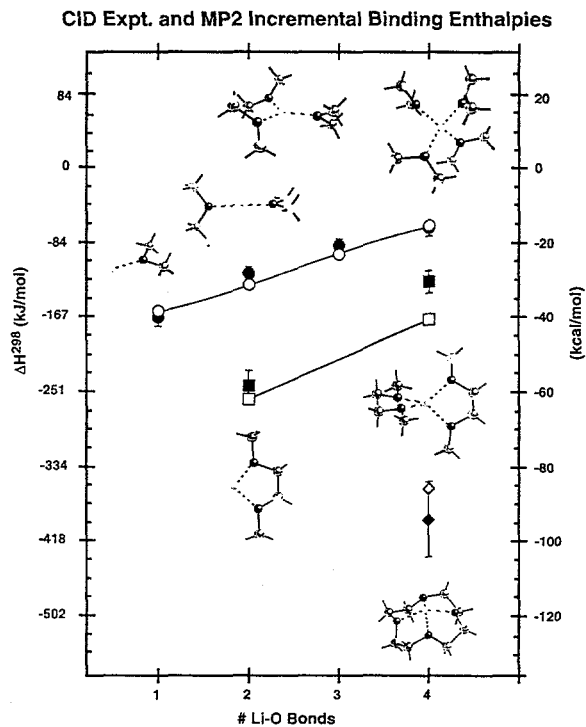


Figure 4.9. Experimental (filled symbols) and computed (open symbols) incremental binding enthalpies for $\text{Li}^+(\text{DME})_n$, $n = 1-4$ (circles), $\text{Li}^+(\text{DXE})_m$, $m = 1-2$ (squares), and $\text{Li}^+[\text{12-crown-4}]$ (diamonds) vs. number of Li^+-O bonds.

gies and the equilibrium structures demonstrate that orientation of the C-O-C moieties relative to the metal cation is more important than the Li^+-O bond length in determining the stability of the complexes, as predicted by Hay *et al.*^{7,8}

References

1. See, for example, D. A. Dougherty, *Science* **271**, 163 (1996).
2. E. P. Horwitz, M. L. Dietz, and D. E. Fisher, *Solvent Extract. Ion Exch.* **9**, 1 (1991).
3. J. W. Grate, R. Strebin, J. Janata, O. Egorov, and J. Ruzicka, *Anal. Chem.* **68**, 333 (1996).
4. M. B. More, E. D. Glendening, D. Ray, D. Feller, and P. B. Armentrout, *J. Phys. Chem.* **100**, 1405 (1996).
5. E. D. Glendening, D. Feller, and M. A. Thompson, *J. Am. Chem. Soc.* **116**, 10657 (1994).
6. D. Feller, E. Apra, J. A. Nichols, and D. E. Bernholdt, *J. Chem. Phys.*, to be published.
7. B. P. Hay and J. R. Rustad, *J. Am. Chem. Soc.* **116**, 6316 (1994).
8. B. P. Hay, J. R. Rustad, and C. J. Hostetler, *J. Am. Chem. Soc.* **115**, 11158 (1993).

Spectroscopy and Dynamics of Molecular Clusters

A. H. Bahnmaier, V. A. Venturo,
A. G. Joly, J. M. Price,* and D. Ray

Supported by DOE Office of Basic Energy Sciences.

*Computing and Information Sciences.

The synthesis of clusters in molecular beams affords the opportunity to create model systems exhibiting a rich variety of chemical phenomena. The application of techniques of laser spectroscopy and mass spectrometry to size-selected cluster beams facilitates rigorous studies of fundamental properties (both static and dynamic) of these model systems. The goal of this project is to examine the relationships between cluster structure (geometric and electronic) and function (reaction dynamics and kinetics) in molecular and ionic clusters. Comparison of the experimental results with predictions of emerging theoretical models is an important component of this project.

We are currently developing and applying time-domain spectroscopic techniques to determine the geometric structures of clusters. All of the methods under development are implementations of rotational coherence spectroscopy (RCS), a high-resolution, time-domain spectroscopic method for the determination of the moments of inertia of molecular species isolated in the gas-phase. RCS yields the rotational constants of an absorber to an accuracy of 0.1–1%, without requiring precise measurement or detailed analysis of individual eigenstates. It has become an established technique, principally through the efforts of Felker¹ and coworkers. In many cases, RCS is complementary to high-resolution spectroscopy in the frequency domain. It has great utility as a method providing gross structural data and is a particularly useful technique for species that have prohibitively dense or featureless spectra in the frequency domain.

A photoionization-based implementation of RCS, similar to that used by Ohline *et al.*,² has been implemented to study neutral clusters. In this approach, the rotational coherence transients are obtained via a psec pump-probe scheme by monitoring the production of photoions as a function of the time delay between the pump and probe pulses. Fluorescence-based implementa-

tions of RCS have been used extensively by Felker¹ and coworkers at UCLA and Topp and coworkers at the University of Pennsylvania³ to study the geometric structures of small clusters (dimers and trimers) that are amenable to size-selective photoexcitation. Fluorescence-based implementations of RCS depend upon the judicious choice of excitation energy to effect size selection, and are not suitable for species that do not fluoresce. Clearly, effective ionization-based implementations of RCS can overcome these limitations. In addition, ionization-based implementations may have improved sensitivity due to the efficient detection of photoions. Picosecond time-resolved rotational coherence transients of fluorene and fluorene-Ar obtained with a time-resolved ionization depletion method are shown in Figs. 4.10 and 4.11, respectively.

A photofragmentation-based implementation of RCS, similar to that described by Magnera *et al.*,⁴ has been implemented to study ionic clusters. In this approach, the rotational coherence transients are obtained via a psec pump-probe scheme by monitoring the production of photofragments as a function of the time delay between the pump and probe pulses. A portion of the rotational coherence transient of Ar_3^+ is shown in Fig. 4.12. There have been very few measurements of the rotational constants of ionic clusters due to the difficulty of generating a large enough sample; the RCS methods we are developing are sufficiently sensitive to measure rotational constants of extremely small numbers of ions and should, therefore, have wide applicability.

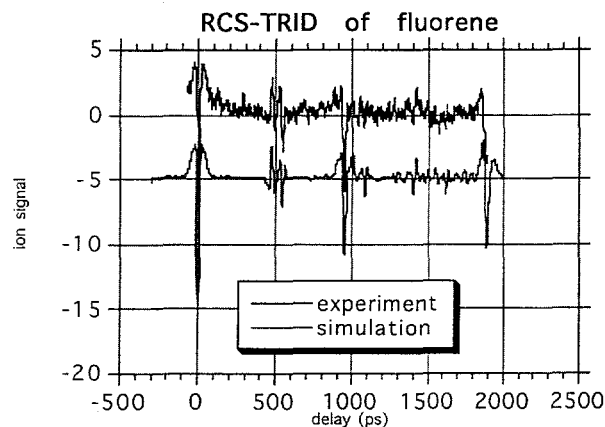


Figure 4.10. RCS trace of fluorene.

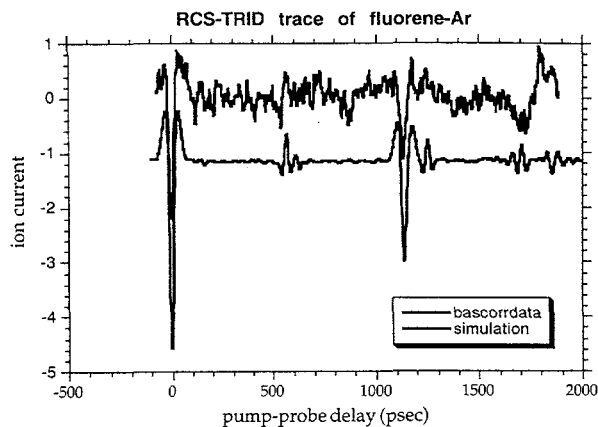


Figure 4.11. RCS trace of fluorene-Ar.

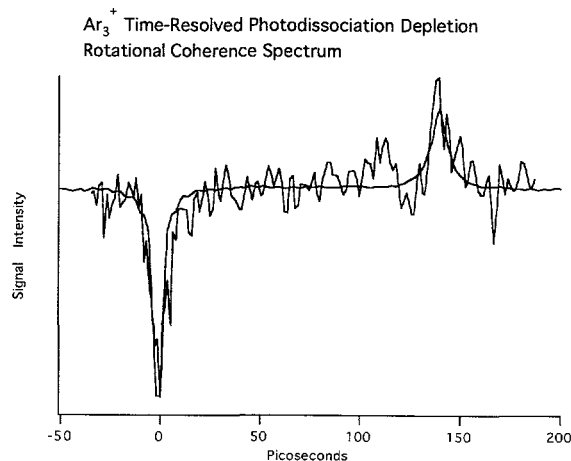


Figure 4.12. RCS trace of Ar_3^+ .

References

1. P. M. Felker, "Rotational coherence spectroscopy: studies of the geometries of large gas-phase species by picosecond time-domain methods," *J. Phys. Chem.* **96**, 7844-7857 (1992).
2. S. M. Ohline, J. Romascan, and P. M. Felker, "Time-resolved ionization depletion. A new picosecond method for molecular beam studies," *Chem. Phys. Lett.* **207**, 563-568 (1993).
3. See, for example, T. Troxler, J. R. Stratton, P. G. Smith, and M. R. Topp, "Photoisomerization of

- molecular van der Waals aggregates. Structural assignments of isomeric forms of 1-chlorobutane/perylene via rotational coherence spectroscopy," *Chem. Phys. Lett.* **222**, 250-256 (1994).
4. T. F. Magnera, D. M. Sammond, and J. Michl, "Ground-state rotational constants of Ar_3^+ by rotational depletion coherence spectroscopy," *Chem. Phys. Lett.* **211**, 378-380 (1993).

5. Miscellaneous

Characteristics of a Weakly-Ionized Nonneutral Plasma

A. J. Peurrung* and S. E. Barlow

Supported by DOE Office of Basic Energy Sciences and Laboratory Directed Research and Development (LDRD).

*Materials and Chemical Sciences Center.

A new scheme that allows the stable confinement of a weakly-ionized nonneutral plasma (WINP) has been investigated. The method requires the forced rotation of the neutral gas within the trap about an axis that roughly coincides with the trap's magnetic and mechanical axes. The basic equilibrium and transport properties of the weakly-ionized nonneutral plasma can be readily calculated.

Recent advances in the understanding of trapped ions in Penning traps have allowed these ion traps to see service in a wide variety of roles.¹⁻⁷ One of the most important and useful characteristics of Penning traps is their ability to store an ion cloud indefinitely at thermal equilibrium.⁸ The equilibrium properties of the stored ion cloud may be found by solving the force balance equations:

$$\begin{aligned} F_B &= -(q\omega_r Br / c)\hat{r}, \\ F_E &= qE, \\ F_P &= -(k_B T \nabla n) / n, \end{aligned} \tag{1}$$

where F_B , F_E , and F_P are the magnetic, electric and pressure gradient forces, respectively; q , c , and k_B are the charge, the speed of light, and Boltzmann's constant; ω_r is the rotation frequency of the nonneutral plasma; B is the applied magnetic field, assumed to be uniform; E is the electric field; r is a radial distance; T is the temperature; and $n = n(r, z)$ is the ion distribution. When the vector sum of all of the forces is zero, equilibrium has been achieved. Equations (1) can then be solved self-consistently to give the ion distribution.⁸

Interestingly, if we add to the above conditions a rotating neutral gas of sufficient density that the ion-neutral collision frequency is large compared to the ion cyclotron frequency, we can also find a stable equilibrium for ion confinement. We show this by writing down the particle flux equations:

$$\begin{aligned} \Gamma_B &= -\left(\frac{\mu n \omega_n B r}{c}\right)\hat{r}, \\ \Gamma_E &= n\mu E, \\ \Gamma_D &= -D\nabla n, \\ \Gamma_M &= \left(\frac{\delta m n \mu \omega_n^2 r}{q}\right)\hat{r}, \end{aligned} \tag{2}$$

where μ is the mobility, ω_n is the rotational frequency of the neutral gas, D is the diffusion constant, Γ_M is an additional (but generally small) inertial force, and

$$\delta m = (m_i - m_n), \tag{3}$$

where m_i is the ion mass and m_n is the neutral mass. Note that with this definition, the last of Eqs. (2) can be of either sign. In this case, when the vector sum of the fluxes is zero, equilibrium is reached. The formal similarity of Eqs. (1) and (2) with respect to n , the ion density distribution, means that the ion cloud shapes will be identical to those in a Penning trap. In particular, at its edge the WINP density profile will fall off over a characteristic distance on the order of the thermal Debye length, $\lambda_D = \sqrt{k_B T / 4\pi n q^2}$. We can also estimate the characteristic relaxation times, and we find two important time scales: an electrostatic time with $\tau_f \approx c / 2\mu\omega_n B$, and a slower thermal one given by $\tau_s \approx \lambda_D^2 / D$. Note that $\tau_s / \tau_f = 1/2$.

The WINP contrasts in several important ways from the standard, fully-ionized nonneutral plasma. First, it is not subject to the rich diocotron mode structure found in Penning-trapped ion clouds. Second, no equivalent exists to the Brillouin limit. Third, we are not limited to only gaseous media; liquids and solids should work just as well, provided the ions or electrons have sufficient mobility.

References

1. J. H. Malmberg and J. S. deGrassie, *Phys. Rev. Lett.* **35**, 577 (1975).
2. C. M. Surko and T. J. Murphy, *Phys. Fluids B* **2**, 1372 (1990).
3. G. Gabrielse, X. Fei, L. A. Orozco, R. L. Tjoelker, J. Haas, H. Kalinowsky, T. A. Trainor, and W. Kells, *Phys. Rev. Lett.* **65**, 1317 (1990).
4. J. J. Bollinger, D. J. Wineland, and D. H. E. Dubin, *Phys. Plas.* **1**, 1403 (1994).

5. J. D. Daugherty, J. E. Eninger, and G. S. Janes, *Phys. Fluids* **12**, 2677 (1969).
6. W. W. Yin, M. Wang, A. G. Marshall, and E. B. Ledford, *J. Am. Soc. Mass Spectrom.* **3**, 188 (1992).
7. P. Zaveri, P. I. John, K. Avinash, and P. K. Kaw, *Phys. Rev. Lett.* **68**, 3295 (1992).
8. S. A. Prasad and T. M. O'Neil, *Phys. Fluids* **22**, 278 (1979).

Ultrafast Infrared Pulse Generation and Measurement of Vibrational Decay in Water

G. R. Holtom

Instrument development supported by
Environmental Molecular Sciences
Laboratory (EMSL).

Water, a hydrogen-bonded liquid, has been much studied, but no direct measurements of the intramolecular forces have been performed. We have developed an ultrafast laser system to address this measurement. While a number of femtosecond-duration lasers have been made, our requirement for a source at a wavelength of 3 μm , with short pulses and the high energies required to do nonlinear spectroscopic measurements, demanded a new approach.

Ti:sapphire is the basis for our visible ultrafast laser oscillator and amplifier, and these devices are available commercially. Our contribution is designing and testing wavelength conversion devices based on optical parametric amplification. This method is stable, efficient, and with suitable nonlinear materials can reach the mid-infrared spectral region. Figure 5.1 shows the temporal and spectral width of our amplified pulses. These are generated at a repetition rate of 250 kHz, and have an energy of 400 nJ, giving us a unique experimental capability.

We are starting measurements on water and related liquids, using photon-echo and pump-probe methods. A fundamental question that we hope to answer involves the relative contributions of inhomogeneous and homogeneous broadening,

which depend upon the lifetime of the vibrational excitations that are pumped directly. This result should also address the question of the intramolecular potential of water.

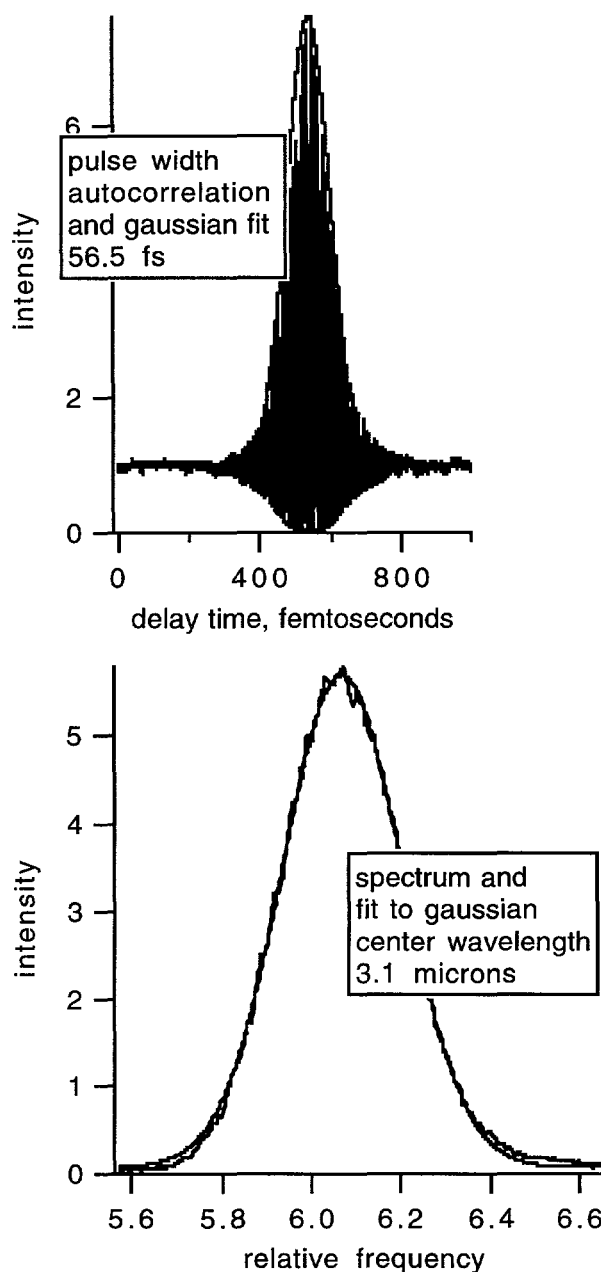


Figure 5.1. Traces of amplified pulses, demonstrating temporal width of 56.5 fs and spectral width at 3.1 μm .

Breath Analysis by Laser-Based Spectroscopy

S. W. Sharpe, T. A. Blake,
and R. L. Sams*

Supported by PNNL Medical Technologies Initiative.

*Associated Western Universities Fellow.

We are developing a portable near-infrared laser-based device for diagnosis of human pathologies by breath analysis. We are monitoring for specific biomarkers that appear only when the patient has a specific pathology or disease. These biomarkers could be a direct consequence of a pathology, such as the presence of elevated ketone concentrations in the breath of diabetics. Alternatively, a stable isotopically-tagged species could be introduced either by injection or ingestion. This tagged species would be metabolized only by a specific bacterium, giving a unique signature in the breath.

A case in point is the development of a non-invasive, rapid, and inexpensive diagnosis procedure for *Helicobacter pylori*, which is often associated with gastritis and stomach ulcers. Of the world's population, 60% has been estimated as being infected with *H. pylori*. While relatively easy to treat with conventional antibiotics, this disease is currently detected via examination of biopsy samples acquired by endoscopy, a most unpleasant, time-consuming, and expensive procedure, and not feasible for mass use. *H. pylori* is known to have an appetite for urea, breaking it down into ammonia and carbon dioxide. We propose tagging urea with ^{15}N , having the patient ingest a small amount of the tagged material, and monitoring the breath for $^{15}\text{NH}_3$. We are currently collaborating with a local gastroenterologist and hope to start preliminary human studies in early 1996.

The instrument used for this analysis is an ultrasensitive, quantitative gas-phase analyzer called a Sniffer, based on a Herriot cell multi-pass

design. Although the Sniffer is highly specific to a particular molecule, it can be configured for detection of almost any infrared-active molecular species. Extremely high sensitivity (i.e., ppb) and excellent speciation are obtained by combining a highly monochromatic laser source with a long optical path length, low-pressure, Doppler-limited sampling system. The device consists of a mid- or near-infrared tunable diode laser, which repeatedly ramps over a specific spectral region known to contain rotational-vibrational transitions of the target molecule. Sample is continuously admitted to the Sniffer absorption cell, which is maintained at a pressure of 30 Torr or less to remove pressure-broadening effects. Ultimate spectral resolution is limited by Doppler broadening, and will depend upon temperature and molecular weight of the effluent molecule, but will typically be on the order of 150 MHz (i.e., 0.005 cm^{-1}). The Sniffer cell contains a pair of spherical mirrors separated by 55 cm, which create a 100-m folded optical path for increased optical depth. Figure 5.2 shows typical signals for various ammonia sources.

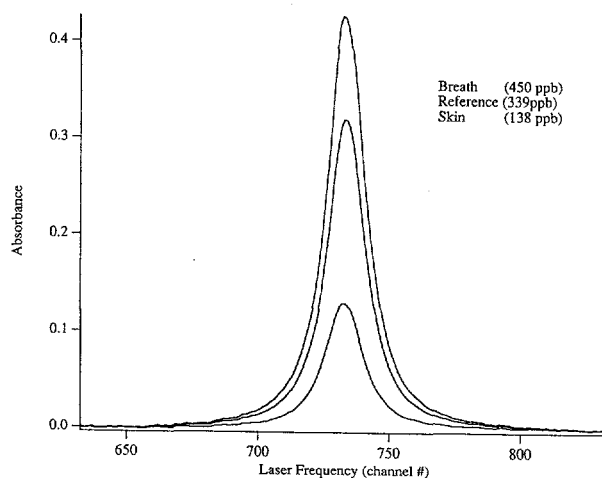
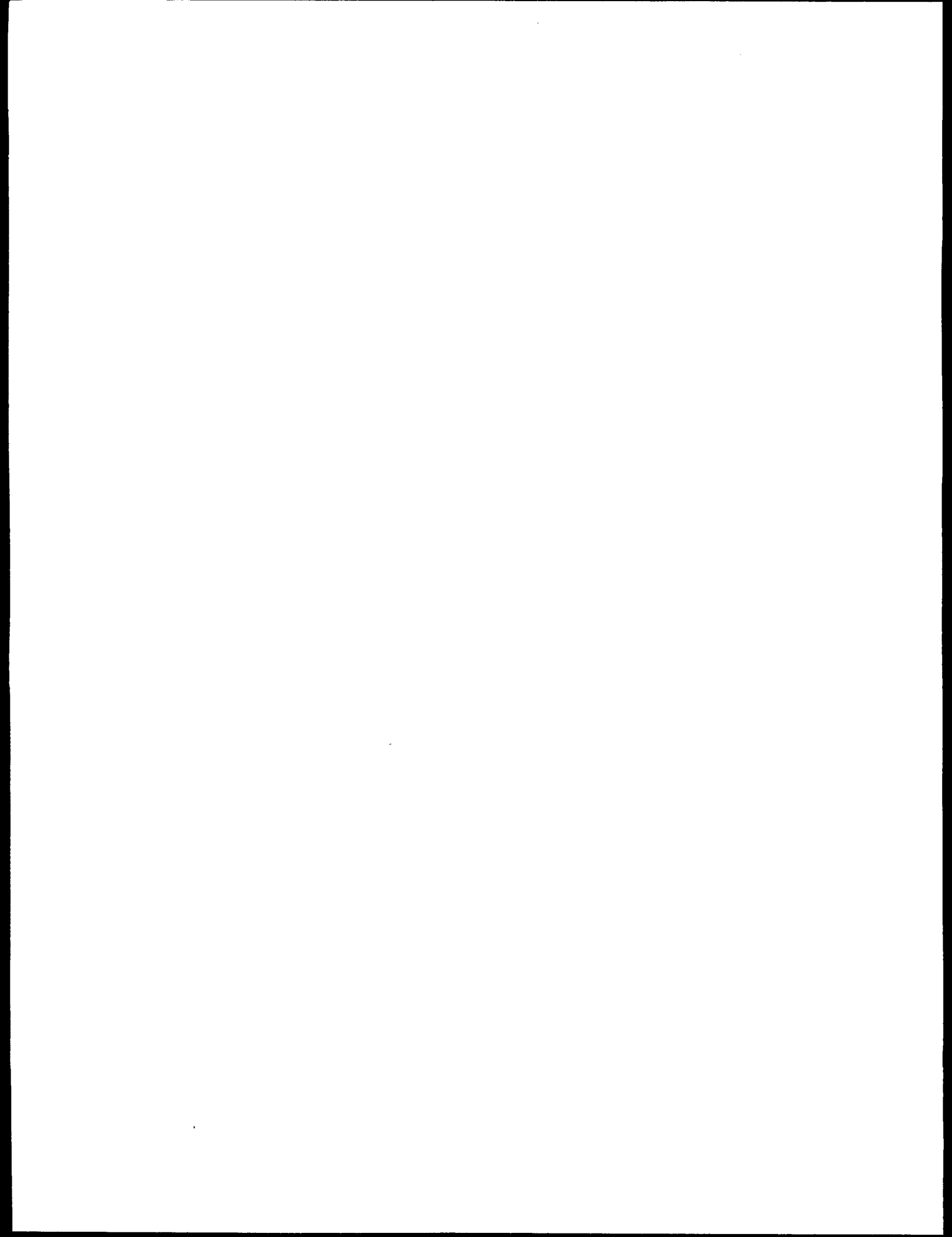


Figure 5.2. Single rotational-vibrational transition of v_2 for the ammonia molecule. The line shape is best described as a Voigt profile and arises from a convolution of the Doppler and pressure-broadening effects.



6. Appendix

Chemical Structure and Dynamics Staff

Associate Director, EMSL

Steven D. Colson

B.S. Utah State University 1963; Ph.D. California Institute of Technology 1968; Postdoctoral Fellow, National Research Council (Ottawa) 1968; Assistant Professor to Professor of Chemistry, Yale University, 1968–1989; joined PNNL as Associate Director for Chemical Structure and Dynamics June 1989. Research interests: photochemistry, photophysics, and molecular dynamics; electronic structures of molecules; processes at the molecule/surface interface.

(509) 375-6882

sd_colson@pnl.gov

Program Manager

Robin S. (Rod) McDowell

B.A. Haverford College 1956; Ph.D. M.I.T. 1960; Staff Member, Assistant Group Leader, and Laboratory Fellow, Los Alamos National Laboratory, 1960–1991; joined PNNL as Program Manager for Chemical Structure and Dynamics April 1991. Research interests: high-resolution infrared and Raman spectroscopy applied to molecular structure and bonding; molecular dynamics and force fields; statistical mechanics; infrared analytical techniques.

(509) 375-6681

rs_mcdowell@pnl.gov

Staff

Stephan E. Barlow

B.A. Southern Oregon State College 1976; Ph.D. University of Colorado 1984, Postdoctoral Fellow 1984–1989; Senior Instructor in Chemistry, University of Denver 1989–1991; joined PNNL June 1991. Research interests: development and application of mass spectrometric techniques to gas-phase chemical kinetics, reaction mechanisms, and structure.

(509) 375-2959

se_barlow@pnl.gov

James P. Cowin

B.S. Case Western Reserve University 1974; Ph.D. University of Chicago 1981; Postdoctoral Fellow, University of Toronto 1981–1983; Assistant Professor of Chemistry, University of California, Santa Barbara, 1983–1990; joined PNNL July 1990. Research interests: molecular motions

at interfaces, especially energy and charge transfer, bond formation dynamics, and light-stimulated surface reactions.

(509) 375-6838

jp_cowin@pnl.gov

Donald M. Friedrich

B.S. University of Michigan 1966; Ph.D. Cornell University 1973; Associate Professor of Chemistry, Hope College, 1975–1985; joined PNNL August 1985; transferred to EMSL Environmental Dynamics and Simulation April 1995. Research interests: mechanisms by which solvent molecules and surface structures interact at solid/liquid interfaces to control sorbate reactions such as complexation, electron transfer, proton transfer, and hydrogen bonding.

(509) 375-3643

dm_friedrich@pnl.gov

Wayne P. Hess

B.A. University of Colorado 1981; M.S. University of Oregon 1983; Ph.D. University of Colorado 1988; Postdoctoral Fellow, Sandia Livermore Combustion Research Facility 1988–1990; joined PNNL January 1990. Research interests: modeling condensed phase chemistry through the study of energetic reactive processes in molecular solids and thin films (dissociation and fragmentation, electronic and vibrational energy transfer), using FTIR and laser-induced desorption and ablation of adsorbed molecules and solid surfaces.

(509) 375-2555

wp_hess@pnl.gov

Gary R. Holtom

B.A. Pfeiffer College 1969; Ph.D. University of California, Berkeley, 1978; Postdoctoral Fellow, Wesleyan University 1978–1979; Head of Laser Operations, University of Pennsylvania Regional Laser and Biotechnology Laboratory, 1979–1989; joined PNNL September 1989. Research interests: short-pulse laser spectroscopy; condensed-phase photochemistry, in particular the dynamics of electronically-excited organic molecules.

(509) 375-2459

gr_holtom@pnl.gov

Stephen A. Joyce

B.S. Boston College 1982; Ph.D. M.I.T. 1987; Postdoctoral Fellow, National Institute of Standards and Technology 1987–1989; Sandia National Laboratories 1989–1991; joined PNNL October 1991. Research interests: scanning probe microscopies for studying molecularly-resolved chemistry on solid surfaces.

(509) 375-6459

sa_joyce@pnl.gov

Bruce D. Kay

B.S. University of Illinois 1976; Ph.D. University of Colorado 1982; Senior Member of the Technical Staff, Sandia National Laboratories, 1982–1991; joined PNNL November 1991. Research interests: chemical dynamics and kinetics of molecular processes occurring at the gas-surface interface; interaction of water and halogenated hydrocarbons on model oxide surfaces; trapping and "solvation" of ions and molecules on multilayer ice surfaces; chemical physics of liquids and amorphous solids; phase transitions and critical phenomena.

(509) 375-6484

bd_kay@pnl.gov

Thomas M. Orlando

B.S. Southampton College 1982; Ph.D. State University of New York at Stony Brook 1988, Postdoctoral Fellow 1988–1989; Postdoctoral Fellow, Sandia National Laboratory 1989–1991; joined PNNL September 1991. Research interests: non-thermal interfacial reaction dynamics; electron, photon, and hyperthermal ion-beam induced surface chemistry; dissociative electron attachment; laser spectroscopy.

(509) 375-6404

tm_orlando@pnl.gov

Douglas Ray

B.A. Kalamazoo College 1979; Ph.D. University of California, Berkeley, 1985; Postdoctoral Fellow, Joint Institute for Laboratory Astrophysics 1985–1990; joined PNNL June 1990. Research interests: the experimental study of dynamical processes in clusters and at liquid interfaces using techniques of laser spectroscopy and mass spectrometry.

(509) 375-2104

d_ray@pnl.gov

Steven W. Sharpe

B.S. University of Bridgeport 1979; Ph.D. State University of New York at Stony Brook 1986; Postdoctoral Fellow, University of Southern California 1987–1990; joined PNNL May 1990. Research interests: high-resolution molecular spectroscopy.

(509) 375-5942

sw_sharpe@pnl.gov

Lai-Sheng Wang

B.S. Wuhan University 1982; Ph.D. University of California, Berkeley, 1989; Postdoctoral Fellow, Rice University 1990–1992; joint Washington State University/PNNL appointment January 1993. Research interests: physical and chemical properties of metal and semiconductor clusters using techniques of molecular-beam and photoelectron spectroscopy; using clusters as model

systems to study surface and interfacial phenomena.

(509) 375-5976

ls_wang@pnl.gov

Xiaoliang (Sunney) Xie

B.S. Peking University 1984; Ph.D. University of California at San Diego 1990; Postdoctoral Fellow, University of Chicago 1990–1991; joined PNNL January 1992. Research interests: chemical physics in liquids and in biological systems, using ultrafast laser techniques; molecular-level understanding of chemical reactions at interfaces and biological membranes, using near-field single-molecule spectroscopy.

(509) 375-6372

xs_xie@pnl.gov

Research Scientists

Thomas A. Blake

B.S. University of Bridgeport 1981; Ph.D. Wesleyan University 1989; Postdoctoral Fellow, University of Washington 1988–1991; NRC Research Associate, NASA Ames Research Center 1991–1994; joined PNNL September 1994.

(509) 375-4341

ta_blake@pnl.gov

Martin J. Iedema

B.S. University of Southern California 1988; Technician, Mt. Wilson Observatory 1987–1990; joined PNNL September 1990.

(509) 375-2354

mj_iedema@pnl.gov

Alan G. Joly

B.S. University of Rochester 1985; Ph.D. M.I.T. 1990; Postdoctoral Fellow, PNNL 1990–1993; joined PNNL staff June 1993.

(509) 375-2729

ag_joly@pnl.gov

Gregory A. Kimmel

B.S. Cornell University 1984, Ph.D. 1992; Postdoctoral Fellow PNNL, 1992–1995; joined PNNL staff September 1995.

(509) 375-6611

ga_kimmel@pnl.gov

R. Scott Smith

B.S. Northern Arizona University 1983; Ph.D. University of Utah 1988; Postdoctoral Fellow, University of Arizona 1988–1989, PNNL 1990–1992; joined PNNL staff October 1992.

(509) 375-2697

rs_smith@pnl.gov

Russell G. Tonkyn

B.A. Reed College 1978; Ph.D. University of Wisconsin 1988; Postdoctoral Fellow, Brookhaven National Laboratory 1988–1991, PNNL 1991–1992; joined PNNL staff November 1992.

(509) 375-6481

rg_tonkyn@pnl.gov

Visiting Scientist

Robert L. Sams

B.A. Western Washington University 1962; M.S. University of Washington 1967; National Bureau of Standards/National Institute of Standards and Technology 1967-1995; Associated Western Universities fellowship at PNNL December 1995. (509) 375-6456 rl_sams@pnl.gov

Technical Specialist

Greg A. Ritter

B.S. Oregon Institute of Technology 1991; PNNL June 1991 to September 1995.

Operations Administrator

Denise A. Motsenbocker

B.A. University of Washington 1975.

Office Support

Debra M. Hinton (from June 1995)

Cynthia A. Irwin

Brenda K. Neeley (to May 1995)

Postdoctoral Fellows

Albert H. Bahnmaier

Ph.D. University of Ulm 1993; Postdoctoral Fellow, CS&D, with Doug Ray, 1993-.

Richard A. Bradley Jr.

B.A. Reed College 1986; Ph.D. University of Oregon 1992; Postdoctoral Fellow, CS&D, with Wayne Hess, 1993-1995; now Scientist at OCLI, Inc., Santa Rosa, Cal.

Robert A. Crowell II

B.S. University of California, Riverside, 1987, Ph.D. 1992, Postdoctoral Fellow 1992-1993; Postdoctoral Fellow, CS&D, with Sunney Xie, 1993-1995; now Staff Member at Argonne National Laboratory.

Sunil R. Desai

B.S. Guilford College 1990; Ph.D. University of Tennessee 1995; Postdoctoral Fellow, CS&D, with Lai-Sheng Wang, 1993-.

Robert Doolen

B.S. University of New Mexico 1989; Ph.D. University of California, San Diego, 1994; Postdoctoral Fellow, CS&D, with Doug Ray, 1994-.

Robert C. Dunn

B.S. California State University, Sacramento, 1988; M.S. University of California, San Diego, 1990, Ph.D. 1992; Postdoctoral Fellow, CS&D, with Sunney Xie, 1993-1995; now Assistant Pro-

fessor at University of Kansas.

Jiawen Fan

B.S. Jinan University 1982, M.S. 1985; M.S. Washington State University 1989, Ph.D. 1991, Postdoctoral Fellow 1992-1993; Postdoctoral Fellow, CS&D, with Lai-Sheng Wang, 1993-1995; now Scientist/Group Leader at North American Scientific, Hollywood, Cal.

Mark C. Gallagher

B.Sc. University of Calgary 1982; Ph.D. University of Alberta 1990; Postdoctoral Fellow, Pennsylvania State University 1990-1993; Postdoctoral Fellow, CS&D, with Jim Cowin, 1993-1995; now Assistant Professor at Lakehead University, Thunder Bay, Ont.

Kristine A. H. German

B.A. Carleton College 1983; M.S. University of California, Riverside, 1989, Ph.D. 1993; Postdoctoral Fellow, CS&D, with Wayne Hess, 1994-1995; now at Xerox Corporation, Rochester, N.Y.

Nigel G. Gotts

B.Sc. University of Sussex 1987, D.Phil. 1991; Postdoctoral Fellow, University of California, Santa Barbara, 1992-1994; Postdoctoral Fellow, CS&D, with Jim Cowin, 1994-1995; now with PNNL Energy Division, Transportation Technology Department, Sensors and Measurement Systems Group.

Chen (Chris) Huang

B.S. Xiamen University 1982; M.A. University of California, Santa Barbara, 1987, Ph.D. 1990, Postdoctoral Fellow 1990-1993; Postdoctoral Fellow, CS&D, with Bruce Kay, 1993-1995; Postdoctoral Fellow in PNNL Earth and Environmental Sciences Division 1995-1996; now with Charles Evans Associates, Redwood City, Cal.

Naushad Kizhakevariam

B.Tech. Indian Institute of Technology 1985; Ph.D. University of Washington 1991; Postdoctoral Fellow, Purdue University 1991-1994; Postdoctoral Fellow, CS&D, with Jim Cowin, 1994-.

Karen Knutsen

B.A. Linfield College 1981; Ph.D. University of Colorado 1992; Postdoctoral Fellow, CS&D, with Thom Orlando, 1994-.

Hong (Peter) Lu

B.A. Beijing University 1982, M.Sc. 1984; M. Phil. Columbia 1987, Ph.D. 1991; Postdoctoral Fellow, Northwestern 1991-1995; Postdoctoral Fellow, CS&D, with Sunney Xie, 1995-.

Michael J. Stirniman

B.S. University of Illinois 1988; Ph.D. University of Chicago 1995; Postdoctoral Fellow, CS&D, with Bruce Kay, 1995- .

Vincent A. Ventura

B.S. Rutgers University 1985; M.S. University of California, Berkeley, 1988; Ph.D. University of California at Los Angeles 1993; Postdoctoral Fellow, CS&D, with Doug Ray, 1994- .

Hong Wang

B.S. Peking University 1987; M.S. Michigan State 1992, Ph.D. 1994; Postdoctoral Fellow, CS&D, with Jim Cowin, 1995- .

Zheming Wang

B.S. Northwestern Normal University, Lanzhou, 1982, M.S. 1985; Ph.D. Florida State University 1994; Postdoctoral Fellow, CS&D, with Don Friedrich, 1995.

Eric K. L. Wong

B.S. University of Oregon 1985, Ph.D. 1992; Postdoctoral Fellow, CS&D, with Bruce Kay, 1993-1995; now Computer Scientist at Intel, Beaverton, Ore.

Songlin Xu

B.S. Xiamen University 1982, M.S. 1985; Ph.D. University of Kansas 1993; Postdoctoral Fellow, CS&D, with Steve Sharpe, 1994-1995; now Senior Process Engineer at Applied Materials, Santa Clara, Cal.

Graduate Students

John P. Biesecker

University of Colorado, Boulder, working with Jim Cowin.

Milton R. Cornwall-Brady

Washington State University, working with Lai-Sheng Wang.

Margaret S. Fyfield

Portland State University, working with Jim Cowin.

Jennifer M. Gaudioso

B.A. Bard College 1995; Science and Engineering Research Semester (SERS) student with Doug Ray.

Erik D. Sanchez

Portland State University, working with Sunney Xie.

Richard Webb

Washington State University, working with Wayne Hess; Ph.D. August 1995, now at Pacific Union College, Angwin, Cal.

Hongbin Wu

Washington State University, working with Lai-Sheng Wang.

Publications and Presentations

Publications

- A. H. Bahnmaier, A. G. Joly, J. M. Price, and D. Ray, "Ionization-Detected Rotational Coherence Spectroscopy of Mass-Selected Clusters," *Proc. SPIE* **2548**, 182-188 (1995) (*Laser Techniques for State-Selected and State-to-State Chemistry III*).
- R. X. Bian, R. C. Dunn, X. S. Xie, and P. T. Leung, "Single Molecule Emission Characteristics in Near-Field Microscopy," *Phys. Rev. Lett.* **75**, 4772-4775 (1995).
- T. A. Blake, C. Chackerian, Jr., and J. R. Podolske, "Prognosis for a Mid-Infrared Magnetic Rotation Spectrometer for the *in situ* Detection of Atmospheric Free Radicals," *Appl. Opt.* **35**, 973-985 (1996).
- T. A. Blake, S. Xu, and S. W. Sharpe, "High-Resolution Infrared Spectroscopy of the ν_4 Fundamental Band of Chlorine Nitrate," *J. Mol. Spectrosc.* **175**, 303-314 (1996).
- R. A. Bradley, Jr., E. Lanzendorf, M. I. McCarthy, T. M. Orlando, and W. P. Hess, "Molecular NO Desorption from Crystalline Sodium Nitrate by Resonant Excitation of the $\text{NO}_3^- \pi-\pi^*$ Transition," *J. Phys. Chem.* **99**, 11715-11721 (1995).
- B. M. Britt, J. L. McHale, and D. M. Friedrich, "Application of Time-Dependent Raman Theory to Raman Excitation Profiles of Hexamethylbenzene-Tetracyanoethylene Electron Donor-Acceptor Complex," *J. Phys. Chem.* **99**, 6347-6355 (1995).
- J. Conceicao, T. Laaksonen, L. S. Wang, T. Guo, P. Norflander, and R. E. Smalley, "Photoelectron Spectroscopy of Transition Metal Clusters: Correlation of Valence Electronic Structure to Reactivity," *Phys. Rev. B* **51**, 4668-4671 (1995).
- R. A. Crowell, G. R. Holtom, and X. S. Xie, "Infrared Free Induction Decay of Liquid Water Molecules," *J. Phys. Chem.* **99**, 1840-1842 (1995).
- R. Doolen and D. Ray, "Uptake of Gases by Aqueous Solutions Probed by Surface Nonlinear Optical Spectroscopy," *Proc. SPIE* **2547**, 364-370 (1995) (*Laser Techniques for Surface Science II*).
- R. C. Dunn, E. V. Allen, S. A. Joyce, G. A. Anderson, and X. S. Xie, "Near-field Fluorescent Imaging of Single Proteins," *Ultramicroscopy* **57**, 113-117 (1995).
- R. C. Dunn and X. S. Xie, "Characterization of the Temporal Behavior of Ultrashort Pulses Emerging from a Near-Field Fiber Probe," *Ultramicroscopy* **57**, 169-172 (1995).
- J. Fan, L. Lou, and L. S. Wang, " FeC_n^- and FeC_nH^- ($n = 3,4$): A Photoelectron Spectroscopic and Density Functional Study," *J. Chem. Phys.* **102**, 2701-2707 (1995).
- J. Fan, J. B. Nicholas, J. M. Price, S. D. Colson, and L.-S. Wang, " Si_3O_4^- : Vibrationally Resolved Photoelectron Spectrum and *ab Initio* Calculations," *J. Am. Chem. Soc.* **117**, 5417-5418 (1995).
- J. Fan and L.-S. Wang, "Photoelectron Spectroscopy of FeO^- and FeO_2^- : Observation of Low-Spin Excited States of FeO and Determination of the Electron Affinity of FeO_2^- ," *J. Chem. Phys.* **102**, 8714-8717 (1995).
- M. C. Gallagher, M. S. Fyfield, J. P. Cowin, and S. A. Joyce, "Imaging Insulating Oxides: Scanning Tunneling Microscopy of Ultrathin MgO Films on Mo(001)," *Surf. Sci.* **339**, L909-L913 (1995).
- G. R. Holtom, R. A. Crowell, and L. K. Cheng, "Femtosecond Mid-Infrared Optical Parametric Oscillator Based on CsTiOAsO_4 ," *Opt. Lett.* **20**, 1880-1882 (1995).
- G. R. Holtom, R. A. Crowell, and X. S. Xie, "High-Repetition-Rate Femtosecond Optical Parametric Oscillator-Amplifier System near $3 \mu\text{m}$," *J. Opt. Soc. Am. B* **12**, 1723-1731 (1995).
- J. F. Kelly and R. S. McDowell, "Environmental Analysis (Optical Spectroscopy)," *Encyclopedia of Energy Technology and the Environment*, A. Bisio and S. Boots, eds. (John Wiley & Sons, New York, 1995), 1268-1292.
- J. F. Kelly, S. W. Sharpe, and N. Chonacky, "FM Laser Techniques and Experiments," *CALIOPE Program Second Interim Technical Review* [Los Alamos, N.M., 28-30 Mar. 1995], *Proceedings* (U.S. Dept. of Energy, Office of Nonproliferation and National Security, Office of Research and Development, 1995), 1:223-234.
- G. A. Kimmel and T. M. Orlando, "Low-Energy (5-120 eV) Electron-Stimulated Dissociation of Amorphous D_2O Ice: $\text{D}(^2\text{S})$, $\text{O}(^3\text{P}_{2,1,0})$, and $\text{O}(^1\text{D}_2)$ Yields and Velocity Distributions," *Phys. Rev. Lett.* **75**, 2606-2609 (1995).
- G. A. Kimmel, R. G. Tonkyn, and T. M. Orlando, "Kinetic and Internal Energy Distributions of Molecular Hydrogen Produced from Amorphous Ice

- by Impact of 100 eV Electrons," *Nucl. Instrum. Methods Phys. Res., Sect. B* **101**, 179-183 (1995).
- K. Knutsen and T. M. Orlando, "Low-Energy (5-80 eV) Electron-Stimulated Desorption of H^+ (D^+), OH^+ (OD^+), O^+ , and NO^+ from Solution-Grown $NaNO_3$ Crystals," *Surf. Sci.* **348**, 143-152 (1996).
- B. Lerner, J. Birmingham, R. Tonkyn, S. Barlow, and T. Orlando, "Decomposition of Trichloroethylene by a Large Scale, High Flow Packed-Bed Gas Phase Corona Reactor," *Proceedings of the 12th International Symposium on Plasma Chemistry*, J. V. Heberlein, D. W. Ernie, and J. T. Roberts, eds. (Univ. Minnesota, 1995), 697-703.
- R. S. McDowell, J. F. Kelly, and S. W. Sharpe, "Pacific Northwest Laboratory CALIOPE Overview," *CALIOPE Program Second Interim Technical Review* [Los Alamos, N.M., 28-30 Mar. 1995], *Proceedings* (U.S. Dept. of Energy, Office of Nonproliferation and National Security, Office of Research and Development, 1995), 1:13-15.
- M. B. More, E. D. Glendening, D. Ray, D. Feller, and P. B. Armentrout, "Cation-Ether Complexes in the Gas Phase: Bond Dissociation Energies and Equilibrium Structures of $Li^+(O(CH_3)_2)_x$ ($x = 1-4$)," *J. Phys. Chem.* **100**, 1605-1614 (1996).
- R. J. Nemzek, J. J. Tiee, L. J. Jolin, S. W. Sharpe, J. F. Kelly, and R. S. McDowell, "Albedo Measurements at CO_2 Laser Wavelengths," *CALIOPE Program Second Interim Technical Review* [Los Alamos, N.M., 28-30 Mar. 1995], *Proceedings* (U.S. Dept. of Energy, Office of Nonproliferation and National Security, Office of Research and Development, 1995), 1:312-316.
- J. B. Nicholas, J. Fan, H. Wu, S. D. Colson, and L.-S. Wang, "A Combined Density Functional Theoretical and Photoelectron Spectroscopic Study of Ge_2O_2 ," *J. Chem. Phys.* **102**, 8277-8280 (1995).
- A. J. Peurrung, S. E. Barlow, and R. T. Kouzes, "Coupled Gyrotors: A Paradigm for Space-Charge Effects in Cyclotron Mass Spectrometry," *Non-Neutral Plasma Physics II*, J. Fajans and D. H. E. Dubin, eds. (AIP Conference Proceedings **331**, American Institute of Physics, New York, 1995), 129-138.
- A. Peurrung, J. P. Cowin, G. Teeter, S. E. Barlow, and T. M. Orlando, "Space-Charge-Induced Acceleration of Ions Emitted by Laser-Irradiated Surfaces," *J. Appl. Phys.* **78**, 481-488 (1995).
- S. W. Sharpe, Book Review: *Introduction to Modern Vibrational Spectroscopy* by Max Diem, *Laser Focus World* **31** (9), 188 (Sept. 1995).
- S. W. Sharpe, "Adhesives," *Sailplane Modeler* **1** (3), 18-24 (Feb. 1996).
- S. W. Sharpe, R. S. McDowell, and J. F. Kelly, "Infrared Spectroscopy Efforts for CALIOPE," *CALIOPE Program Second Interim Technical Review* [Los Alamos, N.M., 28-30 Mar. 1995], *Proceedings* (U.S. Dept. of Energy, Office of Nonproliferation and National Security, Office of Research and Development, 1995), 1:208-214.
- R. J. Speedy, P. G. Debenedetti, C. Huang, R. S. Smith, and B. D. Kay, "The Entropy of Glassy Water," *Physical Chemistry of Aqueous Systems: Meeting the Needs of Industry*, J. H. J. White, J. V. Sengers, D. B. Neumann, and J. C. Bellows, eds. (Proc. 12th Internat. Conf. on Properties of Water and Steam, Orlando, Fla., September 12-16, 1994) (Begell House, New York, 1995), 347-354.
- L.-S. Wang, H.-S. Cheng, and J. Fan, "Photoelectron Spectroscopy of Size-Selected Transition Metal Clusters: Fe_n^- , $n = 3-24$," *J. Chem. Phys.* **102**, 9480-9493 (1995).
- L.-S. Wang, H.-S. Cheng, and J. Fan, "Probing the Electronic Structure of Small Iron Clusters," *Chem. Phys. Lett.* **236**, 57-63 (1995).
- L. S. Wang, H. Wu, S. R. Desai, and L. Lou, "Electronic Structure of Small Copper Oxide Clusters: From Cu_2O to Cu_2O_4 ," *Phys. Rev. B* **53**, 8028-8031 (1996).
- H. Wu, S. R. Desai, and L.-S. Wang, "Two Isomers of CuO_2 : The $Cu(O_2)$ Complex and the Copper Dioxide," *J. Chem. Phys.* **103**, 4363-4366 (1995).
- H. Wu, S. R. Desai, and L.-S. Wang, "Electronic Structure of Small Titanium Clusters: Emergence and Evolution of the 3d Band," *Phys. Rev. Lett.* **76**, 212-215 (1996).
- X. S. Xie and R. C. Dunn, "Near-Field Single Molecule Spectroscopy," *Proc. SPIE* **2385**, 95-102 (1995) (*Advanced Optical Methods for Ultrasensitive Detection*).
- S. Xu, R. S. McDowell, S. W. Sharpe, and B. J. Krohn, "Rovibrational Spectroscopy of $C^{35}Cl_4$," *J. Mol. Spectrosc.* **173**, 431-441 (1995).
- X.-L. Zhou and J. P. Cowin, "Photodestruction of CCl_4 on MgO Films with/without Water," *J. Phys. Chem.* **100**, 1055-1065 (1996).

In Press and Submitted

- C. C. Ainsworth, D. M. Friedrich, P. L. Gassman, and Z. Wang, "Fluorescence Spectroscopy of Salicylate Sorbed at the Al_2O_3 Surface," *Geochim. Cosmochim. Acta*, submitted.
- K. M. Beck, K. A. H. German, and W. P. Hess, "Thermal Distributions Deduced from (2+1) REMPI of CO Products," *Chem. Phys. Lett.*, submitted.
- D. E. Brown, S. M. George, C. Huang, E. K. L. Wong, K. B. Rider, R. S. Smith, and B. D. Kay, " H_2O Condensation Coefficient and Refractive Index for Vapor-Deposited Ice From Molecular Beam and Optical Interference Measurements," *J. Phys. Chem.*, in press.
- J. A. Campbell, S. C. Goheen, K. L. Wahl, and W. P. Hess, "Matrix-Assisted Laser Desorption Ionization-TOF of Low Molecular Weight Organics," *J. Anal. Chem.*, submitted.
- H. S. Cheng and L. S. Wang, "Dimer Growth, Structure Transition, and Antiferromagnetic Ordering in Small Chromium Clusters," *Science*, submitted.
- S. R. Desai, H. Wu, and L.-S. Wang, "Vibrationally Resolved Photoelectron Spectroscopy of AlO^- and AlO_2^- ," *Int. J. Mass Spectrom. Ion Processes*, submitted.
- G. S. Herman, M. C. Gallagher, S. A. Joyce, and C. H. F. Peden, "Epitaxial Growth of Thin TiO_x Films on W(110)," *J. Vac. Sci. Technol.*, in press.
- W. P. Hess, K. A. H. German, R. A. Bradley, and M. I. McCarthy, "Laser Ablation of Sodium Nitrate: NO Desorption Following Excitation of the $\pi-\pi^*$ Band of the Nitrate Anion," *Appl. Surf. Sci.*, in press.
- M. C. Hsiao, B. T. Merritt, B. M. Penetrante, G. E. Vogtlin, P. H. Wallman, R. G. Tonkyn, R. Shah, and T. M. Orlando, "Plasma Assisted Oxidation of Propene," *J. Oxid. Tech.*, in press.
- O. Kornienko, S. Brynjelsen, L. Hanley, and T. M. Orlando, "Analysis of Ethylenediaminetetraacetic acid (EDTA) by Laser Desorption Ion Trap Mass Spectrometry," *Anal. Chem.*, submitted.
- B. L. Maschhoff, M. J. Iedema, M. Kwini, and J. P. Cowin, "Long-Range Electrostatic Forces in the Coadsorption of CH_3Cl and Water," *Surf. Sci.*, in press.
- M. I. McCarthy, K. A. Peterson, and W. P. Hess, "Electronic Structure of Sodium Nitrate: Investigations of Laser Desorption Mechanisms," *J. Phys. Chem.*, in press.
- R. S. McDowell, "Infrared Spectroscopy" and (in part) "Molecular Structure and Spectra," *McGraw-Hill Encyclopedia of Science & Technology*, 8th ed. (McGraw Hill Book Co., 1996), in press.
- A. J. Peurrung, S. E. Barlow, and R. T. Kouzes, "The Nonneutral Plasma: an Introduction to Physics with Relevance to Cyclotron Resonance Mass Spectrometry," *Int. J. Mass Spect. Ion Processes*, in press.
- R. S. Smith, C. Huang, E. K. L. Wong, and B. D. Kay, "Desorption and Crystallization Kinetics in Nanoscale Thin Films of Amorphous Water Ice," *Phys. Rev. Lett.*, submitted.
- R. J. Speedy, P. G. Debenedetti, R. S. Smith, C. Huang, and B. D. Kay, "The Evaporation Rate, Free Energy, and Entropy of Amorphous Water at 150 K," *J. Chem. Phys.*, submitted.
- M. J. Stirniman, C. Huang, R. S. Smith, S. A. Joyce, and B. D. Kay, "The Adsorption and Desorption of Water on Single-Crystal $\text{MgO}(100)$: The Role of Surface Defects," *J. Chem. Phys.*, submitted.
- S. C. Stone, L. A. Philips, G. T. Fraser, F. J. Lovas, L.-H. Xu, and S. W. Sharpe, "High-Resolution Microwave and Infrared Molecular Beam Studies of the Conformers of 1,1,2,2-Tetrafluoroethane," *J. Mol. Spectrosc.*, submitted.
- K. D. Thrall, J. J. Toth, and S. W. Sharpe, "Analysis of Exhaled Breath by Laser Detection," *Proc. SPIE*, in press (*Bios '96 Conference*).
- R. G. Tonkyn, S. E. Barlow, and T. M. Orlando, "Destruction of Carbon Tetrachloride in a Dielectric Barrier/Packed Bed Corona Reactor," *J. Appl. Phys.*, accepted.
- L. S. Wang, "Study of Iron-Carbon Mixed Clusters, FeC_n ($n = 2-5$): A Possible Linear to Cyclic Transition From FeC_3 to FeC_4 ," *Surf. Rev. Lett.*, in press.
- L. S. Wang, J. Fan, and L. Lou, "Iron Clusters and Oxygen-Chemisorbed Iron Clusters," *Surf. Rev. Lett.*, in press.
- L. S. Wang and H. Wu, "A Comparative Study of the Electronic Structure of the First Row Transition Metal Clusters," *Proc. Int. Symp. on the Science and Technology of Atomically Engineered Materials*, Oct. 30 - Nov. 4, 1995, Richmond, Va., in press.

L. S. Wang, H. Wu, and S. R. Desai, "Sequential Oxygen Chemisorption on Surfaces of Small Iron Clusters," *Phys. Rev. Lett.*, submitted.

L. S. Wang, H. Wu, S. R. Desai, J. Fan, and S. D. Colson, "A Photoelectron Spectroscopic Study of Small Silicon Oxide Clusters: SiO_2 , Si_2O_3 , and Si_2O_4 ," *J. Phys. Chem.*, submitted.

H. Wu, S. R. Desai, and L. S. Wang, "Observation and Photoelectron Spectroscopic Study of Novel Mono- and Di-iron Oxide Molecules: FeO_y^- ($y = 1-4$) and Fe_2O_y^- ($y = 1-5$)," *J. Am. Chem. Soc.*, submitted.

X. S. Xie, R. X. Bian, and R. C. Dunn, "Near-Field Microscopy and Spectroscopy of Single Molecules, Single Proteins, and Biological Membranes," in *Focus of Modern Microscopy*, J. L. Wu and P. C. Chen, eds. (World Scientific, 1996), in press.

Presentations (Presenter underlined)

C. C. Ainsworth, D. M. Friedrich, and P. L. Gassman, "Fluorescence Spectroscopy of Salicylate-Aluminum Oxide Surface Complexes," Western Spectroscopy Association, Pacific Grove, Cal., Feb. 1-3, 1995.

R. Doolen and D. Ray, "Uptake of Gases by Aqueous Solutions Probed by Surface Nonlinear Optical Spectroscopy," SPIE 40th Annual Meeting on Laser Spectroscopy and Molecular Dynamics, San Diego, Cal., July 9-14, 1995.

R. C. Dunn, L. Mets, and X. S. Xie, "Application of Near-Field Spectroscopy to Photosynthetic Research," 3rd International Conference on Near-Field Optics, Brno, Czech Repub., May 9-11, 1995.

J. Fan, J. B. Nicholas, S. D. Colson, and L. S. Wang, " Si_3O_x : Photoelectron Spectra and Theoretical Calculations," Gordon Research Conference on Molecular and Ionic Clusters, Oxnard, Cal., Jan. 8-13, 1995.

J. Fan, J. B. Nicholas, S. D. Colson, and L. S. Wang, "Structure and Bonding of Silicon Oxide Clusters," APS 1995 March Meeting, San Jose, Cal., March 20-24, 1995.

J. Fan and L. S. Wang, "Photoelectron Spectroscopy of Fe_xO_y^- Clusters," APS 1995 March Meeting, San Jose, Cal., March 20-24, 1995.

J. Fan, L. S. Wang, and L. Lou, "Metal-Carbon Bond: A Photoelectron Spectroscopy Study of FeC_xH_y^- ($x = 2-5$, $y = 0,1$)," 209th ACS National

Meeting, Anaheim, Cal., April 2-7, 1995.

M. S. Fyfield, M. C. Gallagher, J. P. Cowin, and S. A. Joyce, "STM of Thin-Film MgO Grown on Mo(001)," Oregon Academy of Sciences, Portland, Feb. 1995.

M. S. Fyfield, M. C. Gallagher, J. P. Cowin, and S. A. Joyce, "STM of Thin-Film MgO Grown on Mo(001)," Department of Chemistry, University of California at Irvine, Feb. 14, 1995.

M. S. Fyfield, M. C. Gallagher, J. P. Cowin, and S. A. Joyce, "STM of Thin-Film MgO Grown on Mo(001)," Environmental Engineering Department, California Institute of Technology, Pasadena, Feb. 15, 1995.

M. C. Gallagher, M. S. Fyfield, and S. A. Joyce, "Stranski-Krastanov Growth of Mg on Mo(001)," Pacific Northwest Symposium of American Vacuum Society, Troutdale, Ore., Sept. 21, 1995.

M. C. Gallagher, M. S. Fyfield, and S. A. Joyce, "Growth of Mg on Mo(001)," National Meeting, American Vacuum Society, Minneapolis, Minn., Oct. 16-20, 1995.

M. C. Gallagher, M. S. Fyfield, and S. A. Joyce, "Stranski-Krastanov Growth of Mg on Mo(001)," Materials Research Society, Boston, Nov. 26-30, 1995.

M. C. Gallagher, G. S. Herman, C. H. F. Peden, and S. A. Joyce, "Structure of Ultrathin TiO_x Films Grown on W(110)," American Physical Society, San Jose, Cal., Mar. 20-24, 1995.

M. C. Gallagher, G. S. Herman, C. H. F. Peden, and S. A. Joyce, "Structure and Growth of Ultrathin TiO_x Films Grown on W(110)," STM '95, Snowmass, Col., July 23-28, 1995.

M. C. Gallagher, G. S. Herman, C. H. F. Peden, and S. A. Joyce, "Structure and Growth of Ultrathin TiO_x Films on W(110)," American Vacuum Society 42nd National Symposium, Minneapolis, Minn., Oct. 16-20, 1995.

M. C. Gallagher, S. A. Joyce, M. S. Fyfield, and J. P. Cowin, "Growth of Ultrathin Films of MgO on Mo(001)," STM '95, Snowmass, Col., July 23-28, 1995.

G. S. Herman, M. C. Gallagher, S. A. Joyce, and C. H. F. Peden, "Interaction of D_2O with Model Oxide Single Crystal Surfaces: Clean and Oxidized W(110)," American Chemical Society, Chicago, Aug. 1995.

- G. S. Herman, M. C. Gallagher, S. A. Joyce, and C. H. F. Peden, "Interaction of D₂O with Model Oxide Single Crystal Surfaces: Clean and Oxidized W(110)," American Vacuum Society 7th Annual Pacific Northwest Symposium, Troutdale, Ore., Sept. 20–21, 1995.
- W. P. Hess, K. A. H. German, R. A. Bradley, T. Orlando, and M. I. McCarthy, "Surface Photochemistry without an Adsorbate, or Laser Desorption of Sodium Nitrate in the 6 eV Band," Western Spectroscopy Association, Asilomar, Cal., Feb. 1995.
- W. P. Hess, K. A. H. German, and R. Webb, "Laser Ablation/Ionization Characterization of Solids," Strategic Environmental Research Development Program Symposium, Washington, D.C., April 1995.
- W. P. Hess, K. A. H. German, R. A. Bradley, T. Orlando, and M. I. McCarthy, "Laser Ablation of Sodium Nitrate: NO Desorption Following Excitation of the π - π^* Band of the Nitrate Anion," European Materials Research Society Spring Meeting, Conference on Laser Ablation, Strasbourg, France, May 1995.
- W. P. Hess, K. A. H. German, R. A. Bradley, K. Peterson, T. Orlando, and M. I. McCarthy, "Molecular NO Desorption from Sodium Nitrate by Resonant Excitation of a π - π^* Transition in NO₃ Anion," American Chemical Society Regional Meeting, Park City, Utah, June 1995.
- W. P. Hess, S. Deshmukh, and R. A. Bradley, "Laser Ionization Probing of Molecular Product State Distributions: Photodissociation of Isolated Molecules and Photodesorption from Ionic Crystals," Physics Department Colloquium, Washington State University, Pullman, Sept. 1995.
- W. P. Hess, K. A. H. German, R. A. Bradley, and M. I. McCarthy, "Laser Desorption from Resonant Excitation of Molecular Ionic Crystals," Chemistry Department Colloquium, Colorado State University, Fort Collins, Sept. 1995.
- W. P. Hess, K. A. H. German, R. A. Bradley, and M. I. McCarthy, "Laser Desorption from Resonant Excitation of Molecular Ionic Crystals," Chemical Physics Colloquium, University of Colorado, Boulder, Sept. 1995.
- S. A. Joyce and M. C. Gallagher, "A Model for Scanning Tunneling Microscopy of Ultrathin Film Insulators," National Meeting, American Vacuum Society, Minneapolis, Minn., Oct. 16–20, 1995.
- S. A. Joyce, M. C. Gallagher, M. S. Fyfield, and J. P. Cowin, "Growth of Ultrathin Films of MgO on Mo(001)," American Physical Society, San Jose, Cal., Mar. 20–24, 1995.
- B. D. Kay, "Overview of Recent Advances in Gas-Surface Dynamics," 1995 Conference on the Dynamics of Molecular Collisions, Asilomar, Cal., July 16–21, 1995. (Invited.)
- B. D. Kay, "Adsorption, Desorption, Phase Transformation, and Diffusion Kinetics in Nanoscale Ice Films," Workshop on the Nature of Hydrogen Bonding in Ice and Water, Richland, Wash., September 25, 1995. (Invited.)
- B. D. Kay, "Adsorption, Desorption, Mixing, and Solvation Kinetics of Mixed Methanol and Water Multilayer Ices," American Vacuum Society 42nd National Symposium, Minneapolis, Minn., Oct. 16–20, 1995.
- B. D. Kay, "Adsorption, Desorption, Mixing, and Solvation Kinetics of Mixed Methanol and Water Multilayer Ices," Argonne National Laboratory, Argonne, Ill., Oct. 23, 1995.
- B. D. Kay and K. R. Lykke, "Quantum-Resolved Reactive Gas-Surface Scattering: H + Au(111):Cl → HCl(*v*,*j*)," 209th American Chemical Society National Meeting, Anaheim, Cal., April 2–6, 1995. (Invited.)
- G. A. Kimmel, "A REMPI Study of Low-Energy (5–120 eV) Electron-Stimulated Interactions in Amorphous D₂O Ice," American Vacuum Society 42nd National Symposium, Minneapolis, Minn., Oct. 16–20, 1995.
- B. Lerner, J. Birmingham, R. Tonkyn, S. Barlow, and T. Orlando, "Decomposition of Trichloroethylene by a Large Scale, High-Flow Packed Bed Gas Phase Corona Reactor," 12th International Symposium on Plasma Chemistry, Minneapolis, Minn., Aug. 12–15, 1995.
- R. S. McDowell, "PNL/CALIOPE Overview," Second Annual Interim Technical Review, CALIOPE Program (Chemical Analysis by Laser Interrogation of Proliferant Effluents), Los Alamos, N.M., March 28–30, 1995.
- T. M. Orlando, "Quantum-Resolved Studies of Low-Energy (5–120 eV) Electron-Stimulated Interactions at Wet Interfaces," Argonne National Laboratory, May 16, 1995.

T. M. Orlando, "Quantum-Resolved Studies of Low-Energy (5–120 eV) Electron-Stimulated Interactions at Wet Interfaces," Physical Chemistry Colloquium, Northwestern University, Evanston, Ill., May 17, 1995.

T. M. Orlando, "Quantum-Resolved Studies of Low-Energy (5–120 eV) Electron-Stimulated Interactions at Wet Interfaces," Radiation Laboratory, Notre Dame University, South Bend, Ind., May 18, 1995.

T. M. Orlando, R. G. Tonkyn, and S. E. Barlow, "The Destruction of Chlorinated Hydrocarbons in Packed-Bed Coronas," APS 48th Annual Gaseous Electronics Conference, Berkeley, Cal., Oct. 9–13, 1995. (Invited.)

T. M. Orlando, "Quantum-Resolved Studies of Electron-Stimulated Reactions in Amorphous and Crystalline Water Ice," Physical Chemistry Colloquium, University of Utah, Salt Lake City, Oct. 16, 1995.

T. M. Orlando, "Quantum-Resolved Studies of Electron-Stimulated Reactions in Amorphous and Crystalline Water Ice," Physical Chemistry Colloquium, University of Rochester, Nov. 27, 1995.

T. M. Orlando, "Probing Radiolysis via Quantum-Resolved Studies of Low-Energy (5–120 eV) Electron Stimulated Reactions in Amorphous Ice," Brookhaven National Laboratory, Upton, N.Y., Nov. 28, 1995.

D. Ray, "Collective Effects on Electronic Structure and Reaction Dynamics in Molecular Clusters," NAIR '95 Workshop on Cluster Science, Tsukuba, Japan, March 7–9, 1995. (Invited.)

D. Ray, "Collective Effects on Electronic Structure and Reaction Dynamics in Molecular Clusters," Department of Pure and Applied Sciences, College of Arts and Sciences, University of Tokyo, March 10, 1995. (Invited.)

D. Ray, "Transport of Molecules across the Liquid Water–Vapor Interface Probed by Surface Nonlinear Optical Spectroscopy," Department of Chemistry, University of Utah, Salt Lake City, Nov. 1995. (Invited.)

D. Ray, A. H. Bahnmaier, A. G. Joly, and J. M. Price, "High Resolution Time Domain Spectroscopy of Mass Selected Clusters," Gordon Research Conference on Molecular and Ionic Clusters, Oxnard, Cal., Jan. 8–13, 1995.

D. Ray, A. H. Bahnmaier, V. A. Venturo, A. G. Joly, and J. M. Price, "High Resolution Time Domain Spectroscopy of Mass Selected Clusters," SPIE 40th Annual Meeting on Laser Spectroscopy and Molecular Dynamics, San Diego, Cal., July 9–14, 1995.

D. Ray, M. B. More, P. B. Armentrout, E. D. Glendening, and D. Feller, "Bond Dissociation Energies and Structures of Complexes of Li⁺ with Monodentate and Multidentate Ether Ligands," Gordon Research Conference on Structure, Energetics, and Reaction Dynamics of Gaseous Ions, Ventura, Cal., Feb. 27 – March 3, 1995.

S. W. Sharpe, "Analysis of Automobile Exhaust by FTIR and Chemometrics for Ozone Formation Potential," Energy Research Consortium, Detroit, Mich., Jan. 17, 1995.

S. W. Sharpe, "Infrared Spectroscopy Efforts for CALIOPE," Second Annual Interim Technical Review, CALIOPE Program (Chemical Analysis by Laser Interrogation of Proliferant Effluents), Los Alamos, N.M., March 28–30, 1995.

S. W. Sharpe, "High-Resolution Infrared Spectroscopy at PNL," National Institute of Standards and Technology, Gaithersburg, Md., April 24, 1995.

S. W. Sharpe, "High-Resolution Infrared Spectroscopy at PNL," Oregon State University Chemistry Seminar, Corvallis, Oct. 10, 1995.

R. S. Smith, C. Huang, M. J. Stirniman, E. K. L. Wong, and B. D. Kay, "Molecular Beam Studies of Adsorption, Desorption, and Diffusion Kinetics in Nanoscale Ice Films," American Vacuum Society 42nd National Symposium, Minneapolis, Minn., Oct. 16–20, 1995. (Invited.)

R. S. Smith, C. Huang, E. K. L. Wong, and B. D. Kay, "Adsorption, Desorption and Phase Transformation Kinetics in Nanoscale Ice Films," Gordon Research Conference on Surface Reactions, Ventura, Cal., January 22–27, 1995. (Invited.)

R. S. Smith, C. Huang, E. K. L. Wong, and B. D. Kay, "Adsorption, Desorption and Phase Transformation Kinetics in Nanoscale Ice Films," American Physical Society 1995 National Meeting, San Jose Cal., March 20–24, 1995. (Invited.)

R. S. Smith, C. Huang, E. K. L. Wong, and B. D. Kay, "Mobility and Crystallization of Amorphous Water Ice in Nanoscale Thin Films," 55th Physical Electronics Conference, Flagstaff, Ariz., June 10–15, 1995.

R. S. Smith, C. Huang, E. K. L. Wong, and B. D. Kay, "Adsorption, Desorption, Phase Transformation and Diffusion Kinetics in Nanoscale Ice Films," Conference on the Dynamics of Molecular Collisions, Asilomar, Cal., July 16–21, 1995.

R. S. Smith, C. Huang, E. K. L. Wong, and B. D. Kay, "Adsorption, Desorption, Phase Transformation and Diffusion Kinetics in Nanoscale Ice Films," Gordon Research Conference on Dynamics at Surfaces, Andover, N.H., Aug. 6–11, 1995.

R. S. Smith, C. Huang, E. K. L. Wong, and B. D. Kay, "Adsorption, Desorption, Phase Transformation and Diffusion Kinetics in Nanoscale Ice Films," Gordon Research Conference on the Physics and Chemistry of Liquids, Plymouth, N.H., August 6–11, 1995.

M. J. Stirniman, C. Huang, R. S. Smith, S. A. Joyce, and B. D. Kay, "Kinetics of Water Adsorption, Desorption, and Dissociation on MgO(100)," American Vacuum Society 7th Annual Pacific Northwest Symposium, Troutdale, Ore., Sept. 20–21, 1995.

R. G. Tonkyn, S. E. Barlow and T. M. Orlando, "Destruction of Chlorinated Hydrocarbons in a Packed-Bed Corona Reactor," 1995 World Environmental Congress, London, Ont., Sept. 17–22, 1995.

M. J. Stirniman, C. Huang, R. S. Smith, S. A. Joyce, and B. D. Kay, "Kinetics of Water Adsorption, Desorption, and Dissociation on MgO(100)," American Vacuum Society 42nd National Symposium, Minneapolis, Minn., Oct. 16–20, 1995.

L. S. Wang, "On the Electronic Structure of Transition Metal Clusters," APS 1995 March Meeting, San Jose, Cal., March 20–24, 1995.

L. S. Wang, "Studying the Surface Chemical Bond by Using Cluster Models," 209th ACS National Meeting, Anaheim, Cal., April 2–7, 1995.

L. S. Wang, "Oxidation of Metal and Semiconductor Clusters," Gordon Research Conference on Metal and Semiconductor Clusters, Colby-Sawyer College, New London, N.H., Aug. 1995.

L. S. Wang, "A Comparative Study of the Electronic Structure of the First Row Transition Metal Clusters," International Symposium of the Sciences and Technology of Atomically Engineered Materials, Richmond, Va., Oct. 30 – Nov. 4, 1995.

L. S. Wang, "Electronic and Structural Evolution of Transition Metal Clusters," Physics Collo-

quium, Department of Physics, Washington State University, Pullman, Nov. 16, 1995. (Invited.)

L. S. Wang, J. Fan, and H.-S. Cheng, "Probing the Electronic Structure of Transition Metal Clusters," 209th ACS National Meeting, Anaheim, Cal., April 2–7, 1995.

L. S. Wang, J. Fan, J. B. Nicholas, L. Lou, and S. D. Colson, "Cluster Models of Surfaces," 209th ACS National Meeting, Anaheim, Cal., April 2–7, 1995.

H. Wu, J. Fan, and L.-S. Wang, "Evolution of the Electronic Structure of Small Chromium Clusters: A Possible Nonmetal-Metal Transition," 209th ACS National Meeting, Anaheim, Cal., April 2–7, 1995.

X. Xie, "Molecular Spectroscopy on a Single-Molecule Basis," Portland State University, Portland, Ore., Jan. 12, 1995. (Invited.)

X. Xie, "Studying Single-Molecule Dynamics with Near-Field Fluorescence Spectroscopy," 42nd Western Spectroscopy Association, Pacific Grove, Cal., Jan. 26–28, 1995. (Invited.)

X. Xie, "Near-Field Time-Resolved Fluorescence Spectroscopy of Single Molecules and Photosynthetic Membranes," Photonics West '95, San Jose, Cal., Feb. 4–10, 1995. (Invited.)

X. Xie, "Near-Field Spectroscopy of Single Molecules and Photosynthetic Membranes," Arizona State University, Tempe, Feb. 16, 1995. (Invited.)

X. Xie, "Probing Single-Molecule Dynamics," American Physical Society, San Jose, Cal., Mar. 20–24, 1995. (Invited.)

X. Xie, "Single-Molecule Fluorescence Microscopy and Spectroscopy with Near-Field Optics," International Conference of Confocal Microscopy, Taipei, Taiwan, Apr. 18–20, 1995. (Invited.)

X. Xie, "Probing Single-Molecule Dynamics," Hong Kong University of Science and Technology, Apr. 25, 1995.

X. Xie, "Near-Field Fluorescence Spectroscopy on Single Molecules and Photosynthetic Systems," 9th DOE Solar Photochemistry Research Conference, Tamiment, Pa., June 5–9, 1995. (Invited.)

X. Xie, "Single Molecule/ Single Protein Fluorescence Spectroscopy," STM '95—8th International Conference on Scanning Tunneling Microscopy/ Spectroscopy, Snowmass Village, Col., July 23–28, 1995. (Invited.)

X. Xie, "Probing Single-Molecule Dynamics with Near-Field Optics," Gordon Research Conference on Dynamics at Surfaces, Andover, N.H., Aug. 6-11, 1995. (Invited.)

X. Xie, "Room-Temperature Single-Molecule Spectroscopy," Dept. of Chemistry, University of California at Los Angeles, Nov. 6, 1995. (Invited.)

X. S. Xie and R. C. Dunn, "Probing Single-Molecule Spectroscopy and Dynamics," 209th American Chemical Society Meeting, Anaheim, Cal., Apr. 2-7, 1995. (Invited.)

X. S. Xie and R. C. Dunn, "Near-Field Single-Molecule Spectroscopy," 3rd International Conference on Near-Field Optics, Brno, Czech Republic, May 9-11, 1995.

S. Xu, T. A. Blake, and S. W. Sharpe, "Rovibrational Spectrum of the ν_4 Band of

ClONO_2 ," 209th American Chemical Society Meeting, Anaheim, Cal., Apr. 2-7, 1995.

S. Xu, T. A. Blake, and S. W. Sharpe, "High Resolution Infrared Spectroscopy of the ν_4 Band of Chlorine Nitrate in a Pulsed, Slit Jet Expansion: Observation and Analysis," 50th Ohio State University International Symposium on Molecular Spectroscopy, Columbus, June 12-16, 1995.

S. Xu, R. S. McDowell, S. W. Sharpe, and B. J. Krohn, "Rovibrational Spectroscopy of CCl_4 ," 50th Ohio State University International Symposium on Molecular Spectroscopy, Columbus, June 12-16, 1995.

S. Xu, S. W. Sharpe, and G. T. Fraser, "Diode Laser Spectroscopy of Ar-NH_3 Complex," 50th Ohio State University International Symposium on Molecular Spectroscopy, Columbus, June 12-16, 1995.

Awards and Recognition

The Coblenz Society, a professional organization that fosters the understanding and application of vibrational spectroscopy in the academic and industrial communities, announced that **Sunney Xie** is the 1996 winner of the Coblenz Award, presented annually since 1964 to an outstanding spectroscopist under the age of 36, for his work in near-field fluorescence spectroscopy on individual molecules in their natural biochemical environment.

Collaborations

Outside Collaborations

- J. P. Cowin
University of Colorado (G. B. Ellison)
Molecular Dynamics at the Water/Solid Interface
- D. M. Friedrich
University of Idaho (J. L. McHale)
Raman Excitation Profiles of Electron Donor-Acceptor Complexes
- D. M. Friedrich
University of Oregon (B. S. Hudson and H. B. Lueck)
Electronic Structure of Substituent-Perturbed Benzenes by Deep UV Resonance Raman Spectroscopy
- D. M. Friedrich
Oregon State University (G. Turner)
Laser Raman Study of Uranyl Surface Complex Speciation
- W. P. Hess
University of Central Florida (K. M. Beck)
Studies of Laser/Solid Interactions
- W. P. Hess
University of Utah (C. A. Wight)
Photochemistry of Thin Molecular Films
- W. P. Hess
Washington State University (J. T. Dickinson, R. Webb, and K. A. Peterson)
Laser Ablation Characterization of Solids
- B. D. Kay
Chalmers University, Göteborg, Sweden (B. Kasemo)
Desorption and Phase Transformation Kinetics in Amorphous Ice
- B. D. Kay
University of Colorado (S. M. George)
Optical Properties and Porosity of Vapor Deposited Ice Films
- B. D. Kay
University of Wellington, N.Z. (R. J. Speedy) and Princeton University (P. G. Debenedetti)
Metastability of Glassy Water and its Relation to Liquid Water
- R. S. McDowell
Los Alamos National Laboratory (B. J. Krohn)
Rovibrational Analysis of High-Symmetry Molecules
- T. M. Orlando
University of Illinois (L. Hanley)
Laser Ablation Mass Spectrometry
- T. M. Orlando
Lawrence Livermore National Laboratory (J. N. Bardsley and B. M. Penetrante)
Development of Plasma Processing Techniques
- T. M. Orlando
University of Sherbrooke (L. Sanche)
Low-Energy Electron-Stimulated Processes in Water Overlayers
- D. Ray
University of Utah (P. B. Armentrout)
Gas-Phase Cation-Ether Complexes
- S. W. Sharpe
National Institute for Standards and Technology (G. T. Fraser and A. S. Pine)
Rovibrational Spectral Analysis of Molecular Clusters
- S. W. Sharpe
Oregon State University (J. W. Nibler)
Jet Spectroscopy of Metal Borohydrides
- L. S. Wang
Air Products and Chemicals, Inc., Allentown, Pa. (H. S. Chen)
Quantum Chemistry Calculations on Metal Clusters
- L. S. Wang
Rice University (L. Lou)
Density Functional Calculations on Metal Clusters
- L. S. Wang
Washington State University (H. Wu)
Spectroscopy and Structure of Metal Clusters
- X. S. Xie
University of Chicago (L. Mets)
Spectroscopic Mapping of Photosynthetic Membranes
- X. S. Xie
Portland State University (P. T. Leung)
Theoretical Modeling of Molecule-Metal Interactions in Near-Field Spectroscopy

Collaborations within PNNL

S. E. Barlow

Environmental and Energy Sciences Division (EESD), Materials and Chemical Sciences Department (A. J. Peurrung)

Stabilization of Nonneutral Plasmas

S. D. Colson and R. S. McDowell

Energy Division, Engineering and Analytical Sciences Department, Sensors and Measurement Systems Section (J. S. Hartman); and EESD, Materials and Chemical Sciences Department, Atomic and Molecular Chemistry Section (M. L. Alexander)

Waste Tank Speciation Methods

D. M. Friedrich

EESD Earth Systems Sciences Department, Interfacial Geochemistry Section (C. C. Ainsworth)

Bonding and Structure of Organic Ligands at Oxide/Water Interfaces

D. M. Friedrich

EESD Earth Systems Sciences Department, Thermodynamic and Molecular Geochemistry Section (L. Rao and A. R. Felmy)

Lanthanide Carbonate Speciation by Laser-Induced Fluorescence

W. P. Hess

EESD Materials and Chemical Sciences Department, Atomic and Molecular Chemistry Section (J. A. Campbell)

Laser Ablation Characterization of Solids

W. P. Hess

EMSL Theory, Modeling, and Simulation (M. I. McCarthy, S. S. Xantheas, and J. D. Myers)

Studies of Laser/Solid Interactions

S. A. Joyce

EESD Materials and Chemical Sciences Department (B. C. Bunker)

Physics and Chemistry of Ceramic Surfaces

S. A. Joyce

EMSL Materials and Interfaces (M. A. Henderson); and EESD Earth Systems Sciences Department, Thermodynamic and Molecular Geochemistry Section (J. R. Rustad)

Surface Chemistry of Iron Oxides

S. A. Joyce

EMSL Materials and Interfaces (C. H. F. Peden)

Structure of TiO Thin Films

B. D. Kay

EESD Materials and Chemical Sciences Department (B. C. Bunker)

Physics and Chemistry of Ceramic Surfaces

T. M. Orlando

EESD Materials and Chemical Sciences Department, Atomic and Molecular Chemistry Section (D. M. Camaioni)

Tank Waste Chemistry

T. M. Orlando

Environmental Technology Division, Process Technology Department, Electrical and Chemical Processes Group (W. O. Heath and T. M. Bergsman)

Low-Temperature Plasma Destruction Techniques

T. M. Orlando and W. Hess

Environmental Technology Division, Tank Focus Area (K. D. Keefer)

Radiation Damage of Waste Forms

D. Ray

EMSL Computing and Information Sciences (J. M. Price)

Spectroscopy and Dynamics of Molecular Clusters

D. Ray

EMSL Theory, Modeling, and Simulation (D. F. Feller and E. D. Glendening)

Gas-Phase Cation-Ether Complexes

S. W. Sharpe and R. S. McDowell

EESD Materials and Chemical Sciences Department, Atomic and Molecular Chemistry Section (J. F. Kelly)

Spectroscopic Techniques for Atmospheric Monitoring

L. S. Wang

EMSL Theory, Modeling, and Simulation (J. B. Nicholas)

Cluster Model Studies of Chemical Bonding

X. S. Xie

EESD Earth Systems Sciences Department, Atmospheric Sciences Section (R. X. Bian)

Finite Difference Time-Domain Modeling of the Molecule-Probe Interaction in Near-Field Spectroscopy

X. S. Xie

EESD and WSU Tri-Cities (L. Xun)

Single Protein Enzymatic Reactions of Dehalogenase

Acronyms and Abbreviations

AES	Auger electron spectroscopy	IHB	intramolecular hydrogen bond
AFM	atomic-force microscopy	IPT	intramolecular proton transfer
aq	aqueous	IR	infrared
bcc	body-centered cubic	ITO	indium tin oxide
CALIOPE	Chemical Analysis by Laser Interrogation of Proliferant Effluents	LAMS	laser ablation / mass spectrometry
CID	collision-induced dissociation	LDRD	Laboratory Directed Research and Development
CRADA	Cooperative Research and Development Agreement	LEED	low-energy electron diffraction
CS&D	Chemical Structure and Dynamics	ML	monolayer(s)
DE	detachment energy	NSOM	near-field scanning optical microscope
DEA	dissociative electron detachment	PES	photoelectron spectroscopy
DME	dimethyl ether	PNL	Pacific Northwest Laboratory (to Sept. 1996)
DMSO	dimethyl sulfoxide	PNNL	Pacific Northwest National Laboratory (from Oct. 1996)
DOE	Department of Energy	ppb	parts per billion
DXE	dimethoxyethane	ppm	parts per million
EA	electron affinity	RCS	rotational coherence spectroscopy
EDTA	ethylenediaminetetraacetic acid	REMPI	resonance-enhanced multiphoton ionization
EESD	Environmental and Energy Sciences Division	SERDP	Strategic Environmental Research and Development Program
EMSL	Environmental Molecular Sciences Laboratory	SERS	Science and Engineering Research Semester
ESD	electron-stimulated desorption	STM	scanning tunneling microscope/microscopy
ESIPT	excited-state intramolecular proton transfer	TCE	trichloroethylene
fcc	face-centered cubic	TOF	time of flight
FDTD	finite-difference time-domain	TPD	temperature-programmed desorption
FM	frequency modulation	UHV	ultra-high vacuum
FTIR	Fourier-transform infrared	UV	ultraviolet
FTIRS	Fourier-transform infrared spectrometer	VUV	vacuum ultraviolet
FWHM	full width at half maximum	WINP	weakly-ionized nonneutral plasma
GW	Gaussian width	WSU	Washington State University
hcp	hexagonal close-packed	YAG	yttrium-aluminum-garnet
HF	Hartree-Fock		

Where CS&D Fits in PNNL

Environmental and Energy Sciences Division (EES) (M. L. Knotek)

Earth Systems Sciences (R. L. Skaggs)

Environmental Molecular Sciences Laboratory (EMSL) (T. H. Dunning)

EMSL Construction Project (J. W. Bixler)

Chemical Structure and Dynamics (CS&D) (S. D. Colson)

Materials and Interfaces (M&I) (J. Janata)

Macromolecular Structure and Dynamics (MS&D) (P. D. Ellis)

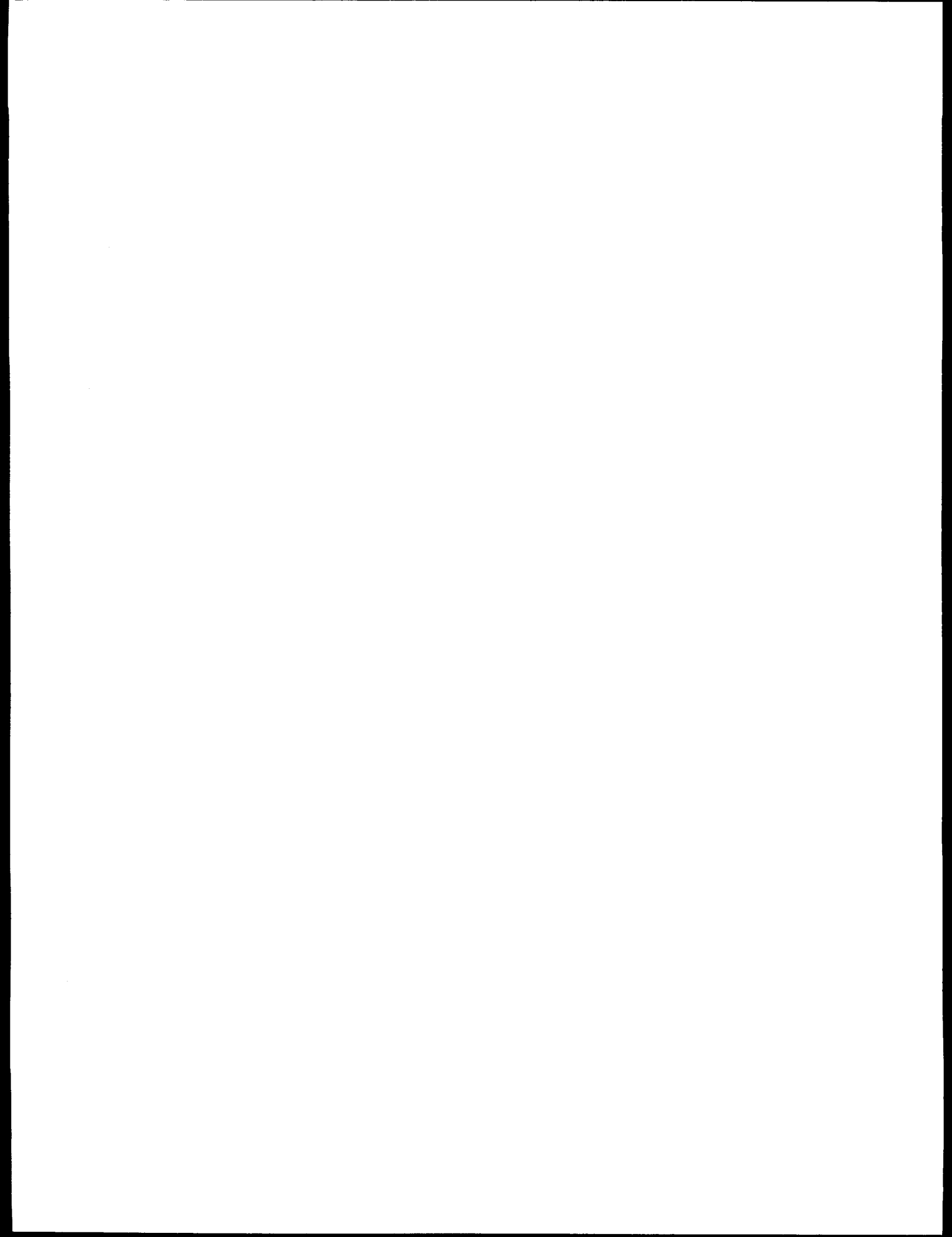
Theory, Modeling, and Simulation (TM&S) (D. A. Dixon)

Environmental Dynamics and Simulation (ED&S) (A. R. Felmy, *Acting*)

Computing and Information Sciences (C&IS) (R. A. Bair)

Processing Science (B. C. Bunker)

Materials and Chemical Sciences (G. L. McVay)



Distribution

No. of Copies		No. of Copies
	Offsite	
2	DOE/Office of Scientific and Technical Information	P. F. Barbara Department of Chemistry University of Minnesota 207 Pleasant Street SE Minneapolis, MN 55455-0431
	A. C. Albrecht Department of Chemistry Cornell University Ithaca, NY 14853-1301	N. F. Barr Office of Health and Environmental Research Office of Energy Research U.S. Department of Energy Washington, D.C. 20545
	J. E. Almloff Department of Chemistry University of Minnesota 207 Pleasant Street S.E. Minneapolis, MN 55455	C. W. Bauschlicher, Jr. NASA Ames Research Center RTC-230-3 Moffett Field, CA 94035
	R. J. Anderson Sandia National Laboratories Livermore, CA 94550	R. A. Beaudet Department of Chemistry University of Southern California Los Angeles, CA 90089-0482
	P. B. Armentrout Department of Chemistry University of Utah 2020 Henry Eyring Bldg. Salt Lake City, UT 84112	B. Bederson Department of Physics New York University Washington Square New York, NY 10003
	G. H. Atkinson Department of Chemistry University of Arizona Tucson, AZ 85721	S. M. Benson Mail Stop 50E Lawrence Berkeley Laboratory 1 Cyclotron Road Berkeley, CA 94720
	D. Auerbach Department K31-802 IBM Almaden Research Center 650 Harry Road San Jose, CA 95120-6099	B. J. Berne Department of Chemistry Box 755 Havemeyer Hall Columbia University New York, NY 10027
	Y. K. Bae SRI International 333 Ravenswood Avenue Menlo Park, CA 94025	

No. of
Copies

No. of
Copies

E. R. Bernstein
Department of Chemistry
Colorado State University
Fort Collins, CO 80523

P. R. Callis
Department of Chemistry
Montana State University
Bozeman, MT 59717

R. Stephen Berry
Department of Chemistry
University of Chicago
5735 South Ellis Avenue
Chicago, IL 60637

C. T. Campbell
Department of Chemistry, BG-10
University of Washington
Seattle, WA 98195-1700

V. E. Bondybey
Insitut fur Physicalische Und
Theor. Chemie der
Technischen Univsersitat Munchen
D-8046 Garching b. Muchen
Deutschland - West Germany

M. Cardillo
AT&T Bell Laboratories
600 Mountain Avenue
Murray Hill, NJ 07974

M. T. Bowers
Department of Chemistry
University of California - Santa Barbara
Santa Barbara, CA 93106

K. L. Carleton
Physical Sciences International
20 New England Business Center
Andover, MA 01810

J. Bradley
Exxon Research and Engineering Co.
Corporate Research
Route 22 East
Clinton Township
Annandale, NJ 08801

A. W. Castleman, Jr.
Department of Chemistry
152 Davey Laboratory
Pennsylvania State University
University Park, PA 16802

M. S. Broido
ER-74, G-155, GTN
U.S. Department of Energy
19901 Germantown Road
Germantown, MD 20874-1290

S. T. Ceyer
Department of Chemistry
Massachusetts Institute of Technology
Cambridge, MA 02139

J. M. Brown
Physical Chemistry Laboratory
Oxford University
S. Parks Road
Oxford OX1 3QZ
UK

J. Chung
Department of Mechanical &
Materials Engineering
Washington State University
Pullman, WA 99164

R. L. Byer
Department of Applied Physics
Stanford University
Stanford, CA 94305

M. J. Coggiola
Program Manager, Collision Processes
SRI International
333 Ravenswood Avenue
Menlo Park, CA 94025

**No. of
Copies**

D. Cox
Exxon Research and Engineering Co.
Corporate Research, LH378
Route 22 East
Clinton Township
Annandale, NJ 08801

F. F. Crim
Department of Chemistry
University of Wisconsin
Madison, WI 53706

G. A. Crosby
Department of Chemistry
Washington State University
Pullman, WA 99164-4630

C. Crowe
Department of Mechanical &
Materials Engineering
Washington State University
Pullman, WA 99164

R. F. Curl, Jr.
Department of Chemistry
Rice University
Houston, TX 77251-1892

R. C. Dahlman
Office of Health and Environmental
Research
Office of Energy Research
U.S. Department of Energy
Washington, D.C. 20545

H.-L. Dai
Department of Chemistry
University of Pennsylvania
Philadelphia, PA 19104-6323

J. G. Dash
Department of Physics, FM-15
University of Washington
Seattle, WA 98195

**No. of
Copies**

A. E. Depristo
Ames Laboratory
Iowa State University
Ames, IA 50011

J. T. Dickinson
Department of Physics
Washington State University
Pullman, WA 99164-2814

G. P. Drobny
Department of Chemistry
University of Washington
Seattle, WA 98195-1700

J. R. Durig
College of Arts & Sciences
320 Scofield Hall
University of Missouri
Kansas City, MO 64110-2499

T. R. Dyke
Department of Chemistry
University of Oregon
Eugene, OR 97403

G. B. Ellison
Department of Chemistry
University of Colorado
Boulder, CO 80309-0215

M. A. El-Sayed
Department of Chemistry
Georgia Institute of Technology
225 North Ave.
Atlanta, GA 30332

T. Engel
Department of Chemistry
University of Washington
Seattle, WA 98195

P. C. Engelking
Department of Chemistry
University of Oregon
Eugene, OR 97403-1253

No. of
Copies

No. of
Copies

P. Esherick
Department 1126
Sandia National Laboratory
Albuquerque, NM 87165-0601

E. M. Eyring
Department of Chemistry
University of Utah
Salt Lake City, UT 84112

J. Farley
Department of Physics
University of Nevada - Las Vegas
4505 Maryland Parkway
Las Vegas, NV 89154

P. M. Felker
Department of Chemistry
405 Hilgard Avenue
University of California
Los Angeles, CA 90024-1569

R. W. Field
Department of Chemistry, Room 6-219
Massachusetts Institute of Technology
Cambridge, MA 02139

G. Fisk
Supervisor, Combustion Chemistry
Division
Division 8353
Sandia National Laboratories
Livermore, CA 94550

G. R. Fleming
Department of Chemistry
University of Chicago
5735 S. Ellis Ave.
Chicago, IL 60637

C. W. Frank
EM-50, 7A-049
Office of Technology Development
Office of Environmental Management
U.S. Department of Energy
Forrestal Building
1000 Independence Avenue, S.W.
Washington, D.C. 20585-0118

H. Frauenfelder
Department of Physics
University of Illinois
110 West Green Street
Urbana, IL 61801

M. E. Frazier
Office of Health and Environmental
Research
Office of Energy Research
U.S. Department of Energy
Washington, D.C. 20545

B. S. Freiser
Department of Chemistry
Purdue University
West Lafayette, IN 47907-1393

T. E. Furtak
Colorado School of Mines
Physics Department
Golden, CO 80401

J. H. Futrell
Chairman
Chemistry and Biochemistry
University of Delaware
Newark, DE 19716

J. W. Gadzuk
Surface Science Division - Theory
National Institute of Standards &
Technology
Gaithersburg, MD 20899

**No. of
Copies**

**No. of
Copies**

J. F. Garvey
Department of Chemistry
University of New York State at Buffalo
Buffalo, NY 14260-3000

W. R. Gentry
Department of Chemistry
University of Minnesota
Minneapolis, MN 55455

S. M. George
Department of Chemistry
University of Colorado
Boulder, CO 80309

T. F. George
Office of the Provost
Washington State University
Pullman, WA 99164-4660

J. L. Gland
Department of Chemistry
University of Michigan
Ann Arbor, MI 48109-1055

W. A. Goddard III
Division of Chemistry and Chemical
Engineering
California Institute of Technology
Pasadena, CA 99125

D. W. Goodman
Department of Chemistry
Texas A&M University
College Station, TX 77843-3255

L. Goodman
Department of Chemistry
Rutgers University
Piscataway, NJ 08855-0939

T. E. Gough
Department of Chemistry
University of Victoria
P.O. Box 3055
Victoria, BC V8W 3P6
Canada

E. R. Grant
Department of Chemistry
Purdue University
West Lafayette, IN 47907-1393

R. B. Green
Associated Western Universities
723 The Parkway, Suite 100
Richland, WA 99352-4234

R. G. Griffin
Department of Chemistry
Massachusetts Institute of Technology
Cambridge, MA 02139-4307

H. Hamilton
Department of Mechanical &
Materials Engineering
Washington State University
Pullman, WA 99164

K. G. Hancock
Division of Chemistry
National Science Foundation
1800 G Street, NW
Washington, D.C. 20550

D. M. Hanson
Department of Chemistry
SUNY Stony Brook
Stony Brook, NY 11794-3400

C. B. Harris
Chemistry Department
University of California
Berkeley, CA 94720

W. C. Harris
Mathematics and Physical Sciences
National Science Foundation
Washington, D.C. 20205

P. J. Hay
T12, Mail Stop B268
Los Alamos National Laboratory
Los Alamos, NM 87545

No. of
Copies

No. of
Copies

R. Haydock
Materials Science Institute
14 Science 1
University of Oregon
Eugene, OR 97403

V. E. Henrich
Department of Applied Physics
Yale University
P.O. Box 2157
New Haven, CT 06520

J. W. Hepburn
University of Waterloo
Guelph, Ont. N1G 2W1
Canada

W. Hetherington
Department of Physics
Oregon State University
Corvallis, OR 97333

K. W. Hipps
Department of Chemistry
Washington State University
Pullman, WA 99164-4630

J. B. Hopkins
Department of Chemistry
Louisiana State University
Baton Rouge, LA 70803

J. T. Hougen
Molecular Physics Division
U.S. Department of Commerce
National Institute of Standards &
Technology (NIST)
Gaithersburg, MD 20899

B. S. Hudson
Department of Chemistry
Room 189 Science II
University of Oregon
Eugene, OR 97403-1253

J. Jellinek
Chemistry Division
Argonne National Laboratory
Argonne, IL 60439

M. A. Johnson
Department of Chemistry
Yale University
P.O. Box 6666
New Haven, CT 06511

P. M. Johnson
Department of Chemistry
SUNY Stony Brook
Stony Brook, NY 11794

H. Jones
University of Ulm
POB 4066
D-7900 Ulm
Germany

C. D. Jorgensen
Office of Health and Environmental
Research
Office of Energy Research
U.S. Department of Energy
Washington, D.C. 20545

H. Kapteyn
Department of Physics
Washington State University
Pullman, WA 99164-4630

D. F. Kelley
Department of Chemistry
Colorado State University
Fort Collins, CO 80523-1872

S. D. Kevan
Department of Physics
University of Oregon
120 Willamette Hall
Eugene, OR 97403

**No. of
Copies**

W. H. Kirchhoff
Division of Chemical Sciences
Office of Basic Energy Sciences
ER-141, G-343
U.S. Department of Energy
Washington, D.C. 20874-1290

T. A. Kitchens
Office of Scientific Computing
Office of Energy Research
U.S. Department of Energy
Washington, D.C. 20545

W. Klemperer
Department of Chemistry
Harvard University
12 Oxford St
Cambridge, MA 02138

D. S. Kliger
Department of Chemistry
University of California
Santa Cruz, CA 95064

M. Koch
Dow Chemical U.S.A.
1897 Building
Analytical Sciences Laboratory
Midland, MI 48667

B. E. Kohler
Department of Chemistry
University of California, Riverside
Riverside, CA 92521

R. Kopelman
Department of Chemistry
University of Michigan
Ann Arbor, MI 48109-1055

K. Krogh-Jespersen
Department of Chemistry
Rutgers University
New Brunswick, NJ 08903

**No. of
Copies**

R. L. Kuczkowski
Department of Chemistry
University of Michigan
Ann Arbor, MI 48109-1055

A. C. Kummel
Department of Chemistry
University of California - San Diego
La Jolla, CA 92093-0314

M. Kuzyk
Department of Physics
Washington State University
Pullman, WA 99164-4630

P. P. Lambropoulos
Department of Physics
University of Southern California
Los Angeles, CA 90089-0484

M. Lapp
Org 8102, MS 9056
Sandia National Laboratories
Livermore, CA 94551

A. H. Laufer
Division of Chemical Sciences
Office of Basic Energy Sciences
ER-141, G-340A
U.S. Department of Energy
Washington, D.C. 20874-1290

T. J. Lee
NASA Ames Research Center
Moffett Field, CA 94035

S. R. Leone
Department of Chemistry and Joint
Institute for Laboratory Astrophysics
University of Colorado
Boulder, CO 80309-0440

No. of
Copies

S. Leutwyler
Institut für Anorganische, Analytische
und Physikalische Chemie
Universität Bern
Freiestrasse 3
CH-3000 Bern 9
SWITZERLAND

D. H. Levy
Department of Chemistry
University of Chicago
5735 South Ellis Avenue
Chicago, IL 60637

S.C.T. Lien
EM-54
Office of Environmental Management
U.S. Department of Energy
12800 Middlebrook Rd.
Germantown, MD 20874

E. C. Lim
Department of Chemistry
University of Akron
Akron, OH 44325-3601

W. C. Lineberger
Department of Chemistry and Joint
Institute for Laboratory Astrophysics
University of Colorado
Campus Box 215
Boulder, CO 80309-0440

W. C. Luth
Engineering and Geosciences Division
Office of Basic Energy Sciences
Office of Energy Research
U.S. Department of Energy
Washington, D.C. 20545

D. Magde
Department of Chemistry
B-014
University of California - San Diego
LaJolla, CA 92093-0314

No. of
Copies

R. S. Marianelli
ER-14, G-336
U.S. Department of Energy
19901 Germantown Road
Germantown, MD 20874-1290

W. J. Marinelli
Group Leader, Thermophysical Sciences
Physical Sciences International
20 New England Business Center
Andover, MA 01810

R. A. Mathies
Department of Chemistry
University of California
Berkeley, CA 94720

B. W. Matthews
Institute of Molecular Biology
University of Oregon
Eugene, OR 97403-1229

U. M. Mazur
Department of Chemistry
Washington State University
Pullman, WA 99164-4630

W. M. McClain
Department of Chemistry
Wayne State University
Detroit, MI 48202

J. L. McHale
Department of Chemistry
University of Idaho
Moscow, ID 83843

R. D. Mead
Spectra Technology
2755 Northrup Way
Bellevue, WA 98004-1495

H. I. Metiu
Chemistry Department
University of California
Santa Barbara, CA 93106

No. of
Copies

No. of
Copies

J. C. Miller
Chem Physics Section
Oak Ridge National Laboratory
P.O. Box 2008
Oak Ridge, TN 37831-6125

R. E. Miller
Department of Chemistry
University of North Carolina/Chapel Hill
Chapel Hill, NC 27599-3290

T. A. Miller
Department of Chemistry
Ohio State University
120 W. 18th Avenue
Columbus, OH 43210

W. S. Millman
Office of Basic Energy Sciences
U.S. Department of Energy
Washington, D.C. 20545

M. D. Morse
Department of Chemistry
University of Utah
Salt Lake City, UT 84112

J. Muentert
Department of Chemistry
University of Rochester
404 Hutchinson Hall, River Campus
Rochester, NY 14627

K. Muller-Dethlefs
Chemistry Department
Technische Universität München
Lichten Bergstrasse 4
Garching BIE, München D-8046
Germany

M. Murnane
Department of Physics
Washington State University
Pullman, WA 99164-4630

A. B. Myers
Department of Chemistry
University of Rochester
404 Hutchinson Hall, River Campus
Rochester, NY 14627-0216

D. J. Nesbitt
University of Colorado
Joint Institute for Laboratory Astrophysics
Campus Box 440
Boulder, CO 80309-0440

T. L. Netzel
Department of Chemistry
Georgia State University
Atlanta, GA 30303

D. M. Neumark
Department of Chemistry
University of California - Berkeley
Berkeley, CA 94720

T. Oka
Department of Chemistry
University of Chicago
Chicago, IL 60637-1403

M. Okumura
Department of Chemistry
Mail Code 127-72
Cal Tech
Pasadena, CA 91125

A. A. Patrinos
ER-74, E-156/GTN
U.S. Department of Energy
19901 Germantown Road
Germantown, MD 20874

M. Philpott
IBM Almaden Research Center
650 Harry Rd.
San Jose, CA 95120

No. of
Copies

No. of
Copies

D. M. Poutsma
Oak Ridge National Laboratory
MS-6182, Building 4500N
P.O. Box 2008
Oak Ridge, TN 37831-6182

D. W. Pratt
Department of Chemistry
University of Pittsburgh
Parkman Ave & University Dr
Pittsburgh, PA 15260

H. E. Radford
Center for Astrophysics
60 Garden St.
Cambridge, MA 02138

D. A. Ramsay
NRC Canada/100 Sussex Dr.
Ottawa
Ontario K1A 0R6
Canada

M. R. Riches
ER-74, G-141/GTN
U.S. Department of Energy
19901 Germantown Road
Germantown, MD 20874

S. Riley
Argonne National Laboratory
9400 South Cass Avenue
Argonne, IL 60439

G. W. Robinson
Texas Tech University
Lubbock, TX 79409-1061

R. J. Saykally
Department of Chemistry
University of California - Berkeley
419 Lattimer Hall, #1460
Berkeley, CA 94720

E. Schlag
Chemistry Department
Technische Universität München
Lichten Bergstrasse 4
Garching BIE, München D-8046
Germany

T. J. Sears
Chemistry Department
Brookhaven National Laboratory
33 Louis St.
Upton, NY 11973-9999

G. Scoles
Department of Chemistry
Princeton University
Princeton, NJ 08544

H. Sellers
National Center for Supercomputing
Applications
University of Illinois
405 North Matthews Avenue
Urbana, IL 61801

J. M. Shreeve
Department of Chemistry
University of Idaho
Moscow, ID 83844-2343

M. W. Shupe
EM-541, 464/TREV
U.S. Department of Energy
12800 Middlebrook Road
Germantown, MD 20874

J. D. Simon
Department of Chemistry, B-032
University of California - San Diego
La Jolla, CA 92093

T. Slanger
Molecular Physics Laboratory
SRI International
333 Ravenswood Avenue
Menlo Park, CA 94025

**No. of
Copies**

**No. of
Copies**

R. E. Smalley
Department of Chemistry
Rice University
P.O. Box 1892
Houston, TX 77251-1892

D. A. Smith
Office of Health and Environmental
Research
Office of Energy Research
U.S. Department of Energy
Washington, D.C. 20545

M. A. Smith
Department of Chemistry
University of Arizona
Tucson, AZ 85721

AT&T Bell Laboratories
Murray Hill, NJ 07974
Attn: D. K. Stillinger
F. H. Stillinger

P. C. Stair
Department of Chemistry
Northwestern University
2145 Sheridan Road
Evanston, IL 60208-3113

R. M. Stratt
Department of Chemistry
Brown University
324 Brook Street, Box H
Providence, RI 02912

E. M. Stuve
Department of Chemical Engineering
University of Washington BF-10
Seattle, WA 98195

J. A. Syage
Propulsion & Environmental Science
Lab - M5-754
Aerospace Corporation
P.O. Box 92957
Los Angeles, CA 90009-92957

I. Thomas
ER-13, J-317/GTN
U.S. Department of Energy
19901 Germantown Road
Germantown, MD 20874

T. Torgersen
Engineering & Geosciences Division
Office of Basic Energy Sciences
Office of Energy Research
U.S. Department of Energy
Washington, D.C. 20545

F. P. Tully
Div. 8353
Combustion Research Facility
Sandia National Laboratories
Livermore, CA 94551-0969

J. Tully
AT&T Bell Laboratories
600 Mountain Avenue
Murray Hill, NJ 07974

V. Vaida
Department of Chemistry
University of Colorado
Boulder, CO 80309

S. P. Walch
NASA Ames Research Center
Moffett Field, CA 94035

E. A. Walters
Department of Chemistry
University of New Mexico
Albuquerque, NM 87131

F. B. Wampler
Mail Stop J515
Los Alamos National Laboratory
P.O. Box 1663
Los Alamos, NM 87545

No. of
Copies

No. of
Copies

R. O. Watts
School of Chemistry
University of Melbourne
Parkville Victoria 3052
Australia

J. Weaver
Department of Chemical Engineering
and Materials Science
University of Minnesota
Minneapolis, MN 55455

W. H. Weinberg
Department of Chemical and Nuclear
Engineering
University of California, Santa Barbara
Santa Barbara, CA 93106-5080

J. C. Weisshaar
Department of Chemistry
University of Wisconsin
1101 University Avenue
Madison, WI 53706

K. B. Whaley
Department of Chemistry
University of California
Berkeley, CA 94720

R. L. Whetten
School of Chemistry and Biochemistry
Boggs Chemistry Building
Georgia Institute of Technology
Atlanta, GA 30332-0400

M. G. White
Department of Chemistry
Brookhaven National Laboratory
Upton, NY 11973

K. B. Wiberg
Yale University
225 Prospect Street
P.O. Box 6666
New Haven, CT 06511

R. D. Willett
Department of Chemistry
Washington State University
Pullman, WA 99164-4630

M. W. Windsor
Department of Chemistry
Washington State University
Pullman, WA 99164-4630

C. Wittig
Department of Chemistry, SSC-403
University of Southern California
Los Angeles, CA 90089-0482

S. M. Wolf
EM-542, 413/TREV
U.S. Department of Energy
12800 Middlebrook Road
Germantown, MD 20874

J. C. Wooley
Office of Health and Environmental
Research
Office of Energy Research
U.S. Department of Energy
Washington, D.C. 20545

J. T. Yates, Jr.
Director, Pittsburgh Surface
Science Center
Department of Chemistry
University of Pittsburgh
Pittsburgh, PA 15260

R. N. Zare
Department of Chemistry
Stanford University
Stanford, CA 94305-5080

A. H. Zewail
Department of Chemistry
Cal Tech
Pasadena, CA 91125

No. of Copies		No. of Copies			
	T. S. Zwier Department of Chemistry Purdue University West Lafayette, IN 47907-1393		T. A. Fryberger B. C. Garrett J. S. Hartman A. C. Hess W. P. Hess G. R. Holtom J. Janata A. G. Joly D. R. Jones S. A. Joyce B. D. Kay M. L. Knotek W. J. Madia R. S. McDowell (100) G. L. McVay R. L. Ornstein E. W. Pearson G. R. Petersen R. K. Quinn D. Ray J.T.A. Roberts S. W. Sharpe A. A. Shepherd B. D. Shipp R. L. Skaggs R. S. Smith G. M. Stokes B. R. Stults R. G. Tonkyn R. A. Walters L. S. Wang W. R. Wiley G. L. Work Technical Report Files (5)		K2-20 K1-96 K5-25 K1-83 K2-14 K2-14 K2-12 K2-14 K1-90 K2-14 K2-14 K1-48 K1-46 K2-14 K2-45 K2-01 K1-73 K1-71 K9-69 K2-14 K9-78 K3-58 K1-71 K9-09 K9-34 K2-14 K1-74 K9-76 K2-14 K1-50 K2-14 K9-95 K1-40
Onsite					
5	DOE Richland Operations Office				
	H. E. Bell P. W. Kruger J. P. Neath J. J. Sutey D. E. Trader	K8-50 A5-54 K8-50 A4-52 K8-50			
256	Pacific Northwest National Laboratory				
	W. J. Apley J. F. Bagley R. A. Bair S. E. Barlow J. W. Bixler T. A. Blake B. C. Bunker S. D. Colson (50) C. A. Counts (50) J. P. Cowin D. A. Dixon T. H. Dunning, Jr. (5) P. D. Ellis A. R. Felmy B. M. Foley T. R. Fox D. M. Friedrich	P7-75 K1-42 K1-87 K2-14 K2-35 K3-58 K2-45 K2-14 K2-20 K2-14 K1-83 K2-20 P7-55 K9-77 K2-18 K6-48 K2-14			